MODELLING TO SUPPORT POSSIBLE FUTURE REVISIONS OF PROTOCOLS AND STRATEGIES ON TRANSBOUNDARY AIR POLLUTION

DEFRA CONTRACT NO: EPG 1/3/164

FINAL REPORT

JULY 2000 TO JUNE 2003

R G Derwent M G Sanderson W J Collins C E Johnson

Climate Research

Met Office

Bracknell

Berkshire

July 2003

Executive Summary

1. In this report, a state-of-the art global chemistry transport model STOCHEM is used to examine European air quality in the wider context of global atmsopehric chemistry. The aim has been to use a wider range of emission scanrios and trace gases and to address a wider range of environmental issues than has hitherto been used in the context of transboundary air pollution. The intention has been to forewarn policy-makers of the growing understanding of the importance of the linkages between regional and global air quality problems

2. Policy measures to control and abate the emissions of SO_2 and NO_x have been formulated within the aegis of the United Nations Economic Commission for Europe (UN ECE) in Geneva, Switzerland and its international convention on long range transboundary air pollution (CLRTAP). A series of legally-binding protocols have been negotiated to this convention dealing with the control and abatement of SO_2, NO_x, VOCs, NH_3, trace metals, and persistent organic pollutants. The latest protocol, signed in Gothenburg in 1999, is the 'Protocol to Abate Acidification, Eutrophication and Ground Level Ozone'. The ultimate goal of this protocol is to achieve levels of the deposition of acidic and eutrophying species which no longer exceed critical loads and to achieve levels of exposure to ozone which no longer exceed critical levels. The formulation of the underpinning science required to support this protocol envisaged a set of pollutant generating human activities, a set of atmospheric trace gases derived from these activities, and the physico-chemical interations between these trace gases, generating a set of damaging pollutants which cause damage to target ecosystems and human health, see Figure ES1.

3. This report has examined a number of the potential linkages in Figure ES.1 and addressed the growing understanding of the importance of the linkages between global and regional-scale air quality problems. These linkages may require new protocols and strategies and may lead potentially to revisions in the existing protocols.
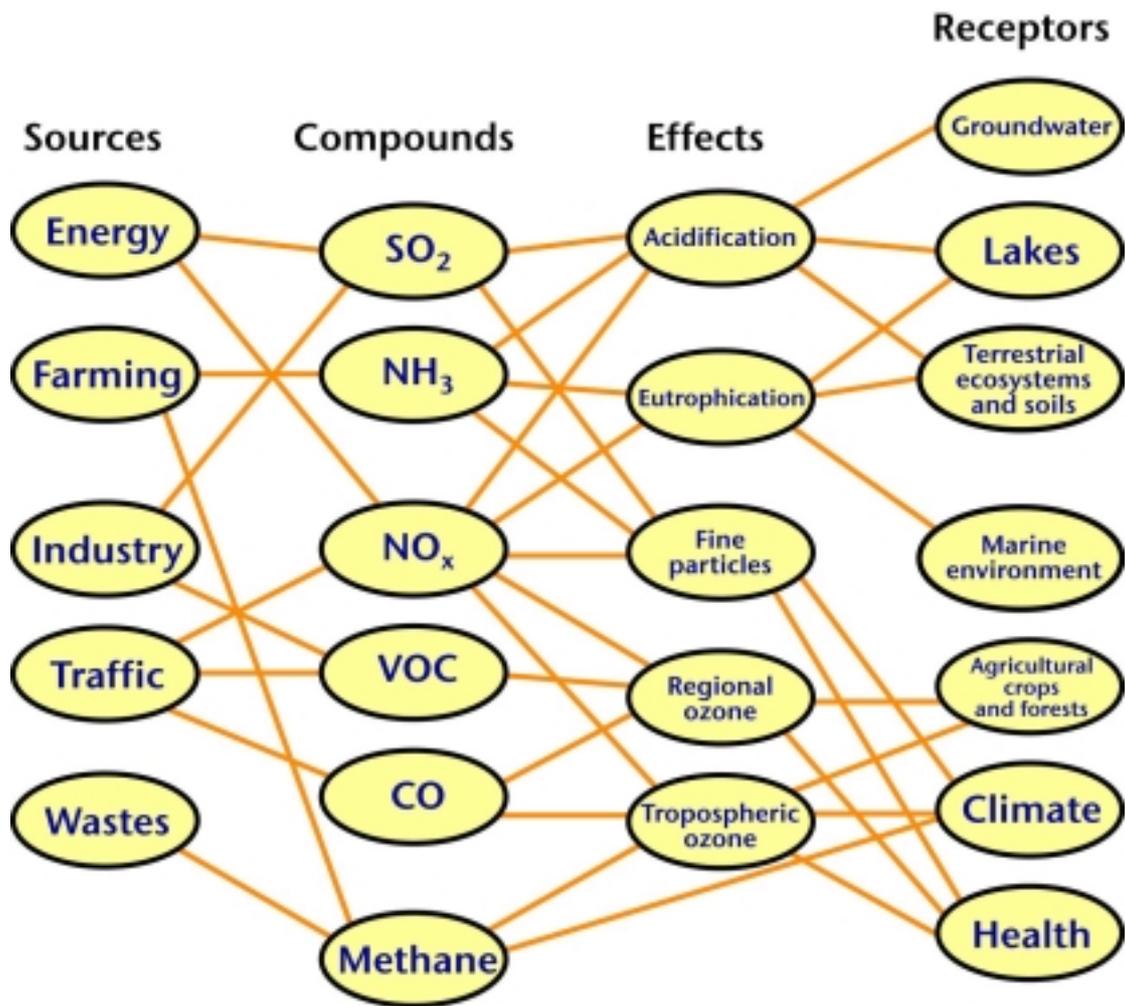
Figure ES.1. Regional air pollution problems in Europe. Relations between dominant sources, emitted compounds and their effects on different receptors.

4. The first issue that has been addressed in this study has been the linkage between CO emissions and acidification and eutrophication. Figure ES.1 shows how CO emissions from human activities on the regional scale arise predominantly from traffic and how they influence the formation of ozone on both the regional and global scale. The potential issue is that this involvement of CO in global and regional ozone formation also influences the production of hydrogen peroxide and of hydroxyl radicals, the main oxidants for the SO_2 emitted from human activities. There is the potential therefore for man-made emissions of CO on the regional scale to influence acidification. By the same argument, the involvement of CO in the production of OH radicals could influence the oxidation of NO_x and hence

eutrophication. The responses in the deposition of acidifying and eutrophying agents due to changes in man-made CO emissions were found to be small and are unlikely to be of any significance in air quality policy terms.

5. It is widely recognised that the growth of greenhouse gases will induce through climate change, widespread and significant changes in atmospheric composition and weather patterns. The impact of the growth in greenhouse gas emissions through to 2030 in the IPCC SRES B2 scenario on the deposition of acidifying and eutrophying compounds has been investigated by calculating the deposition patterns for 2030 with identical emissions but with 1990 and 2030 meteorology. Both deposition maps for 2030 have been calculated with identical 2030 emissions and show similar features. The impact of Asian SO_2 emissions on the wet sulphur deposition fields is clearly apparent across much of the northern hemisphere. Also, the trans-continental transport of acidic sulphur compounds across the North Atlantic Ocean is clearly apparent following the implementation of strict SO_2 emission controls in Europe. Nevertheless, the differences between the deposition maps resulting from changes in meteorology due to climate change are small. There is an indication of increased export across the North Atlantic Ocean into the British Isles but it is difficult to say whether this is a robust feature of the future deposition patterns. It may well be that 2030 is too early for dramatic shifts in the regional deposition patterns of acidifying and eutrophying agents. Nevertheless, such shifts should be taken into account in any wider policy study of the interaction between climate change and critical loads and levels exceedance over the medium to long term future.

6. The formation of secondary particles on the global and regional scales has been investigated. The conversion of SO_2 and DMS to particulate sulphur, of NO_x to particulate nitrate, NH_3 to particulate ammonium and terpenes to secondary organic aerosols has been incorporated into STOCHEM. A reasonable description has been obtained of the observed distributions of secondary particles on the regional and global scales. On the global scale, the fraction of secondary particle mass predicted to be present as sulphate was found to be 0.52, with the fractions of nitrate, ammonium and organics found to be 0.22, 0.09 and 0.17, respectively. This implies that the links between the climate impacts of particles and regional

emissions of SO_2, NO_x and NH_3 in Figure ES.1 are likely to be of strong policy concern. However, the UN Framework Convention on Climate Change as currently formulated does not address the aerosol precursor gases in the basket of gases under control. Overall, there are cogent reasons for extending both the Gothenburg Protocol and the UN Framework Convention on Climate Change to include secondary aerosol species and their precursors: SO_2, NO_x, VOCs and NH_3.

7. It has only recently been recognised that North American ozone precursor emissions may exert an influence on ozone levels in Europe. Similarly, intercontinental transport processes can lead to the export of ozone from Europe to Asia, Asia to the North America and North America to Europe. Labelling techniques have been employed within STOCHEM to ascertain the continental origins of the ozone observed in Europe. Internal ozone production within Europe contributed on average about 20.7 ppb to surface ozone mixing ratios over Europe and provided the largest single source area contribution to annual mean ozone levels. Import from North America contributed about 8.2 ppb and from Asia about 4.5 ppb, to surface ozone mixing ratios over Europe.

8. In view of the importance of intercontinental transport from North America and Asia in determining mean ozone concentrations over Europe, the question remains as to the magnitude of ozone changes resulting in Europe from ozone precursor emission reductions in North America and Asia. An across-the-board 50% reduction in global man-made NO_x emissions reduced the contribution to surface ozone levels from internal ozone production within Europe by 0.9-4.3 ppb. Import from Asia was reduced by 0.5-0.7 ppb and import from North America by 0.8-1.9 ppb. It is likely, therefore, that changes in man-made NO_x emissions made in North America and Asia will have an impact on annual mean ozone levels across Europe, particularly on the Atlantic Ocean seaboard of north west Europe and in Scandinavia. These will need to be taken into account in the revision of the Gothenburg Protocol.

9. The impact of an across-the-board 50% reduction in global man-made carbon monoxide emissions was studied in a similar manner as that for NO_x emission reductions. These responses to CO emissions appear to be close to the level of

noise within the STOCHEM model and may therefore be only of borderline air quality policy significance.

10. STOCHEM has been used to look at the global scale impact of the regional emissions of NO_x and CO and their control on the build-up of the greenhouse gases: methane and ozone. By changing the location and season of an emitted pulse of NO_x or CO, but not its magnitude, differing impacts on methane and ozone have been found for NO_x and CO emitted in Europe, North America and Asia. The influence of the regional emissions of CO and NO_x and their control on the global mean radiative forcing due to methane and ozone and hence on climate change, are large and are likely to be of air quality policy significance. The UN Framework Convention on Climate Change does not currently have tropospheric ozone precursors within its basket of greenhouse gases. It is therefore not possible currently for Europe to claim credit or disbenefit in climate change terms for actions taken on the regional scale to control NO_x and CO emissions.

11. STOCHEM has been used to follow the build-up of methane and ozone in the troposphere during the 21st century and to understand the mechanisms involved in the feedback between the chemical development and the changing weather patterns which result from climate change. Surface ozone concentrations during the summer months over the continental land masses are currently about 30-40 ppb. In the IPCC SRES A2 and A1FI emission scenarios, the corresponding values become 45-50 ppb in 2030, 60 ppb in 2060 and 70 ppb in 2100. These concentrations are well above the internationally-accepted environmental criteria values set to protect human health, sensitive crops and vegetation. This prospect is in store for all of the continental areas of the northern hemisphere, despite the measures being taken to improve urban- and regional-scale ozone air quality in North America and Europe. These ozone increases are more directly relevant to the long term exposure levels of crops and vegetation than to human exposures. However, urban- and regional-scale pollution episodes are built upon these global baseline values and so the future medium to long term increases in the latter may therefore work against regional pollution control strategies, set to reduce exposure levels of both man and vegetation.

12. A feasibility study has been conducted to consider adding the life cycle of mearcury to STOCHEM. Mercury and its compounds are emitted into the atmosphere from a number of natural processes as well as from human activities. Long range and intercontinental transport of atmospheric mercury and its deposition, followed by the biomethylation and the bioaccumulation of the highly toxic methylmercury compounds in the aquatic food chain, pose serious environmental problems. These concerns have been reflected in the incorporation of mercury within the Geneva Convention of the United Nations Economic Commission for Europe on Long-range Transboundary Air Pollution. A protocol to this Convention was signed at Arrhus in Denmark in June 1998 and addresses the emissions of mercury in addition to those of cadmium and lead. Mercury could be added into regional integrated assessment models as it is a substance emitted by coal combustion and from industrial processes. Its oxidation in the atmosphere is driven by ozone and hydroxyl radicals which are controlled by VOCs, CO, methane and NO_x. The receptors for mercury would be the aquatic food chain and human health.

13. It has been shown that it is feasible to fit a simplified treatment of the atmospheric life cycle of mercury and its compounds into the STOCHEM model. The fields of OH radicals and of ozone calculated within STOCHEM have the required accuracy with which to calculate a quantitative description of the fate and behaviour of the mercury compounds emitted from man-made sources.

14. In summary, we have identified a number of reasons why present agreements, protocols and strategies need extending and supplementing with new protocols and strategies. They are given in no particular order in the paragraphs below.

- As concentration levels and deposition loads are progressively reduced by regional pollution controls, originally small and uncontrolled sources within the UN ECE framework assume more significant proportions. Examples include marine sulphur sources from shipping in the North Atlantic Ocean, North Sea, Baltic Sea and Mediterranean Sea. Such sources may have a significant influence on critical load exceedance in sensitive ecosystems on the Atlantic Ocean seaboard of north west Europe and Scandinavia.

- Global baseline levels of ozone in Europe have been rising due to increased man-made emissions elsewhere in the northern hemisphere and threaten to erode the improvements made through European regional pollution controls on NO_x and VOCs. There is currently no framework within European regional air quality policy formulation to address the consequences of changes in global baseline ozone concentrations due to precursor emission changes in North America and Asia.

- Reductions in European regional emissions of CO and NO_x may have a significant influence on the global scale build-up of methane and ozone, the second and third most important greenhouse gases. The UN Framework Convention on Climate Change does not include tropospheric ozone precursor gases within its basket of greenhouse gases. There is therefore no mechanism for Europe to claim any credit or disbenefit in terms of climate change mitigation for it actions to reduce ozone precursor emissions on the regional scale.

- European emissions of SO_2, NO_x and NH_3 play a significant role in the global scale formation of secondary aerosol particles which may have a significant influence on climate change. The UN Framework Convention on Climate Change does not include aerosol precursor gases within its basket of greenhouse gases. Again, there is no mechanism for Europe to claim credit or disbenefit in terms of climate change mitigation for its actions to reduce aerosol precursor emissions on the regional scale.

- European emissions of CO and NO_x exert an influence on the availability of oxidants and hence the deposition of acidifying and eutrophying species on the global scale.

- Mercury deposition over Europe is driven partly by local European emissions of mercury compounds and by the deposition of mercury compounds derived from the global mercury circulation. This material of global origins is not addressed currently by the Arrhus Protocol on heavy metals.

.15. Recommendations have been compiled for further work to take the issues raised in this study through to completion, addressing background ozone, intercontinental transport, global mercury modelling and investigation of the links between air quality and global climate change.

Contents of the Report

Executive Summary

Contents

1. Introduction to the Project

2. The Global 3-D Lagrangian Chemistry-Transport Model STOCHEM

3. The Global and Regional Deposition of Acidifying and Eutrophying Species

4. Global and Regional Distributions of Ozone

5. Global Deposition of Mercury Compounds

6. Discussion and Conclusions

7. Recommendations for Further Work

8. References

Annex A. Published Papers and Reports from this Project

Annex B. Meetings Attended.

1. Introduction to the Project

The adverse environmental impacts of the long range transport and deposition of acidic sulphur and nitrogen species to the remote and sensitive regions of north west Europe have been recognised for over two decades now. Policy measures to control and abate the emissions of SO_2 and NO_x have been formulated within the aegis of the United Nations Economic Commission for Europe (UN ECE) in Geneva, Switzerland and its international convention on long range transboundary air pollution (CLRTAP). A series of legally-binding protocols have been negotiated to this convention dealing originally with the exchange of research and monitoring data and then the control and abatement of SO_2, NO_x, VOCs, NH_3, trace metals, and persistent organic pollutants.

The latest protocol, signed in Gothenburg in 1999, is the 'Protocol to Abate Acidification, Eutrophication and Ground Level Ozone'. The ultimate goal of this protocol is to achieve levels of the deposition of acidic and eutrophying species which no longer exceed critical loads and to achieve levels of exposure to ozone which no longer exceed critical levels. The formulation of the underpinning science required to support this protocol was laid out through the collaboration of research teams in Norway, Sweden and in the United Kingdom. An integrated assessment model using the consensus research base was then used to construct the outline of an agreement which was then negotiated by policy-makers into the final legally-binding protocol.

The requirements for future revisions are built in to the individual protocols. Future revisions depend on the successes of the measures taken to reduce emissions and changing perceptions of the environmental impacts addressed. They also reflect improvements in scientific understanding of the processes involved. The models used to describe the emission, transformation, long-range transport and deposition of air pollutants are becoming more sophisticated with time. They are becoming better able to support the pressure for further emission reductions and to provide the more accurate assessments of source-receptor relationships required to identify the crucial remaining sources to be tackled.

Evidence has begun to accumulate concerning the interhemispheric scale of the long range transport of some of the important air pollutants of concern. Whilst it has been

long recognised that particulate sulphate aerosol can travel from North America and Eurasia to the Arctic, it has only been recognised that North American ozone precursor emissions may exert an influence on ozone levels in Europe. Similar interhemispheric effects may link Asian emissions to North American air quality.

The Met Office has had a long involvement with the modelling of the long-range transport of acidic sulphur and nitrogen species and of ozone in Europe. It has also developed a sophisticated global Lagrangian chemistry model (STOCHEM) to study the build-up of greenhouse gases and aerosols. The STOCHEM model has been used to identify the important coupling between global and regional scale ozone formation and transport. We have identified how European regional ozone concentrations will steadily increase over the next few decades in response to growing global scale emissions of methane, carbon monoxide and NO_x.

The present challenge is to enrol state-of-the-art global chemistry transport models to examine future European air quality in the wider context of global atmospheric composition change. The aim of this project is to follow up these initial studies with a wider range of emission scenarios and to address a wider range of environmental impacts. The intention is to forewarn policy-makers about the growing understanding of interhemispheric long-range transport so that they have the opportunity to consider its wider ramifications for regional and global air quality policy development.

The objectives of the project are as follows:

i.   To quantify global deposition fields of SO_x, NO_y and NH_x based on present day emissions and future emission scenarios and evaluate the policy significance of these deposition fields.

ii.   To quantify ozone fields based on present day and future emissions of NO_x, CH_4 and VOCs and analyse the policy significance of the results.

iii. To evaluate possible lines for the development of integrated assessment models, taking into account improvements in scientific understanding which have taken place in the last decade.

iv.   To investigate and characterise the export of trace gases and aerosols from the European region into the free troposphere and analyse the policy consequences of this export.

2. The Global 3-D Lagrangian Chemistry-Transport Model STOCHEM

2.1 Model Description

The model used in this work is the UK Meteorological Office tropospheric 3-D chemistry transport model (STOCHEM). This model takes a Lagrangian approach by dividing the troposphere into 50,000 air parcels which are advected with a 3 hour time step using archived winds from the Meteorological Office Unified Model. These three-dimensional winds are 6-hourly instantaneous values, taken either from operational meteorological analyses or from climate integrations.

Each parcel holds the concentrations of 70 chemical species including NO_x, O_3, OH, HO_2, PAN, and hydrocarbons. The hydrocarbons modelled are methane (CH_4), ethane (C_2H_6), ethene (C_2H_4), propane (C_3H_8), propene (C_3H_6), n-butane (C_4H_{10}), toluene ($CH_3C_6H_5$), o-xylene (($CH_3)_2C_6H_4$), and isoprene (C_5H_8), along with their oxidation products such as peroxy radicals (RO_2), hydroperoxides (ROOH), and carbonyls (e.g., formaldehyde (HCHO), acetaldehyde (CH_3CHO), acetone (CH_3COCH_3), methyl glyoxal (CH_3COCHO), and methyl vinyl ketone ($CH_3COCH=CH_2$). The chemical species react according to 174 photolytic and thermal reactions, with a 5-minute chemistry time step. The resulting parcel concentrations are mapped to a $5°×5°×9$ pressure level grid for output. The vertical co-ordinate used in STOCHEM and in the GCM is a hybrid co-ordinate equal to P/P_{surf} (terrain-following) near the surface and equal to $P/(1000$ hPa) (pressure following) above 30 hPa.

The physical processes included are emission, dry and wet deposition, convection, and sub-grid scale mixing between parcels. Emissions can be into the boundary layer or three-dimensional (from aircraft and lightning). For a more detailed model description, see Collins et al. (1997), with subsequent improvements to the model described below.

2.2 Meteorological Fields and Processes

The meteorological fields used in the original version of STOCHEM are instantaneous values, available every 6 hours, taken from operational meteorological

analyses at 0.83^o latitude x 1.25^o longitude from the Meteorological Office Unified Model. In the enhanced version of STOCHEM, they are taken from the Hadley Centre climate version (Johns et al., 1997) of the Meteorological Office Unified Model. These data are provided by the global circulation model (GCM) at a resolution 3.75^o longitude $\times$ 2.5^o latitude and on 19 unevenly spaced pressure levels between the surface and 4.6 hPa. Note that this grid applies only to fields imported from the global circulation model. All other input and output data use the grid described in the preceding section.

Air parcels are advected using a Runge-Kutta fourth order method with a time-step of 3 hours. Linear interpolation from the wind grid to the parcel position is used in the horizontal and in time, and a cubic interpolation is used in the vertical direction. Random displacements are added to the parcel each time step based on locally prescribed diffusivities. The horizontal diffusivity K_H is chosen to be 1300 m^2 s^{-1} (5300 m^2 s^{-1} in the boundary layer) and the vertical diffusivity K_h is chosen to be in the range 7×10^{-3}-1×10^{-1} m^2 s^{-1}.

The model convection scheme is unchanged from the previous model version. It uses convective diagnostics from the driving GCM in the form of heights of the convective cloud bases and tops, cloud cover, and precipitation rate. These parameters are used to derive probabilities for a Lagrangian parcel to be involved in convective transport. The convective probability is given by the amount of cloud cover for clouds that are not precipitating, or by a mass flux calculated from the precipitation rate for those that are precipitating using a formula taken from Chatfield and Delany (1990). The mass flux is converted to a probability by dividing it by the mass of air beneath the cloud base. Within each grid square, each parcel below the cloud top is randomly designated (according to the above probability) as convected or not. Those that are convected have their chemical species uniformly redistributed among all the convected parcels below the cloud top within a $5^o\times5^o$ grid square. The advection, convection and mixing schemes have been validated using ^{222}Rn as a tracer (Stevenson et al., 1998). In reality, convection may be more episodic but the present representation represents the best that can be achieved with such large air parcels and grid volumes.

During the advection process the Lagrangian cells are considered to be isolated parcels of air. However in reality the air is mixed with other parcels by diffusion processes characteristic of the size of a parcel. In this model the mixing ratio of a species in a parcel c is brought closer to the average background mixing ratio $\underline{c}$ by adding a term $(c-\underline{c})d$ where d is a parameter representing the degree of exchange, taken to be 10^{-3} in the troposphere and 10^{-6} in the stratosphere. We estimate $\underline{c}$ to be the average mixing ratio of all the cells within a grid volume, which are chosen to be $5°\times5°\times\Delta h = 0.1$ as this gives an average of about one and a half cells per grid volume (more near the equator, less near the poles). The volumes are fixed to the Eulerian grid. The exchange is treated in a more theoretical manner by Walton et al. (1988).

2.3 Surface Deposition and Uptake

In the original version of the STOCHEM model, the deposition velocity v is a combination of a surface term v_d and an aerodynamic term v_a, and is given by $v = 1/([1/(v_a)]+[1/(v_d)])$. Values for v_d are species dependent and have been taken from Hough (1991), v_a is also species independent and is derived from boundary layer theory. The scheme is based on calculating a species loss flux in molecules s^{-1} given by $[S]\times v\times A$ where [S] is the concentration of species S and A is the area of the grid square. This loss is spread equally among all the parcels within the boundary layer in a similar way to the treatment of emissions. If no parcels are within the boundary layer, the loss flux is stored for one or more time-steps until an air parcel enters the boundary layer there and hence this scheme results in a specified loss flux.

The dry deposition scheme in the enhanced version of STOCHEM utilises the surface-exchange scheme from the Met Office Unified Model. A standard surface resistance approach has been employed utilising the following surface types:

- broad-leaved and needle-leaved forests
- grasslands
- shrub
- urban and desert
- water, lakes and oceans

- bare soil

- ice and snow.

The following pollutants have been treated consistently: H_2, CO, CH_4, O_3, SO_2, NO_2, HNO_3, PAN, H_2O_2, ROOH and NH_3. A two-year model run with STOCHEM coupled to both HadAM3 and MOSES 2.2 has been completed covering the years 1995 and 1996. A paper on the simulation of hydrogen levels using STOCHEM coupled to HadAM3 and MOSES 2.2 has been accepted for publication in the Journal of Atmospheric Chemistry. The main sink for hydrogen is dry deposition and so this trace gas provides a good test for the dry deposition scheme.

The new dry deposition scheme uses the well-established "big-leaf" model to calculate dry deposition velocities. Each possible deposition pathway is assigned a resistance term. These resistances are then combined in the same way as electrical resistances. The resistance terms considered are an aerodynamic term, which depends on the stability of the boundary layer, a quasi-laminar resistance which is a function of the friction velocity, and a surface resistance term. The surface resistance is itself a function of many other individual resistances, including uptake up plants (via stomata and the leaf cuticle), and absorption by the surface.

Many of the individual resistance terms above do not have constant values. For example, the uptake of many gases by soils (methane, carbon monoxide and hydrogen) will change with the soil moisture content. As the soil becomes wetter, the pores through which the gas diffuses become smaller or blocked, and hence the rate of uptake decreases. Uptake of some species by the leaf cuticle will change depending on whether the surface is dry or wet. All the necessary data (soil moisture content, stomatal conductance and canopy moisture content) are available from MOSES 2.2. All the relevant resistance terms for the species listed above are then calculated every time step and from these an overall dry deposition velocity is found.

A new coupled scheme to calculate emissions of isoprene and monoterpenes within STOCHEM has been implemented within STOCHEM using the Met Office surface exchange scheme MOSES 2.2 and model calculated photosynthetically-active radiation

and temperature. The scheme gives global emission totals in good agreement with other studies. This coupled scheme has been used to evaluate the impact of climate change on isoprene emissions and surface ozone concentrations. A paper describing these results has been submitted to Geophysical Research Letters.

An interactive scheme to predict the areas and locations of wetlands and rice paddies and their corresponding methane emissions has been developed. Simulation of present and future climate with this scheme is in hand but model simulations over the several decades required for climate timescale integrations are exceedingly computer intensive.

2.4 Wet Deposition

Soluble species are removed by wet deposition depending on the dynamic and convective precipitation rates, using altitude dependent coefficients from Penner et al. (1994). The species deposited are HNO_3, N_2O_5, SO_2, HCHO, H_2O_2, and the organic hydroperoxides (ROOH). The higher organic hydroperoxides are given the same coefficients as methyl hydroperoxide (CH_3OOH).

Convective precipitation is a sub-grid scale process, removing material efficiently over a narrow column. Our removal rate is modified by the algorithm of Walton et al. (1988) to take account of fractional precipitation area, using a fixed fraction of 0.3. At present, we remove by wet scavenging water soluble species from every air parcel equally within the square covered by the precipitation data ($3.75^{o} \times 2.5^{o}$) regardless of whether that parcel is subject to convective mixing. This means that the convective wet deposition is not completely coupled to the convective transport scheme.

2.5 Stratospheric sources of ozone and NO_y

The upper boundary of our model is set at ~ 100 hPa and hence we do not include stratospheric ozone production. To allow for this, 6-hourly vertical wind fields are used to calculate an ozone flux across the ~ 100 hPa surface on a $5^{\circ} \times 5^{\circ}$ grid using monthly ozone fields from Li and Shine (1995). Using this parameterisation, a stratospheric source of ozone is injected into the upper model layer. When integrated over one year with the particular meteorological diagnostics used in this study, the

total annual injection amounted to 375 Tg yr^{-1}. No account is taken of any loss of any species due to upward transport into the stratosphere. In the upper troposphere, this stratospheric source dominates during spring in mid-latitudes but other ozone sources dominate during other seasons and in the tropics.

A stratospheric source of NO_y is also included in STOCHEM. This source is scaled directly to the stratospheric ozone source, on a point-by-point basis, and is set, based on the work of Murphy and Fahey (1994), as one thousandth of the ozone flux by mass (as N) and is emitted into the model as HNO_3.

2.6 Chemistry

The main additions to the chemistry since Collins et al. (1997) have been propane and acetone chemistry, organic hydroperoxide formation, dimethyl sulphide oxidation, and aqueous phase SO_2 oxidation. The last two have only small effects on ozone levels (mostly due to the aqueous $H_2O_2+SO_2$ reaction) and will not be discussed further. Of the new species that have been added, those of most importance to this study are HO_2NO_2, C_3H_8, $C_3H_7O_2$, CH_3COCH_3, $CH_3COCH_3O_2$, C_2H_5OOH, C_3H_7OOH, $secC_4H_9OOH$, HOC_5H_8OOH, and MVKOOH. Altogether, 7 additional photochemical and 27 thermal reactions have been added to the model chemistry.

STOCHEM contains a description of the heterogeneous reactions of HNO_3 and N_2O_5 on aerosols. It does not, however, include any treatment of the heterogeneous reactions occurring on cirrus clouds which may deplete NO_x concentrations near the tropopause (Borrmann et al. 1996) nor of the reactions leading to springtime ozone destruction at the polar sunrise (Barrie et al. 1988).

2.7 The Treatment of Emissions

Emissions into the model are implemented as an additional term in the production flux for each species during each integration time-step, exactly as in the Collins et al. (1997) study. The emissions used are listed in Table 2.1. The man-made, biomass burning, vegetation, soil, oceans and 'other' are all surface sources based on two-dimensional (latitude, longitude) source maps. The aircraft and lightning NO_x

TABLE 2.1. Emissions in Tg yr^{-1} employed in the original version of STOCHEM.

species	industrial	biomass burning	vegetation	soil	oceans	aircraft	lightning	other[b]
NO_x	31.7	7.1		5.6		0.5	7.0[f]	
SO_2	71.2	1.4						
H_2	20.0	20.0		5.0	5.0			
CO	650.0	700.0	150.0		50.0			
CH_4	155.0	40.0			10.0			260.0
C_2H_4	12.3	7.7	10.0		1.9			
C_2H_6	7.0	3.6	3.5		1.0			
C_3H_6	19.9	10.9	10.0		1.6			
C_3H_8	13.1	1.1	5.0		1.3			
C_4H_{10}	91.4	1.7	3.0					
C_5H_8			249.3					
C_8H_{10}	17.6	1.2						
C_7H_8	18.7	7.2						
H_2CO	1.2	0.6						
CH_3CHO	2.5	3.2						
CH_3OH	7.6	4.3						
Acetone[c]	4.5	0.4	18.8					
DMS					15.0			
NH_3	39.3	3.5		2.4	8.2			

Notes:
[a]emissions are in Tg yr^{-1} except for NO_x which are in Tg N yr^{-1} and sulphur compounds which are in Tg S yr^{-1}.
[b]includes paddies, tundra, wetlands, termites and animals.
[c]acetone source from vegetation represents production from terpene oxidation.
[d]emission totals and their spatial distributions were based on entries in the EDGAR database (Olivier et al. 1996).
[e]aircraft NO_x emissions for 1992 were taken from IPCC (1999).
[f]Emissions calculated interactively. Exact value could be ± 1 Tg N about this mean value.

TABLE 2.2. Emissions in Tg yr^{-1} employed in the enhanced version of STOCHEM for 1990.

Species	Ind	BioBrn	Veg	Soil	Ocean	Aircraft	Lning	Other
$NO_x{}^a$	22.8	7.1		5.6		0.5	7.0^b	
$SO_2{}^c$	70.9	2.2						
H_2	20.0	20		4.0	4.0			
CO	393.0	500.0	150.0		50.0			
CH_4	282.0	55.0			13.0			266.0^d
C_2H_4	6.8	8.4	20.0					
C_2H_6	6.0	4.4	3.5					
C_3H_6	9.3	9.5	20.0					
C_3H_8	6.2	1.1	3.5					
C_4H_{10}	53.7	2.6	8.0					
C_5H_8			560^e					
C_8H_{10}	9.01	0.46						
C_7H_8	8.93	2.27						
HCHO	1.4	1.5						
CH_3CHO	3.0	4.8						
CH_3OH	7.1	8.8						
Acetone	2.5	0.7	20.0					
DMS^c				1.0	15.0			
$NH_3{}^{a,f}$	39.4	3.5		2.5	8.2			

Notes:
^{a}Emissions are Tg N yr^{-1}.
^{b}Emissions calculated interactively. Exact value could be ± 1 Tg N about this mean value.
^{c}Emissions are Tg S yr^{-1}.
^{d}Emission includes termites, wetlands and rice paddies. Wetland and rice paddy emissions calculated interactively and are 239 ± 33 Tg yr^{-1}.
^{e}Emission calculated interactively. Exact value could be ± 40 Tg about this mean value.
^{f}Emission magnitudes from EDGAR V2.0, as are not specified in SRES A2 scenarios.

sources are three-dimensional. The man-made, paddy, tundra, wetland and 'other animal' methane sources (see Table 2.1 and 2.2) are held constant throughout the year at the yearly average value. Work is in hand to treat the time-dependence and climate sensitivity of these sources using the Met Office surface exchange scheme MOSES 2.2. The other sources vary by calendar month. After each advection timestep the surface emissions for a grid square are distributed equally over all the Lagrangian cells that are within the boundary layer in that grid square. If there are no cells within the boundary layer for a particular emissions grid square then those emissions are stored until a cell does pass through.

The emissions in the enhanced version of STOCHEM have been updated and the corresponding global emission totals are given in Table 2.2, for comparison purposes.

2.8 Parallelisation

The original version of the STOCHEM model was initially developed to run on a single processor DEC Alpha workstation and later on a desk-top pc system. To utilise the advantages of running a code on a massively parallel CRAY T3E computer, each processor needs to compute a fraction of the calculations and hold a fraction of the data. The enhanced version of STOCHEM has been split by geographical region. For optimum efficiency each processor has been assigned a similar number of Lagrangian parcels rather than Eulerian grid points. This means that the geographic regions need to be of equal area. We achieved this by splitting the model domain into a small number of latitude bands, which are divided longitudinally into varying numbers of columns so that each region covers approximately the same surface area. Parcels are allowed to move freely between all the regions. If parcels move out of the geographical region for a particular processor after advection, they are swapped to their new processor, passing over all the information on parcel position and species concentrations.

The geographical division of parcels gives roughly, but not exactly, equal numbers of cells on each processor. Since most of the computational load is in the chemistry integration, it is essential to balance the load between processors as evenly as possible for this routine. This is done by swapping extra parcels on processors responsible for

more than the average number of parcels onto those responsible for less than the average. After the chemical integration, the parcels have to be swapped back to their original processors (geographically allocated). The other routines need the parcels to be grouped geographically and are not so computationally expensive.

2.9 Comparison of Model Results with Observations

The advection, convection and mixing schemes have been validated using ^{222}Rn as a tracer (Stevenson et al., 1998) and careful comparisons made using an Eulerian tracer advection scheme. Although the Lagrangian schemes adopted produce inert tracer fields that agree well with observations, in reality, convection may well be more episodic. The present schemes represent the best that can be achieved with such large air parcels and grid volumes.

We have participated in a number of global 3-D chemistry-transport model intercomparisons to establish the level of STOCHEM model performance. These include intercomparisons of fast photochemistry (Olson et al. 1997), ozone (Kanakidou et al. 1998), carbon monoxide (Kanakidou et al., 1999) and of past, present and future tropospheric ozone distributions (Gauss et al. 2003). In all of these intercomparisons, STOCHEM performs within the range of current models. However, in common with all other complex models, it is sometimes difficult to reconcile good model performance with one species in one location with poor model performance elsewhere or with other species. In this study which focusses on tropospheric ozone sources and sinks, ozone budgets are crucial and their intercomparison with other model budgets is discussed separately and in more detail below.

In previous work, Collins et al. (1997) have described comparisons of model results with observations for global mean OH concentrations, surface ozone concentrations for the Atlantic Ocean cruises of Winkler (1988), surface ozone concentrations at 16 remote background sites from Oltmans and Levy (1994) and others, ozonesondes for 8 sites during summer and winter from Komhyr et al. (1989) and 14 sets of NO_x measurements throughout the troposphere. From these comparisons it was concluded that the model was well able to provide a good approximation to the main controlling processes for OH, NO_x and ozone in both the winter and the summer and that the

model ozone distribution contains all the most important features of the observed distribution.
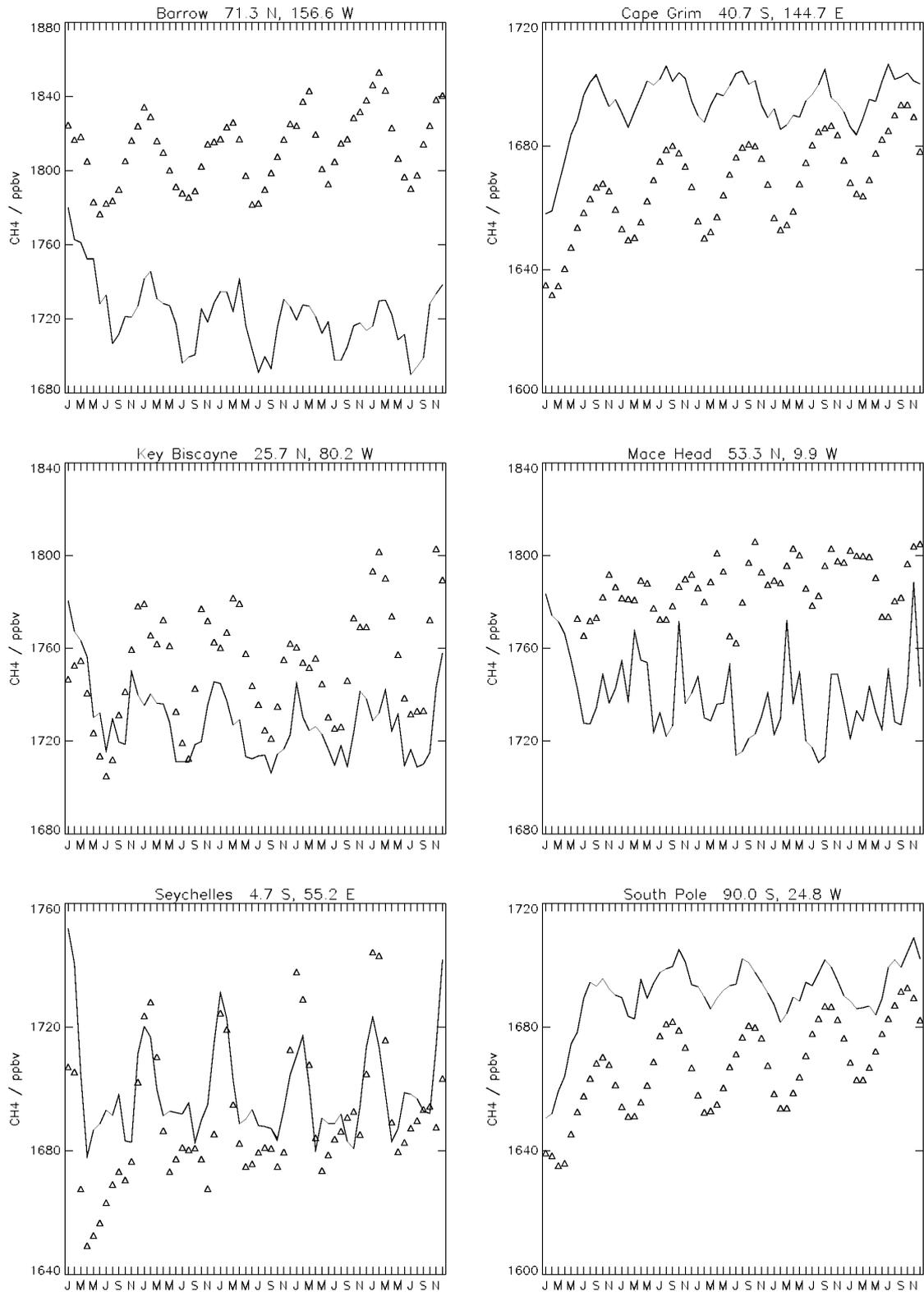

Figure 2.1. Comparison of measured surface methane concentrations (triangles) from the NOAA/CMDL network with modelled concentrations from STOCHEM (lines).
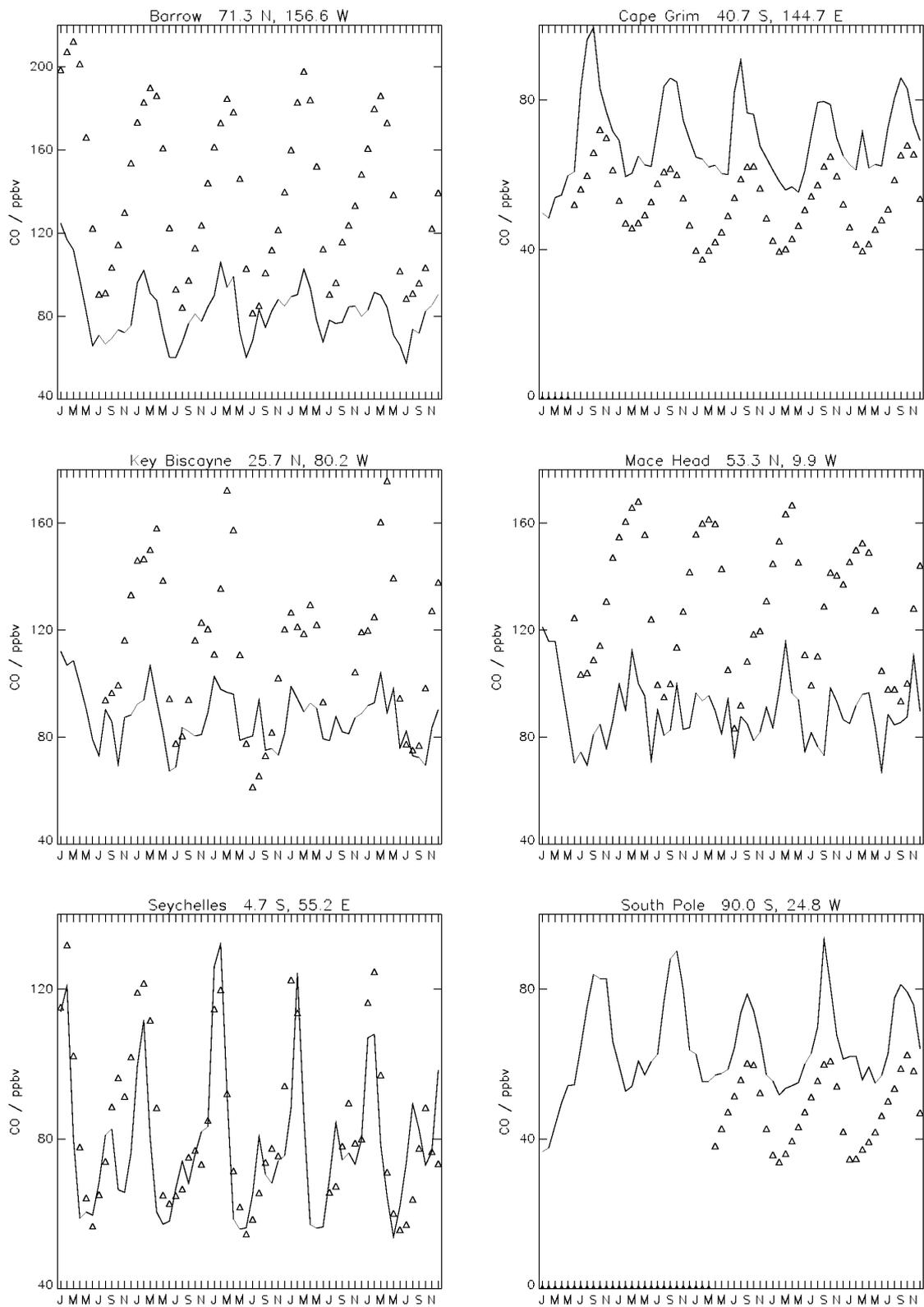
Figure 2.2. Comparison of measured surface carbon monoxide concentrations
(triangles) from the NOAA/CMDL network with modelled concentrations from
STOCHEM (lines).
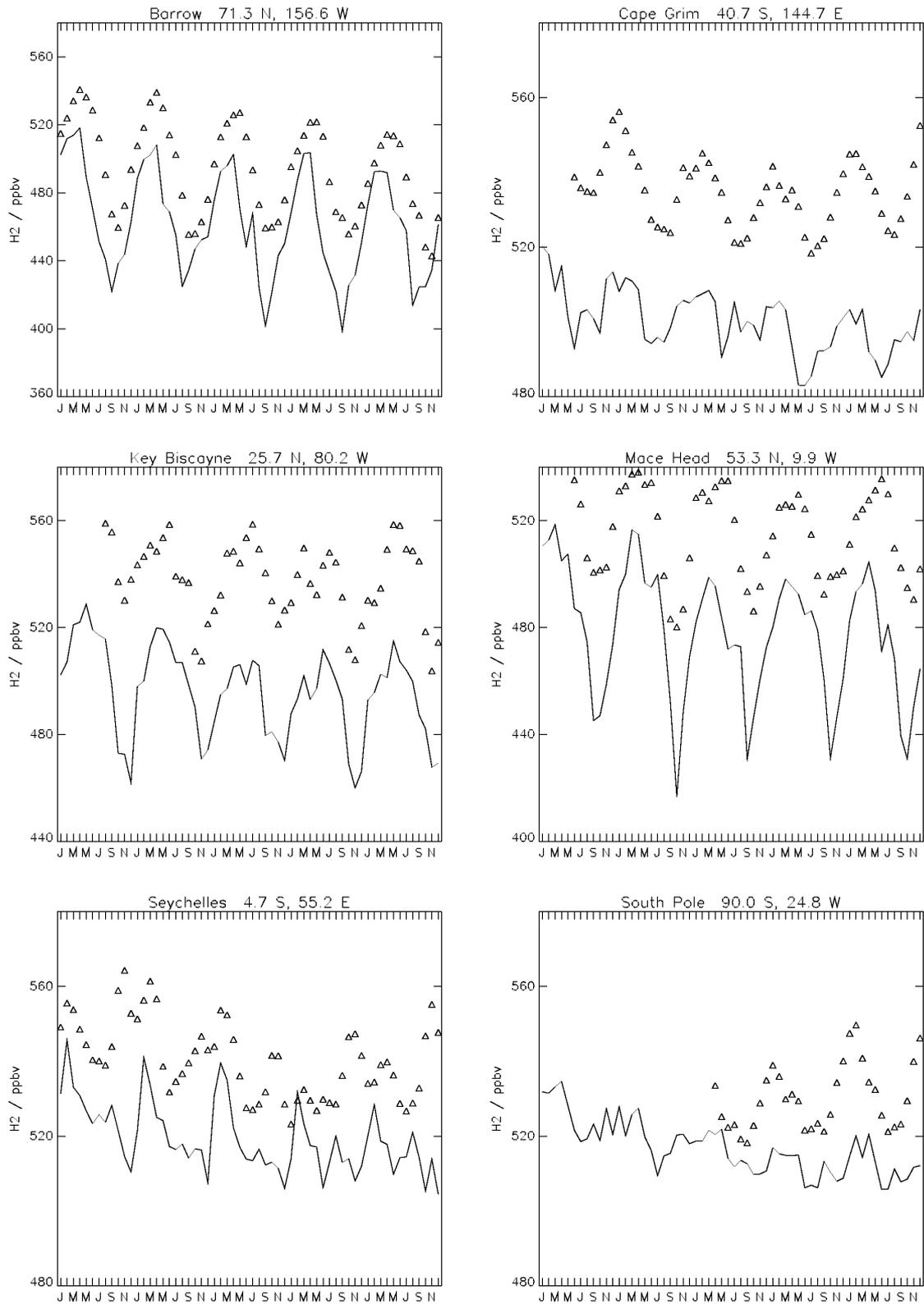
Figure 2.3. Comparison of measured surface hydrogen concentrations (triangles) from the NOAA/CMDL network with modelled concentrations from STOCHEM (lines).

26

Collins et al. (1999) presented comparisons between the model results and observations for hydrogen peroxide, formaldehyde, methyl hydroperoxide and acetone, all potentially important free radical sources in the troposphere. Furthermore, the methane lifetime due to OH removal was found to be 9.0 years, in agreement with the atmospheric lifetime of 8.4 years assessed by IPCC (2001).

Comparison of 5-years of enhanced STOCHEM integration with observations:
Six sites from the NOAA/CMDL monitoring network have been selected, giving a good spread of latitudes. This network measures a number of different trace gases. Measurements of methane, carbon monoxide and hydrogen are compared with the STOCHEM predictions. The comparison focusses on three different features - the absolute concentrations of the trace gases, the amplitude of the seasonal variation, and the phase of the variation. Five years worth of data are shown to illustrate the interannual variability in both the observed and modelled gas concentrations. It should be noted that these simulations were performed using STOCHEM coupled to the UM. The meteorology driving the transport is therefore not "real" (in the sense that, for example, the ECMWF ERA-40 winds are "real" as they are based on assimilations of satellite data). The model may not predict the exact features seen in the observations, but should reproduce the main features.

The methane comparisons, see Figure 2.1, show that the model is reproducing the amplitude and phase of the seasonal variations accurately, except at Mace Head, where the model does not simulate the observed values well at all.. At this latter location, the model results are very noisy, as are the measurements. At Barrow, Cape Grim and the South Pole the model does not reproduce the absolute concentrations very well. This problem is due to the initial methane concentrations which are not fully consistent either with the observations or with the emission fields that would generate them. In the southern hemisphere, the model reproduces the amplitude and phase of the observed carbon monoxide concentrations quite well, see Figure 2.2, but overestimates the absolute values. The observations at the Seychelles are particularly well reproduced. However, the absolute values at Barrow, Mace Head and Key Biscayne are fairly well reproduced, but the model underpredicts the magnitude of the seasonal variation.
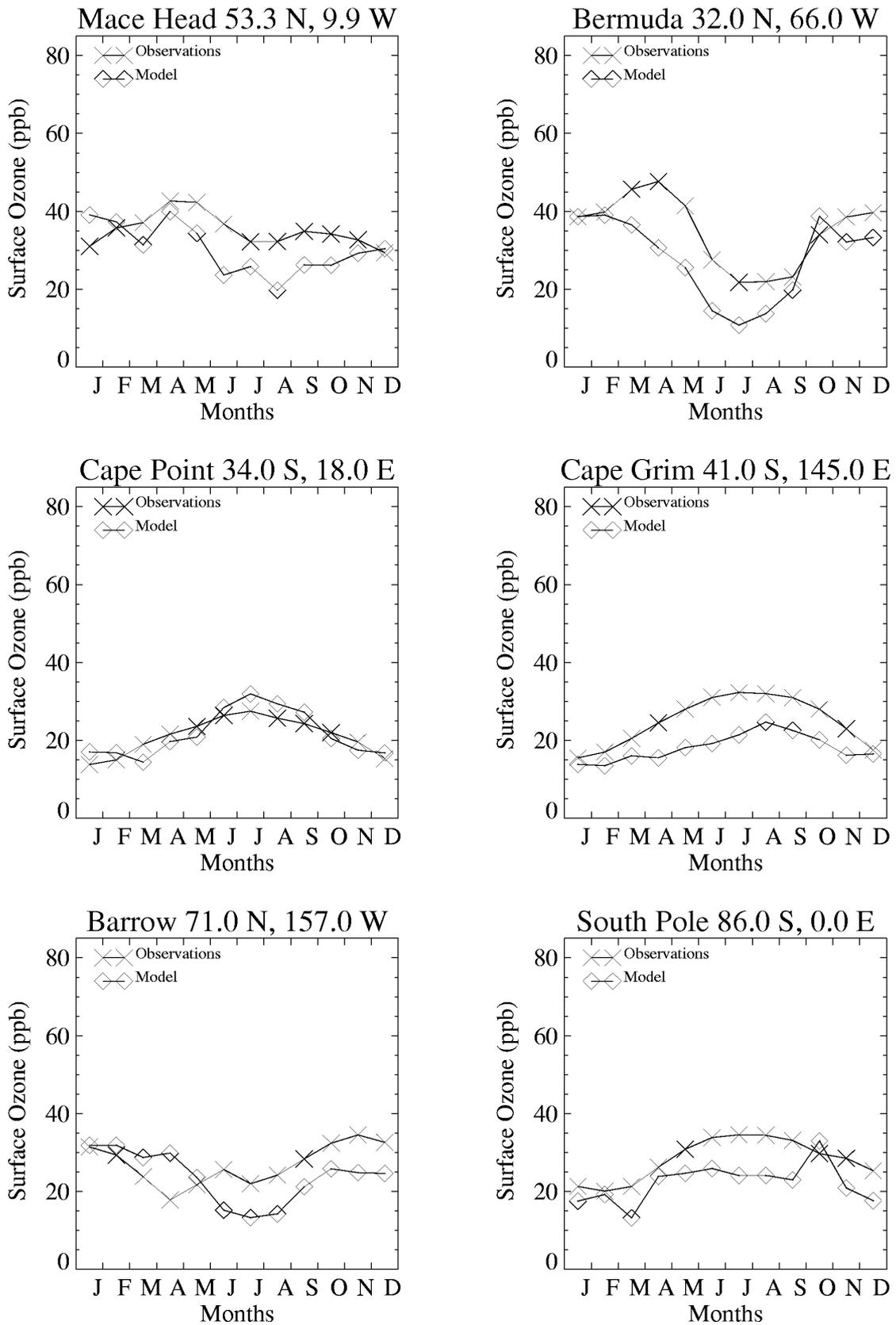
Figure 2.4. Comparison of measured monthly mean surface ozone levels with monthly mean predictions from the lowest layer of STOCHEM.

The model reproduces the phase of the observed hydrogen levels quite well, see Figure 2.3, except at the South Pole and the Seychelles, and tends to slightly over-estimate the amplitude of the seasonal cycle. The model also reproduces the downward trend in the hydrogen concentrations at Barrow, Cape Grim and the Seychelles.

Some comparisons of the modelled ozone levels with surface ozone measurements are shown in Figure 2.4. It should be noted that these ozone data have been compiled from several different sources. The model reproduces the correct levels and seasonal cycle in most places, but does not capture all of the observed features. At Bermuda and Barrow, the modelled seasonal cycle is out of phase with the measurements by 1-2 months and 2-3 months respectively. At the other locations, the model captures the correct levels and seasonal cycles.

The modelled vertical ozone profiles are shown in Figure 2.5 for three seasons, spring (MAM), summer (JJA) and autumn (SON). No observational data are available for the winter months. The model generally reproduces the observed profiles very well, capturing the shape and absolute ozone concentrations. However, the model underestimates the ozone concentrations in the upper troposphere at some locations (Hohenpeissenberg, Wallops Island and Brazzaville) which could be due to either chemical losses or too rapid transport of air downwards from this region. The model also tends to underestimate the ozone levels in the lower atmosphere in some marine locations (e.g. Forster).
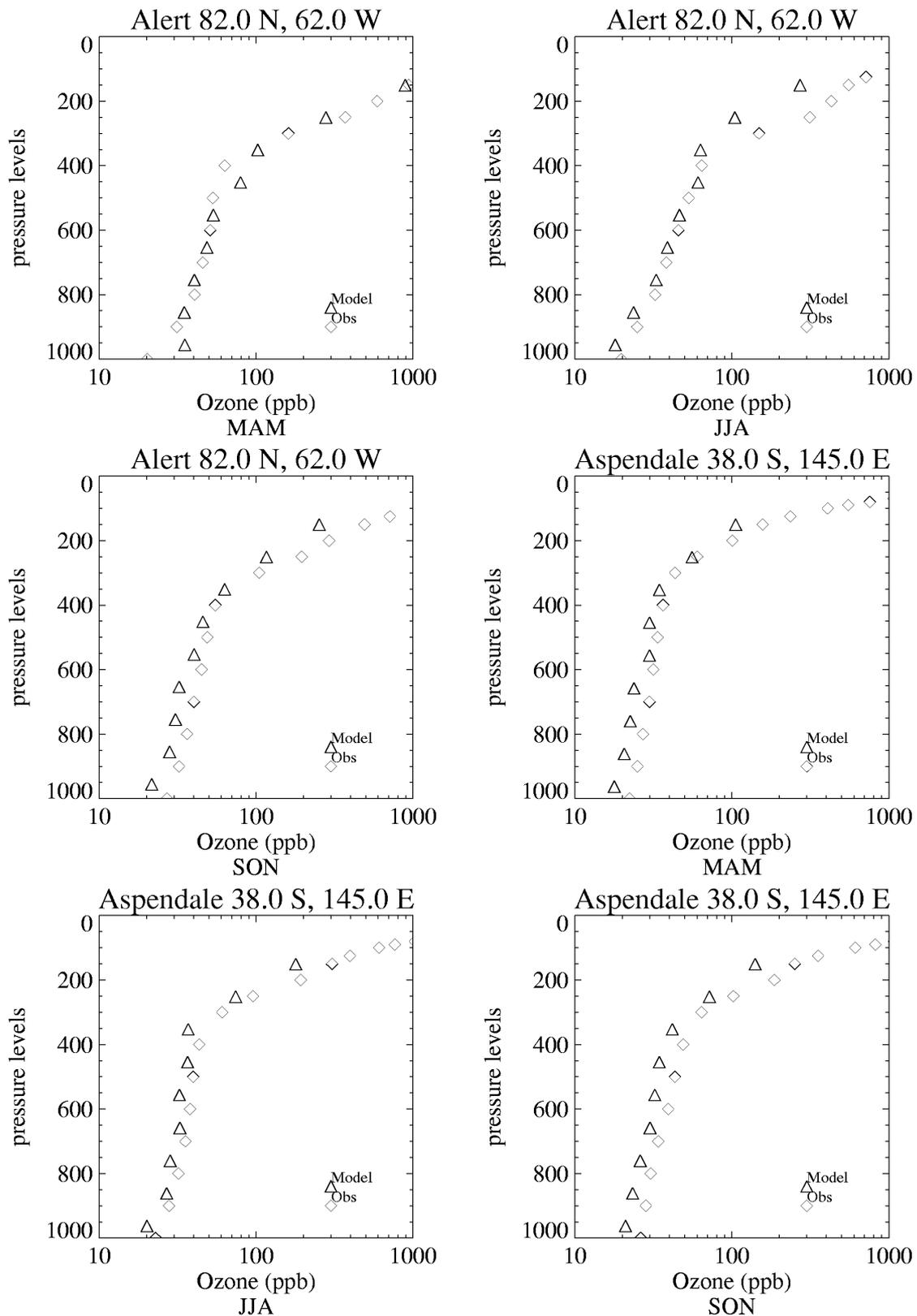
Figure 2.5. Comparison of modelled and measured vertical ozone profiles for three seasons at six different locations. Note that the ozone concentration scale is logarithmic.
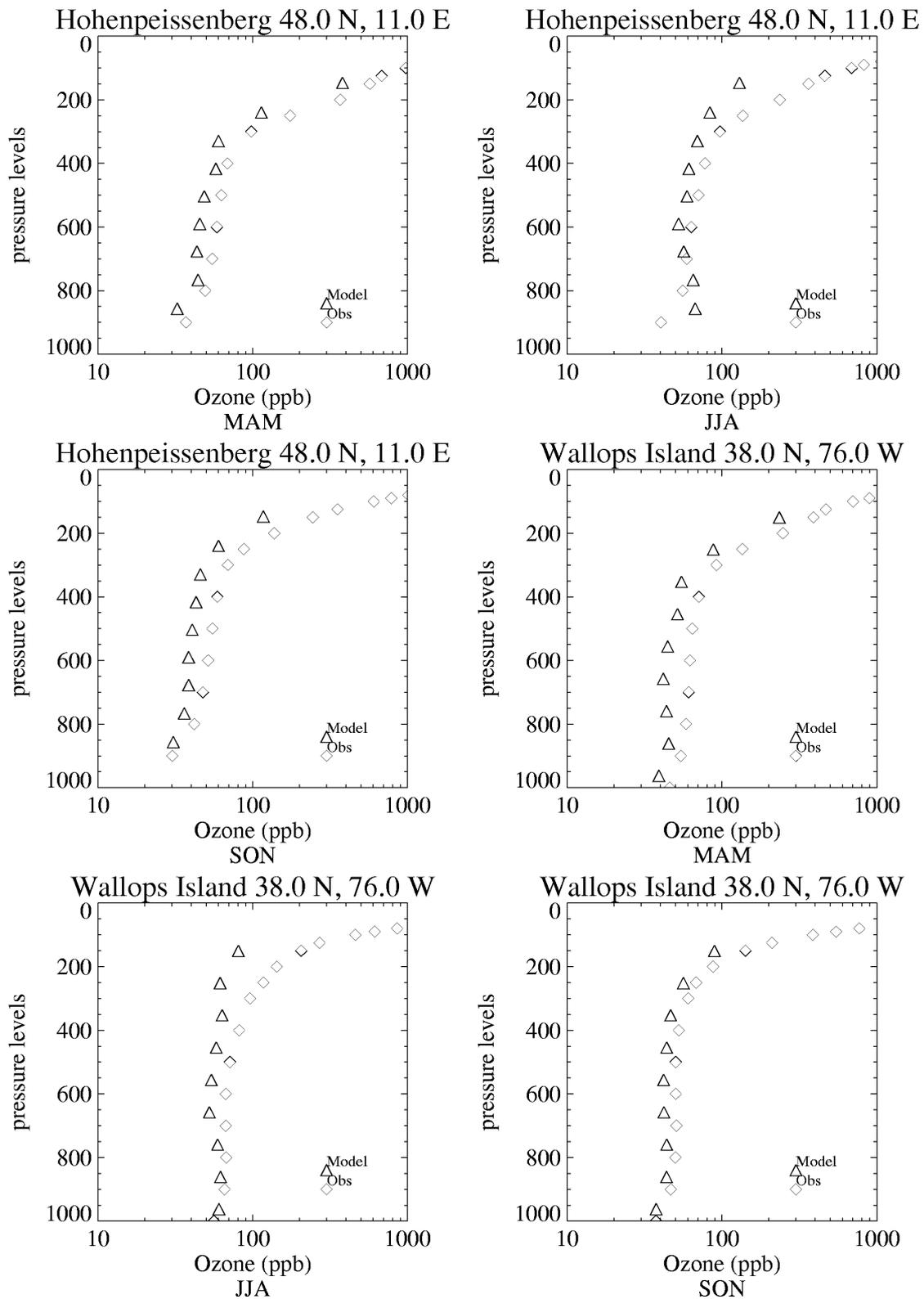
Figure 2.5. (Cont). Comparison of modelled and measured vertical ozone profiles for three seasons at six different locations. Note that the ozone concentration scale is logarithmic.
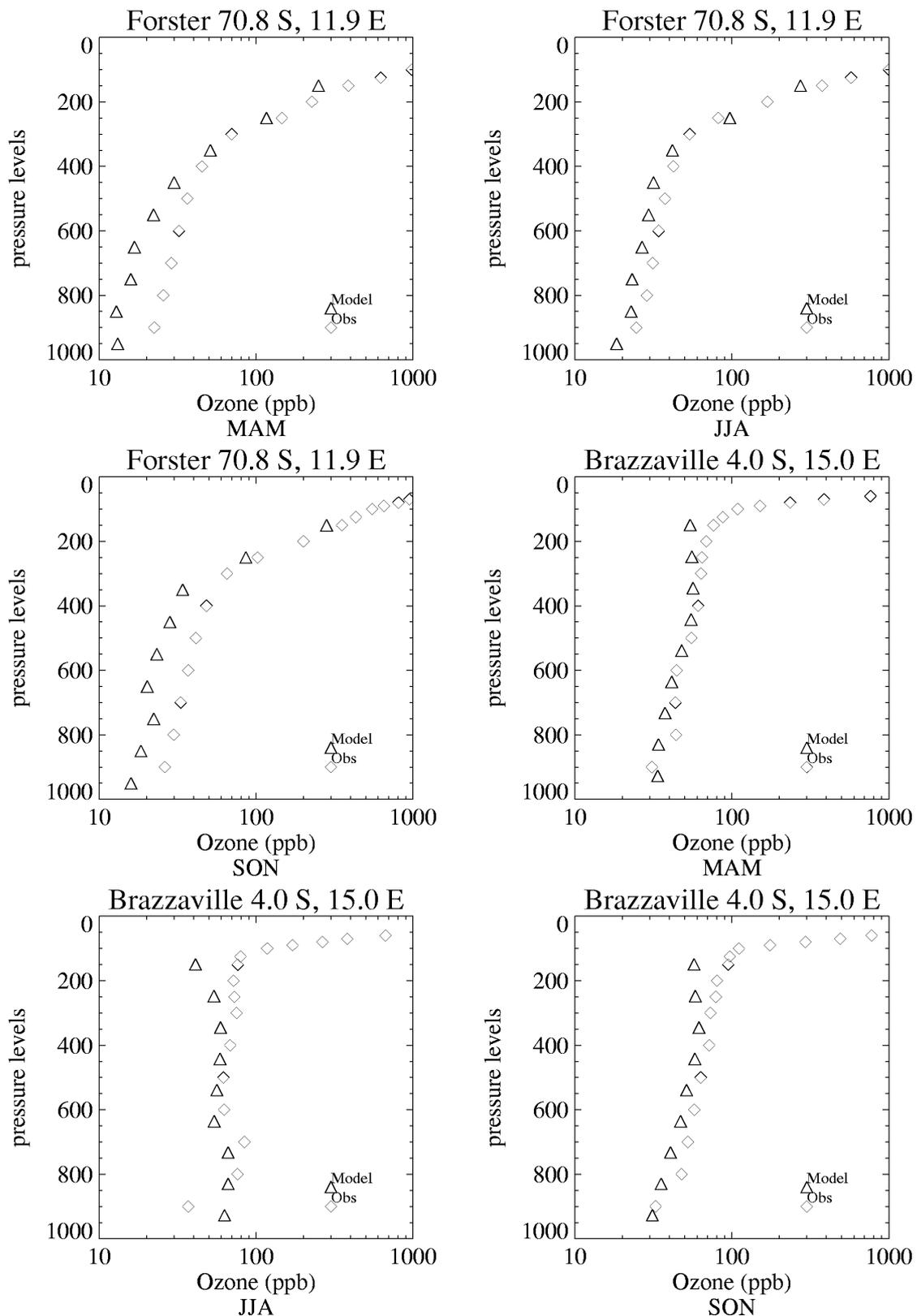
Figure 2.5. (Cont). Comparison of modelled and measured vertical ozone profiles for three seasons at six different locations. Note that the ozone concentration scale is logarithmic.

3. The Global and Regional Deposition of Acidifying and Eutrophying Species

3.1 Introduction

This chapter describes the effects of reducing anthropogenic NO_x and CO emissions on sulphur and nitrogen chemistry. The focus is on the dry and wet deposition of sulphur and nitrogen containing compounds, and how these fluxes are changed by the emission reductions.

One important route by which SO_2 is oxidised to sulphate occurs via reaction with hydrogen peroxide, H_2O_2. This reaction occurs in the aqueous phase, as shown below.

$$SO_2 + H_2O_{(l)} \rightarrow HSO_3^-{}_{(aq)} + H^+{}_{(aq)} \hspace{2cm} \text{(Reaction 1)}$$
$$HSO_3^-{}_{(aq)} + H_2O_{2(aq)} \rightarrow SO_4^{2-}{}_{(aq)} + H_2O_{(l)} + H^+{}_{(aq)} \hspace{1cm} \text{(Reaction 2)}$$

SO_2 dissolves in cloud water droplets, and forms the bisulphite anion (HSO_3^-). This species may then be oxidised by H_2O_2 to form a sulphate anion. Hydrogen peroxide is formed from the self-reaction of HO_2 radicals,

$$HO_2 + HO_2 \rightarrow H_2O_2 + O_2 \hspace{2cm} \text{(Reaction 3)}$$

Another major sink for HO_2 radicals is reaction with nitric oxide, NO:

$$HO_2 + NO \rightarrow OH + NO_2 \hspace{2cm} \text{(Reaction 4)}$$

NO_x emissions are almost exclusively NO. Hence, if the NO emissions are reduced, the amount of HO_2 converted to OH via reaction (Reaction 4) will be reduced, and more hydrogen peroxide can be produced via reaction (Reaction 3), in turn oxidising more SO_2 to sulphate (reactions (Reaction 1) and (Reaction 2)).

Carbon monoxide, CO, reacts exclusively with the OH radical to form carbon dioxide and a HO_2 radical,

$$\text{OH} + \text{CO} \xrightarrow{\text{fast}} \text{CO}_2 + \text{H} \ (+ \text{O}_2) \rightarrow \text{HO}_2 \qquad \text{(Reaction 5)}$$
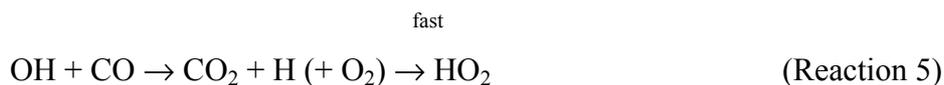
Hence, the OH radical has been converted to a HO_2 radical. Reducing the CO emission will therefore decrease the rate at which OH is converted to HO_2, and the production of hydrogen peroxide via reaction (Reaction 3). It may therefore be expected that the rate of formation of sulphate will be reduced, and so the deposition of SO_2 will increase and the deposition of sulphate will decrease. However, there is also a competing effect. SO_2 reacts directly with the OH radical in the gas phase, eventually forming sulphuric acid aerosols,

$$\text{OH} + \text{SO}_2 \rightarrow \text{HOSO}_2 \qquad \text{(Reaction 6)}$$

$$\text{HOSO}_2 + \text{O}_2 \rightarrow \text{HO}_2 + \text{SO}_3 \qquad \text{(Reaction 7)}$$

$$\text{SO}_3 + \text{H}_2\text{O} \rightarrow \text{H}_2\text{SO}_{4 \ (aq)} \qquad \text{(Reaction 8)}$$
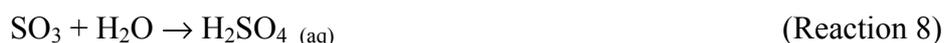
Reducing the amount of CO emitted means that more OH will be present, as the rate of reaction (Reaction 5) will be reduced. Hence, the conversion of SO_2 to sulphuric acid aerosols via reactions (Reaction 6) to (Reaction 8) will be increased, and so the deposition of SO_2 will fall, compensated by a rise in the deposition of sulphate. It is not clear what the exact effect of reducing the CO emissions will be.

Model Integrations:

Three model integrations were run for 13 months (December 1994 to December 1995), and results from the last 12 months were used in the analysis.

- Control Run: The control run for this study used emissions from the SRES A2 scenario.
- Case Study A: 50 % less NO_x. Reducing NO_x emissions will clearly change the oxidised nitrogen deposition fluxes. However, as nitrogen oxides are fundamental species in atmospheric chemistry, affecting production and loss of ozone which in turn controls OH levels. Reducing NO_x emissions may therefore indirectly affect the sulphur chemistry and the loss fluxes.

- Case Study B: 50% less CO. CO is involved in the conversion of OH radicals to HO_2. A reduction in the CO emission may therefore affect the $OH:HO_2$ ratio, which in turn will affect the chemistry. HO_2 radicals self-react to form hydrogen peroxide (H_2O_2) which oxidises SO_2 to sulphate anions in the aqueous phase.

3.2 Results for the sulphur-containing compounds

Maps showing the annual dry and wet deposition fluxes of sulphur compounds, oxidised nitrogen species (NO_y) and reduced nitrogen compounds (NH_x) from the control run are shown in Figures 3.1 to 3.3 respectively. Figures 3.1(a) and 3.1(b) show the dry and wet deposition fluxes of sulphur dioxide. Both of these fluxes have maxima located at the major source regions, which are Europe, North America, and China. The wet deposition flux has minima in regions with little or no rainfall, such as the Sahara and the oceans west of South America and Africa. A similar pattern is seen for the deposition fluxes of sulphuric acid aerosols (Figures 3.1(c) and 3.1(d)). These aerosols are formed from the oxidation of SO_2, and so their deposition patterns should be similar to those of SO_2.

The deposition patterns of ammonium sulphate are shown in Figures 3.1(e) and 3.1(f). The dry deposition flux of ammonium sulphate is similar to that for SO_2 and sulphuric acid aerosols, with maxima over Europe, China, and North America. The wet deposition flux has maxima in these regions, but also additional maxima over parts of South America and Africa. Ammonia is emitted from agricultural practices in these regions, and hence additional ammonium sulphate is formed and deposited there.

The final sulphur species considered in STOCHEM is methylsulphonic acid, MSA. This species is formed from the degradation of dimethyl sulphide (DMS), which in turn is principally emitted from the oceans. Hence, the dry and wet deposition patterns of MSA shown in Figures 1(g) and 1(h) are very different. The magnitudes of the fluxes are much smaller, as MSA is only present in low concentrations. The dry deposition fluxes are smaller than the wet deposition fluxes, because MSA is very soluble. The dry deposition fluxes over land are slightly greater than those over the sea, as the boundary layer over land will be less stable. The wet deposition fluxes have small maxima where strong convective activity and rainfall occur, in the
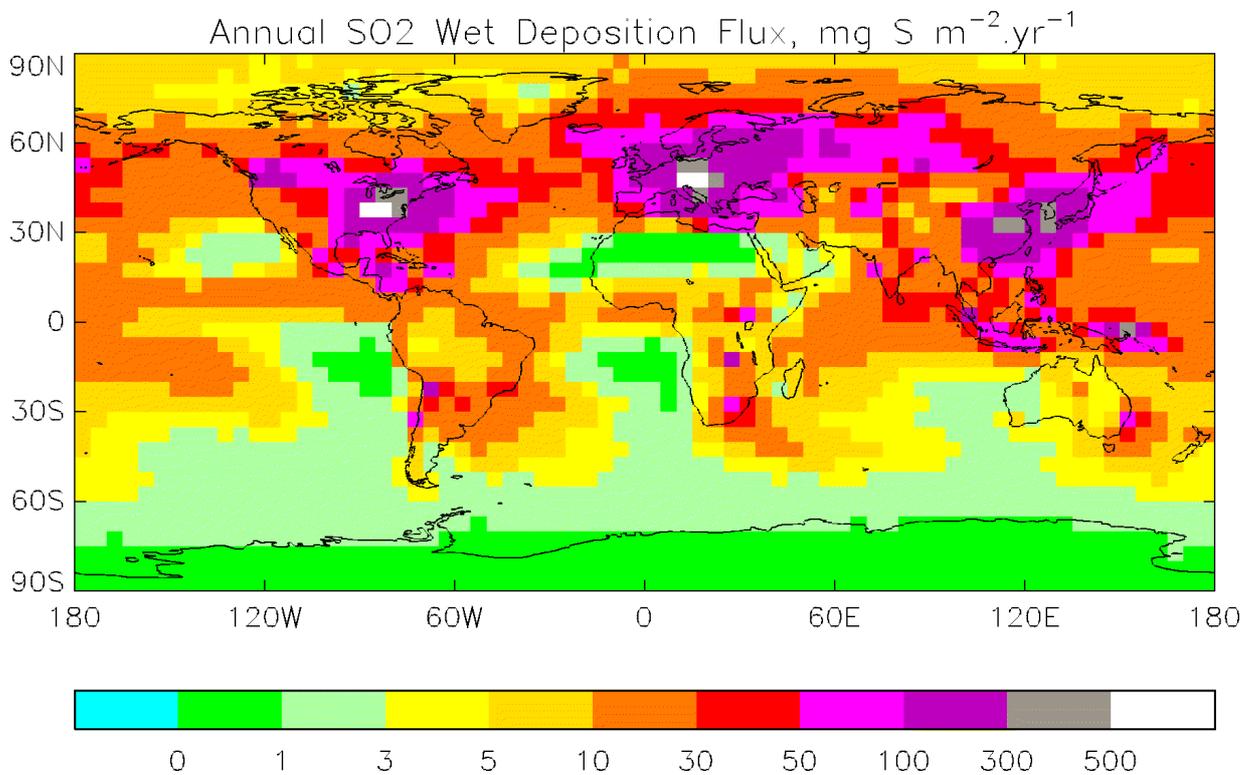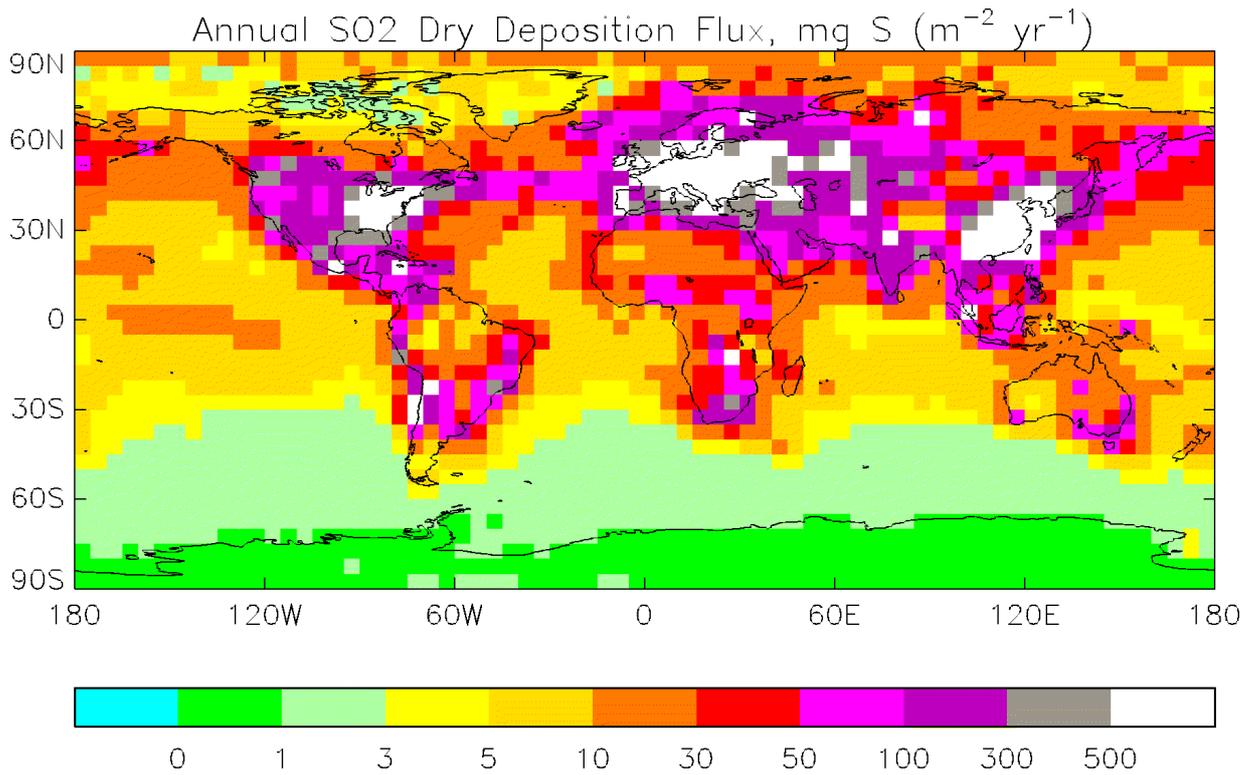
Figure 3.1. Annual deposition fluxes of SO₂. (a) Dry deposition flux (top panel), and
(b) wet deposition flux (lower panel).
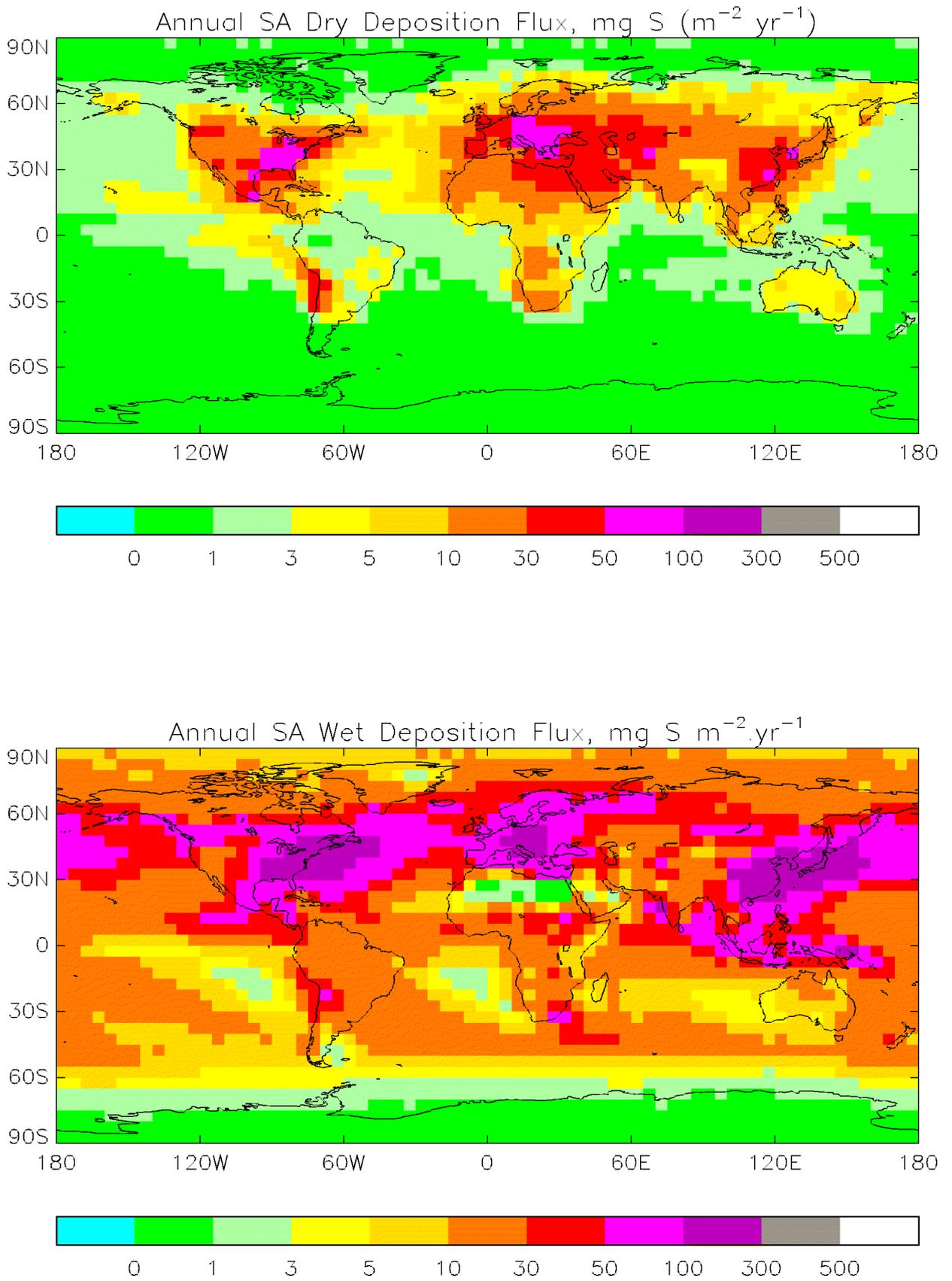
Figure 3.1 (cont.) Annual deposition fluxes of sulphuric acid aerosols. (c) Dry
deposition flux (top panel); (d) wet deposition flux (lower panel).
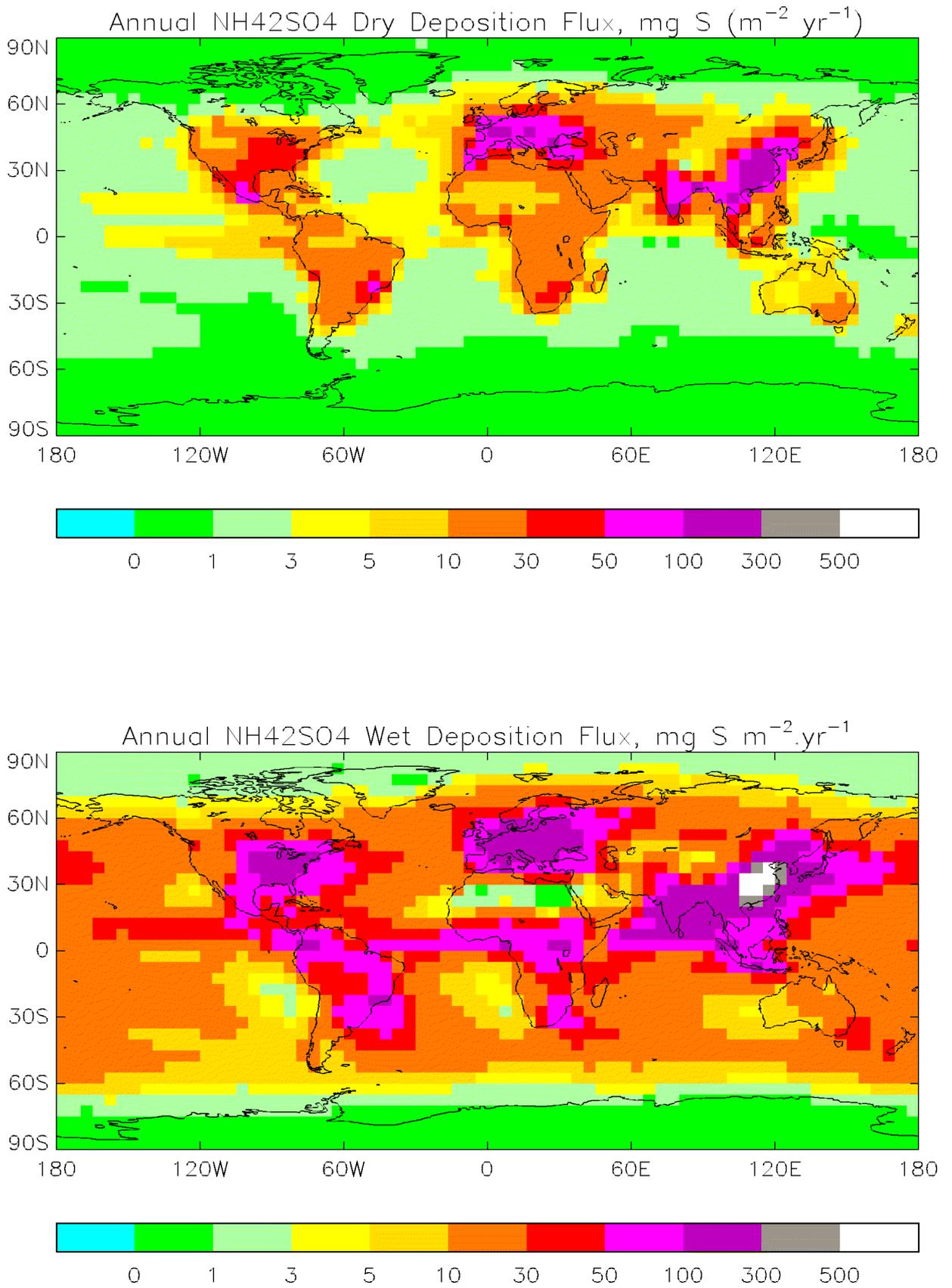
Figure 3.1 (cont.) Ammonium sulphate deposition fluxes. (e) Dry deposition flux (top panel). (f) Wet deposition flux (lower panel).
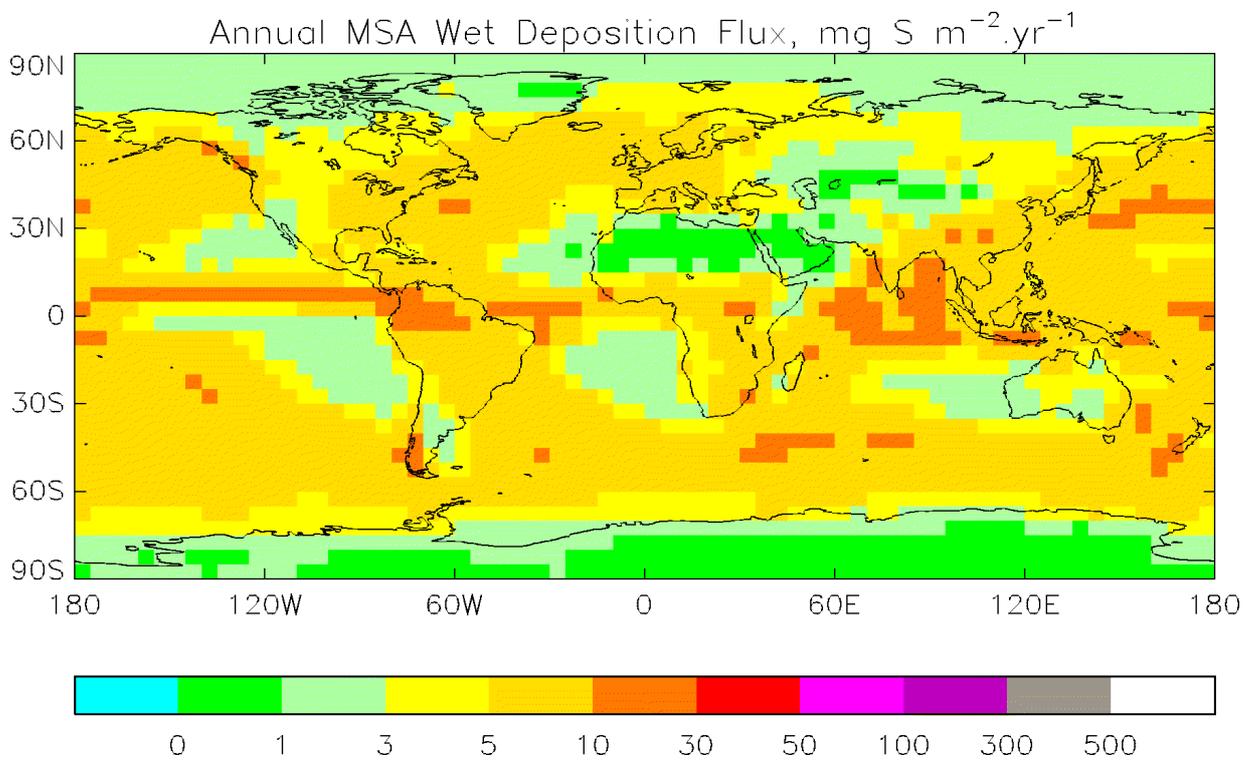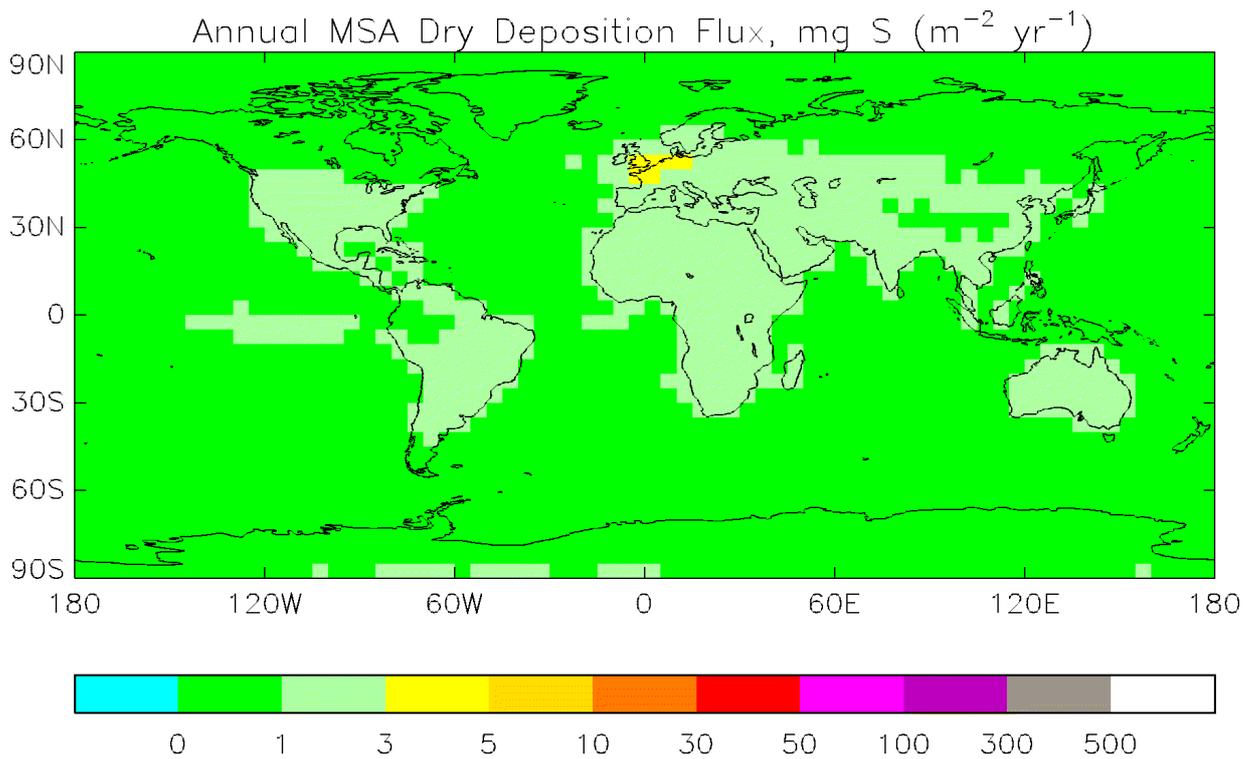
Figure 3.1 (cont.). Annual deposition fluxes of methylsulphonic acid (MSA). (g) Dry deposition flux (top panel). (h) Wet deposition flux (lower panel).

intertropical convergence zone (over the mid Atlantic and Pacifc), and the Indian Ocean.

3.3 Results for the oxidised nitrogen compounds (NOy)

The dry and wet deposition fluxes of NO_y species are shown in Figure 3.2. The dry deposition fluxes of NO_2 and peroxyacetyl nitrate (PAN) are shown in Figures 3.2(a) and 3.2(b) respectively. It is clear that the fluxes are much greater over land than the oceans. Both NO_2 and PAN are very insoluble in water, and wet deposition of these species is not considered in STOCHEM.

NO_2 is not emitted directly, but is mainly formed from the oxidation of NO. The maxima in the NO_2 dry deposition fluxes occur in the same areas as the NO sources, which are combustion of fossil fuels and biomass burning. Soils also emit NO naturally, and this emission is enhanced by fertilizer use. Hence, maxima in the NO_2 dry deposition fluxes occur in Europe, North America and China owing to combustion, the patterns over land being similar to those for SO_2 (see figure 1(a)). However, maxima are also seen over much of Africa and parts of South America. The lifetime of NO_2 is about 2.6 days with the major loss process being conversion to PAN and HNO_3.

Nitric acid, HNO_3, readily dry deposits to all surfaces, and is easily removed by rainwater owing to its high solubility. The lifetime of HNO_3 is therefore very short, about 1.1 days. The only chemical source of nitric acid is from the reaction of OH radicals with NO_2. Hence, the dry deposition of nitric acid over land closely resembles the pattern for NO_2 dry deposition (compare Figures 3.2(a) and 3.2(c)). Extra deposition of HNO_3 occurs over oceans where it is transported from the land. The wet deposition fluxes (Figure 3.2(d)) have a similar pattern to the dry deposition fluxes, owing to the short lifetime of HNO_3. Additional deposition over the oceans can be seen again. Transport of HNO_3 from the continents is also in evidence from this figure. Enhanced fluxes are visible over the north Atlantic, which shows transport of HNO_3 from North America. There is also an enhanced wet deposition flux over northern Asia, owing to transport from Europe. A similar plume can be seen extending from East Asia over the Pacific.
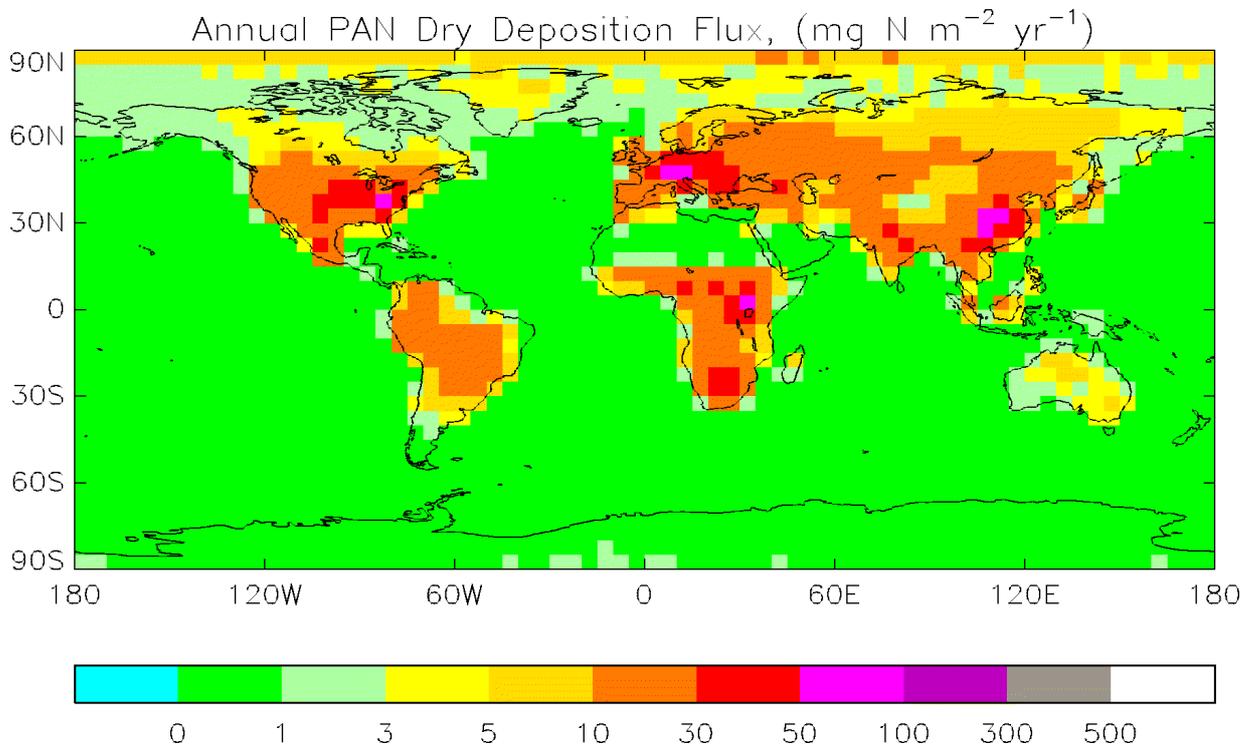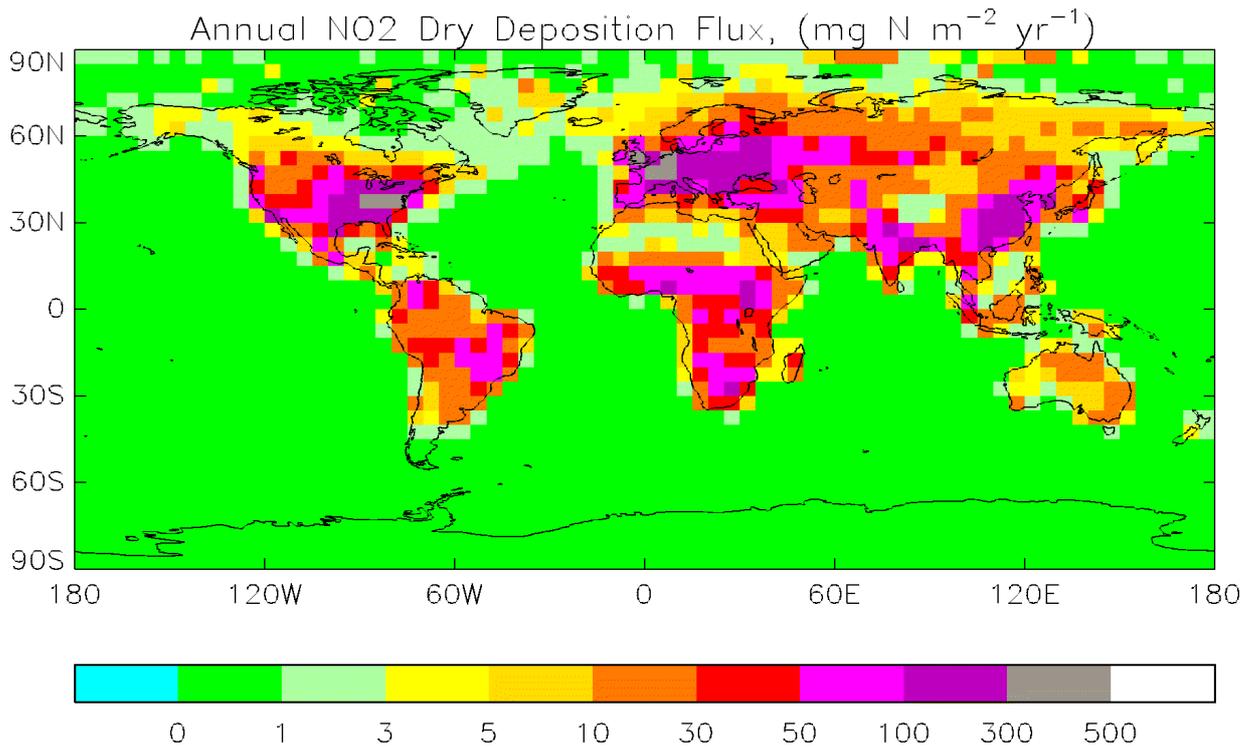
Figure 3.2. Annual deposition fluxes of oxidised nitrogen species (NO_y). (a) Dry deposition flux of NO_2 (top panel). (b) Dry deposition flux of PAN (lower panel).
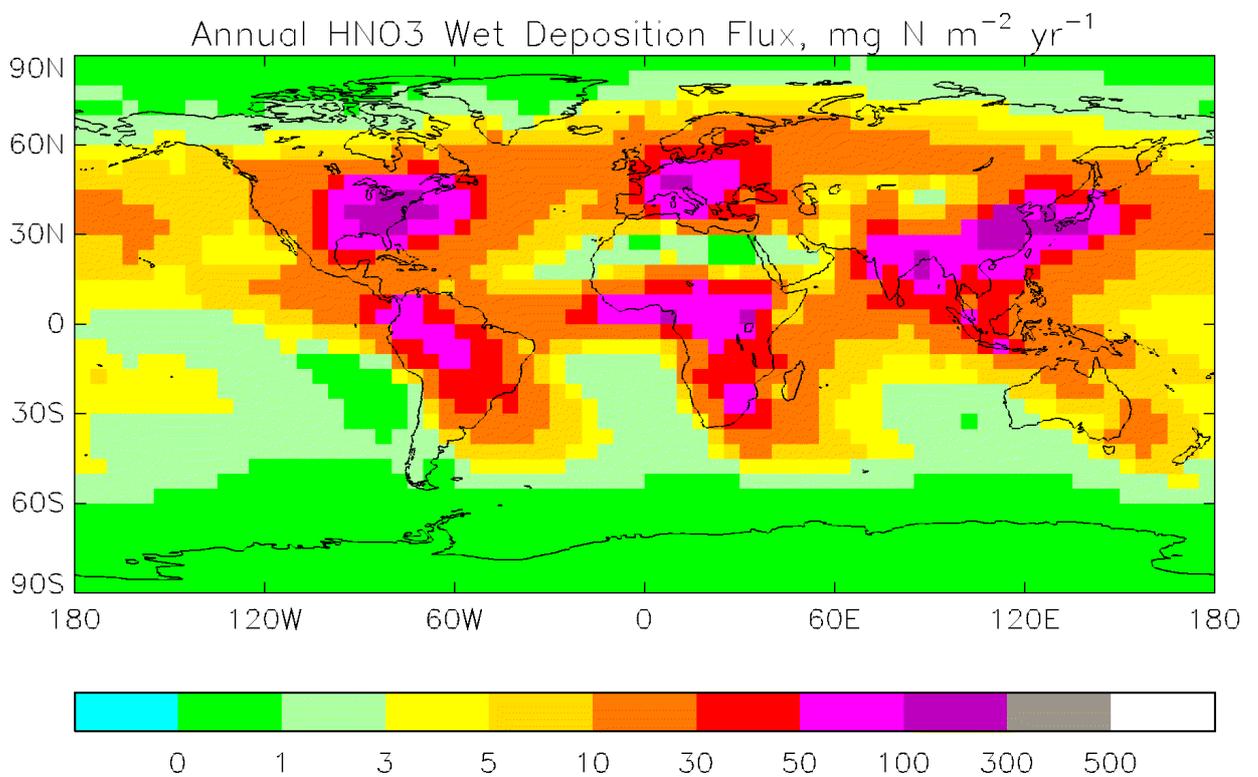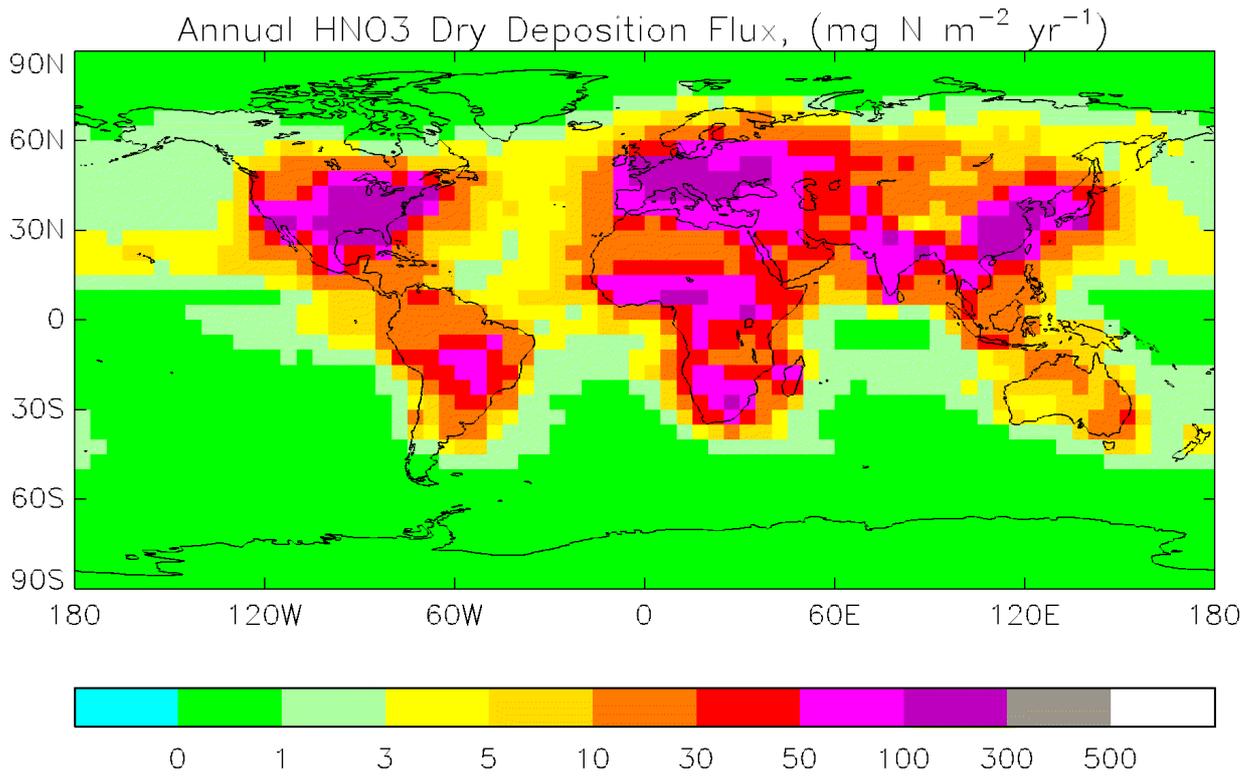
Figure 3.2 (cont.). Annual deposition fluxes of nitric acid (HNO$_3$). (c) Dry deposition flux (top panel). (d) Wet deposition flux (lower panel).
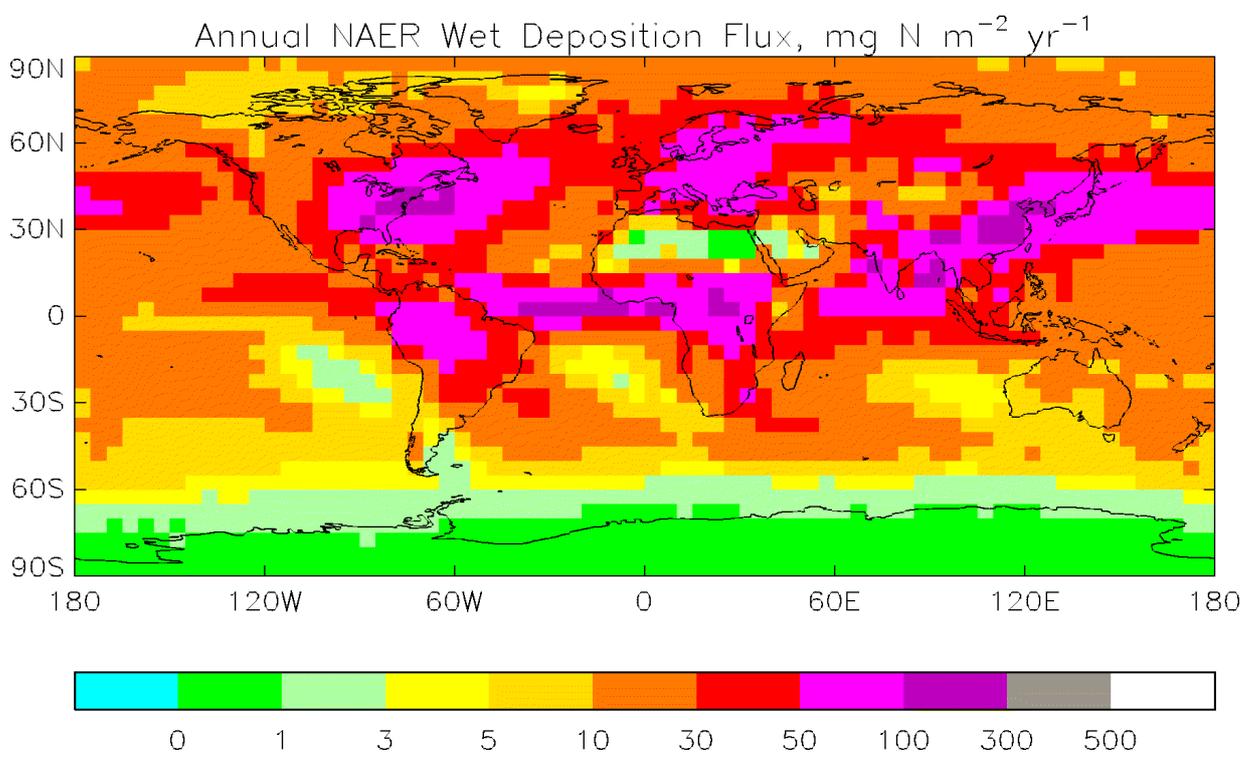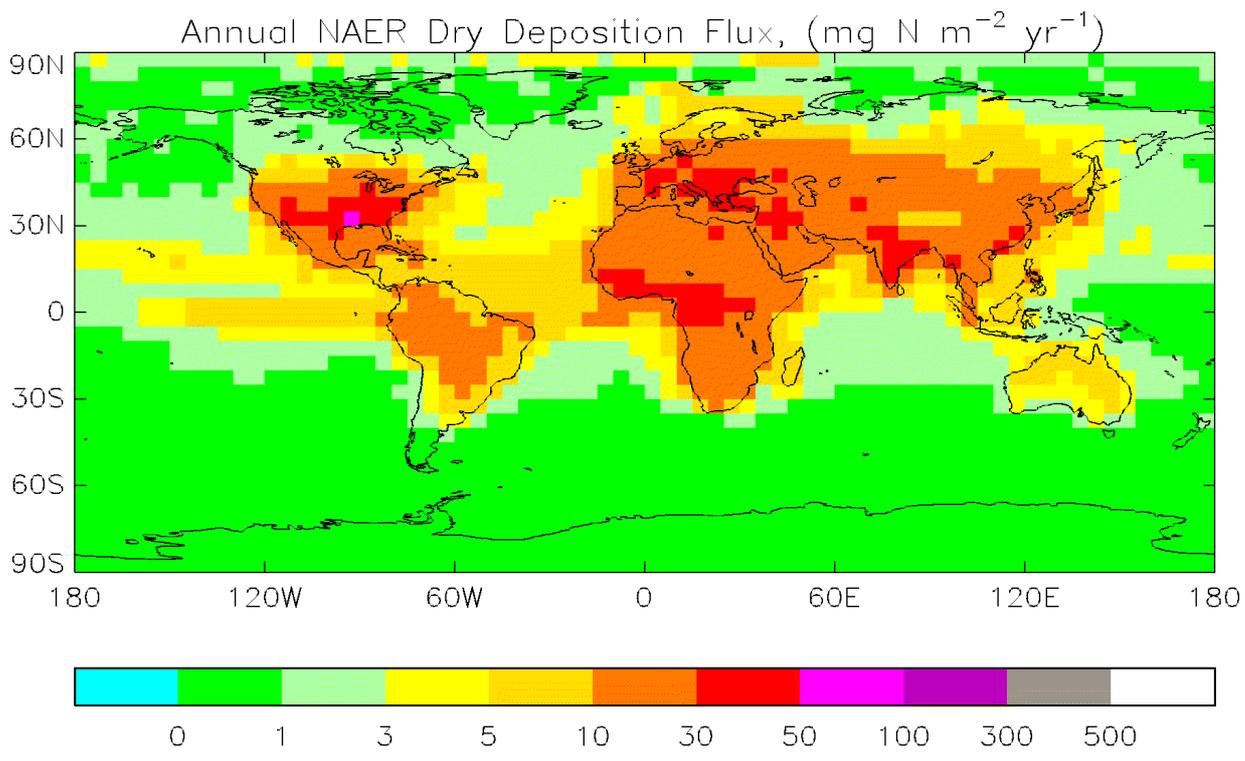
Figure 3.2 (cont.). Annual deposition fluxes of nitrate aerosol (NAER). (e) Dry deposition flux (top panel). (f) Wet deposition flux (lower panel).

The final oxidised nitrogen species considered in STOCHEM is a nitrate aerosol. This is a generic species formed from the uptake of nitric acid, N_2O_5 and organic nitrates by aerosols. In STOCHEM, the uptake of aerosols is parameterised in terms of the stability of the boundary layer, and does not depend on the surface type. Figures 3.2(e) and 3.2(f) show that nitrate aerosol readily deposits to most surfaces. The dry deposition fluxes are larger over land areas than the oceans because the boundary layer is generally less stable. The wet deposition flux does not depend on the stability of the boundary layer, and closely resembles the wet deposition flux pattern for nitric acid (HNO_3). Again, plumes from the continents are visible. The lifetime of nitrate aerosol is quite long, about 12.9 days.

3.4 Results for the reduced nitrogen compounds (NHx)

The deposition fluxes of reduced nitrogen species, ammonia (NH_3) and ammonium sulphate, are shown in Figure 3.3. The ammonium sulphate fluxes have already been discussed earlier. They are reproduced here to illustrate the magnitude of nitrogen deposited. In STOCHEM, ammonia is assumed to be taken up by most surfaces. High uptake rates via both dry and wet deposition are visible over agricultural areas, where there are also large sources of ammonia.

3.5 Global Deposition Fluxes in the Model Integrations

The global dry and wet deposition fluxes of each compound containing sulphur and/or nitrogen are listed in Table 3.1. The changes in the model results in each case study are small. It is important to identify which changes are real, and not just due to "noise" in the model. The magnitude of the noise may be estimated from the emission fluxes in Table 3.1. The SO_2 and NH_3 emissions have not been changed in any of the three runs, yet the totals emitted are slightly different. Similarly, the NO emission in the control run and case study (b), 50 % less anthropogenic CO, are also slightly different. From examination of these differences, it appears that a change of the order of 0.1 Tg yr^{-1} or less in a given flux is indistinguishable from noise.
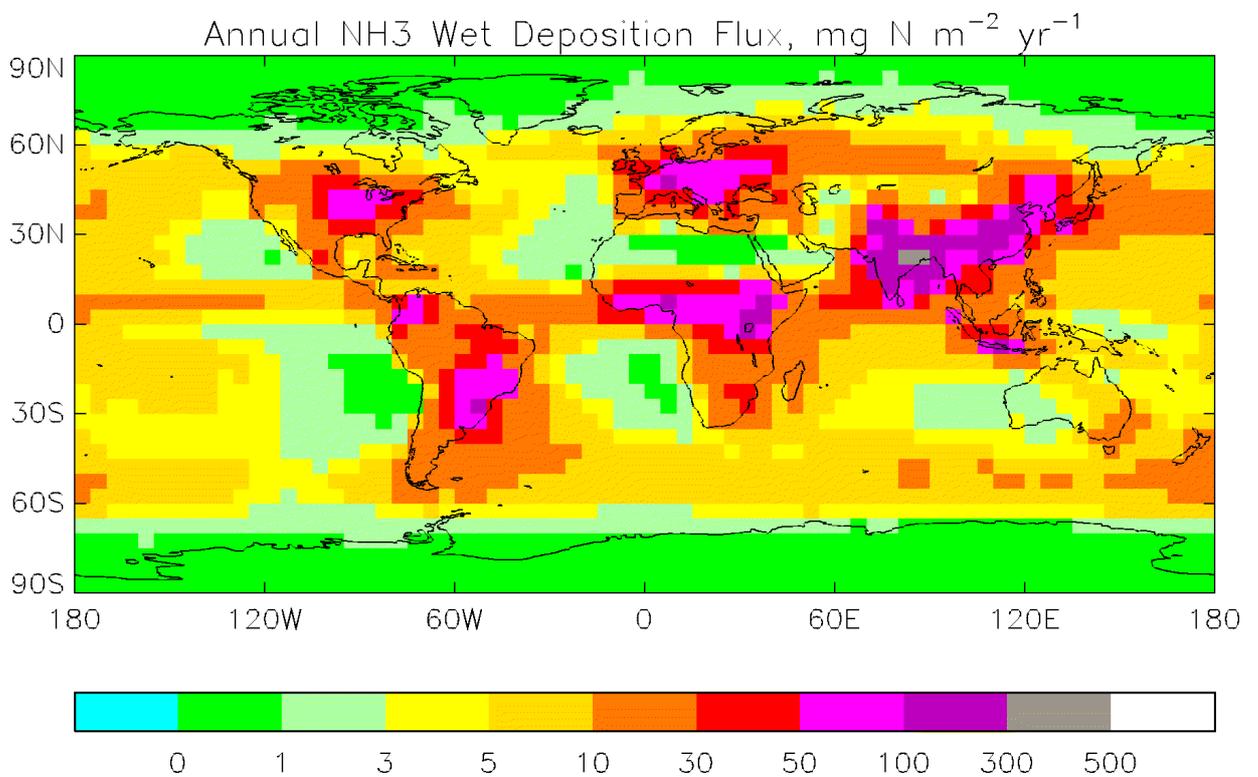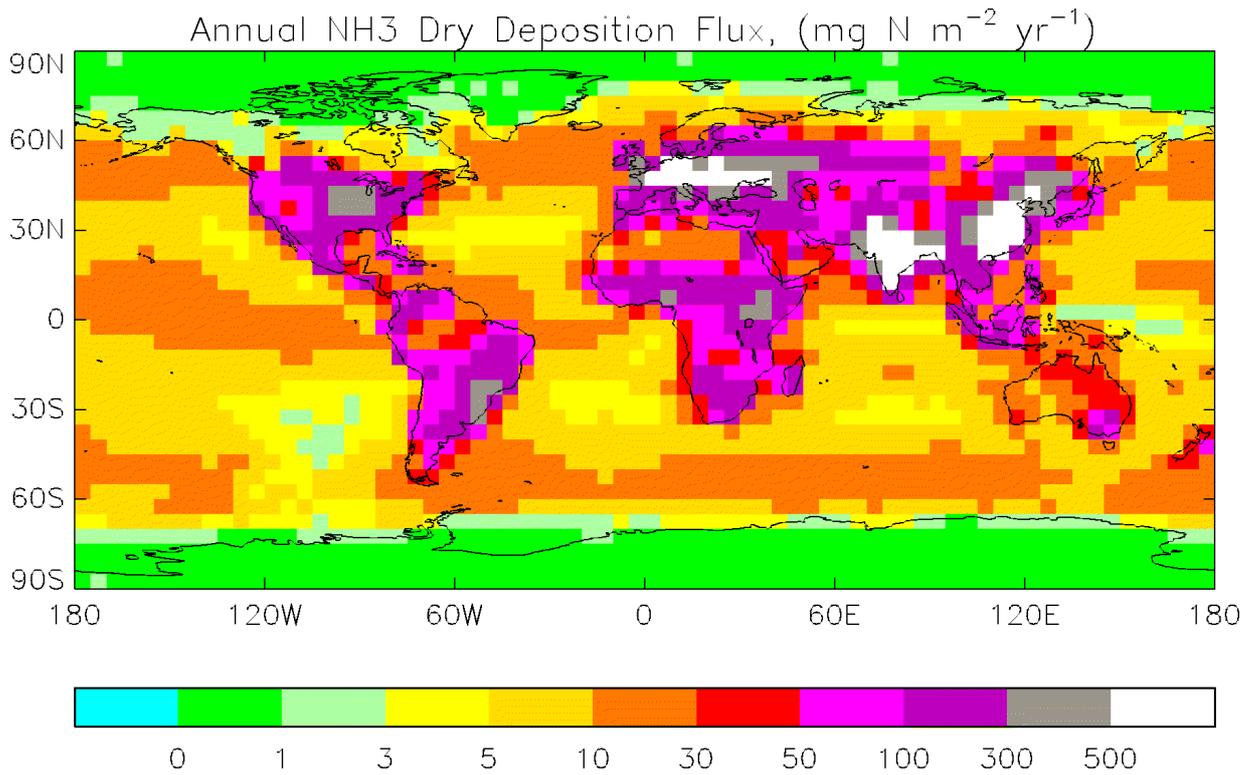
Figure 3. Annual deposition fluxes of reduced nitrogen compounds (NH$_x$). (a) Dry deposition flux of ammonia (NH$_3$; top panel). (b) Wet deposition flux (lower panel).
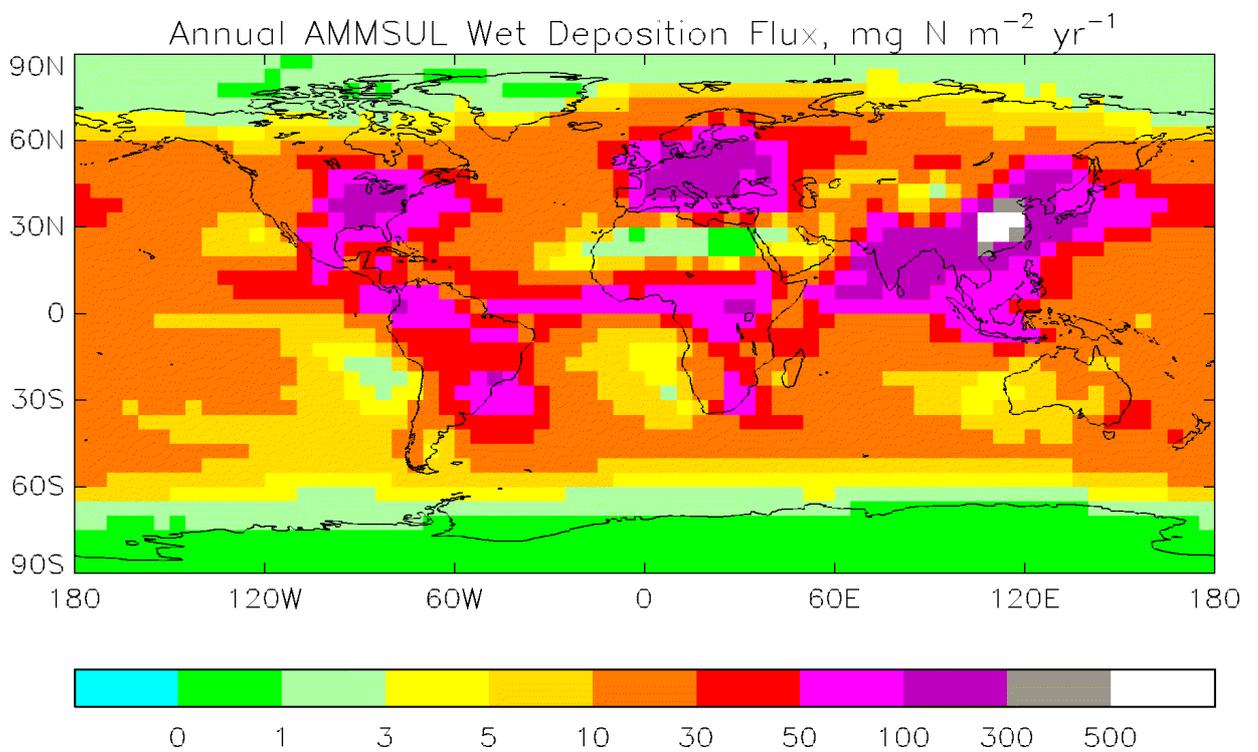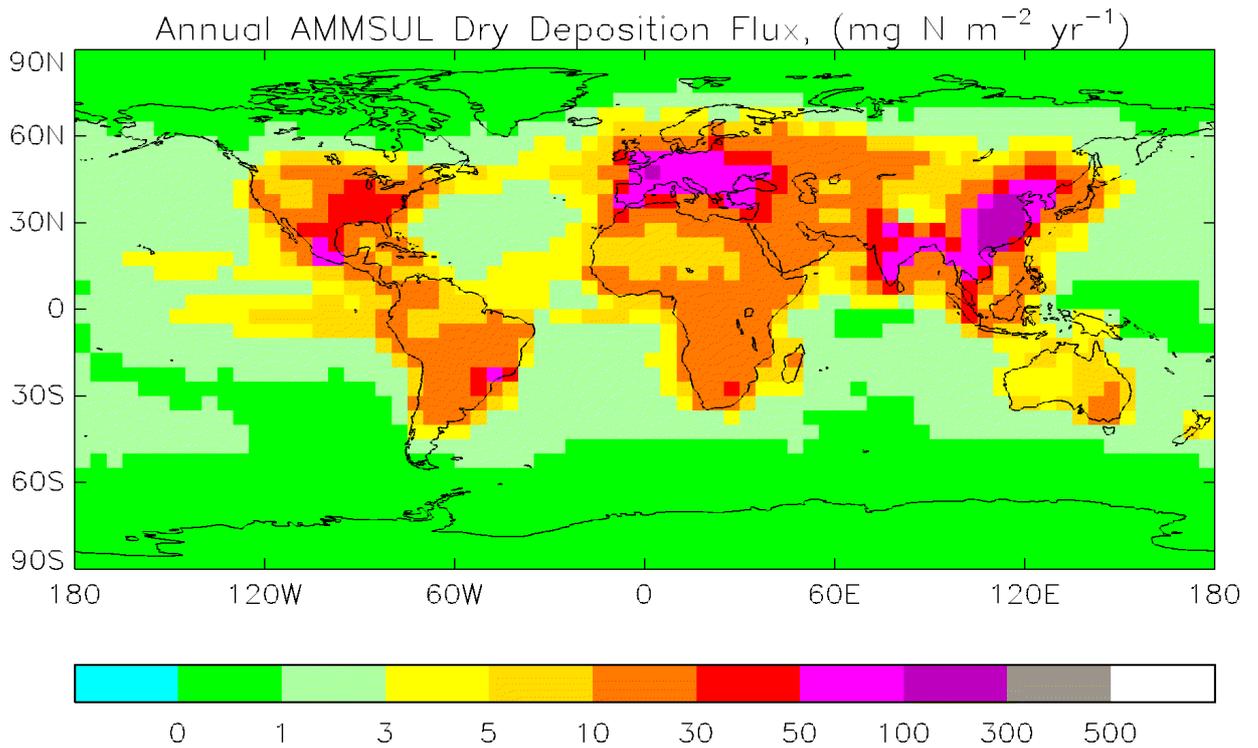
Figure 3 (cont.). Annual deposition flux of ammonium sulphate. (c) Dry deposition flux (top panel). (d) Wet deposition flux (lower panel).

TABLE 3.1. Summary of annual dry and wet deposition fluxes of S- and N-containing compounds in STOCHEM

| Flux	Control Run	Case Study A 50% less NO_x	Case Study B 50% less CO
Sulphur fluxes (Tg S yr^{-1})			
SO_2 dry	39.85	39.48	39.69
MSA CH_3SO_3H dry	0.38	0.36	0.37
$(NH_4)_2SO_4$ dry	4.76	5.01	4.91
H_2SO_4 dry	3.32	3.21	3.32
SO_2 wet	13.01	12.90	13.03
MSA CH_3SO_3H wet	2.97	2.99	2.98
$(NH_4)_2SO_4$ wet	17.78	18.19	17.93
H_2SO_4 wet	14.77	14.85	14.80
SO_2 emission	81.31	81.39	81.39
Nitrogen Fluxes (Tg N yr^{-1})			
NO_2 dry	6.36	4.17	6.33
HNO_3 dry	8.28	5.51	8.32
PAN dry	1.96	1.71	1.98
Nitrate aerosol dry	3.32	2.38	3.31
HNO_3 wet	8.07	5.97	8.13
Nitrate aerosol wet	13.99	10.52	13.96
NO emission	42.24	30.22	42.29
$(NH_4)_2SO_4$ dry	4.17	4.39	4.30
NH_3 dry	25.67	25.31	25.44
$(NH_4)_2SO_4$ wet	15.56	15.92	15.69
NH_3 wet	7.42	7.38	7.44
NH_3 + OH	0.81	0.71	0.84
NH_3 emission	53.64	53.71	53.71

Comparing the fluxes listed in Table 3.1 for the control run and case study A, it can be seen that reducing the anthropogenic NO_x emissions by 50 % results in slightly less dry deposition of SO_2 (a reduction of 0.37 Tg yr^{-1}), and a slightly increased dry and wet deposition of ammonium sulphate (an increase of 0.25 and 0.41 Tg yr^{-1} respectively). These changes suggest that the transformation of SO_2 to ammonium sulphate is more efficient in case study A than the control run. The changes in the dry and wet deposition fluxes of H_2SO_4 are within the noise. The dry deposition flux of ammonia has also decreased slightly, which is consistent with an increased production of ammonium sulphate aerosol. The dry and wet deposition rates of the NO_y species have, not surprisingly, decreased.

Similar results are obtained when the anthropogenic CO emissions are reduced by 50 %. Again, the dry deposition of SO_2 is smaller than in the control run, and the dry and wet deposition fluxes of ammonium sulphate are slightly larger. However, the magnitude of the changes is smaller (approximately 0.15 Tg yr^{-1} in each case), being just greater than the noise level of 0.1 Tg yr^{-1}.

3.6 Changes in SO_2 and total sulphur deposition

The changes in the patterns of SO_2 dry deposition and total sulphate deposition when either the NO_x or CO emissions are halved are shown in Figures 3.5 to 3.7. Figure 3.5 shows the change in the SO_2 dry deposition flux when the NO_x emission is halved. The changes resulting when the CO emission is halved are very similar. Over Europe and parts of North America and China, the SO_2 dry deposition flux is smaller. However, there are some regions where the flux has increased - central Europe, and small parts of central Asia, south-east Asia and western North America. Overall, however, the dry deposition flux of SO_2 has fallen.

Figure 3.6 shows the corresponding change in total sulphur deposition when the anthropogenic NO_x emission has been halved. It can be seen that this flux has increased, generally in the places where the SO_2 dry deposition flux has decreased. There are also regions where the total sulphur deposition flux has decreased, over parts of Europe and North America, and particularly northern China.
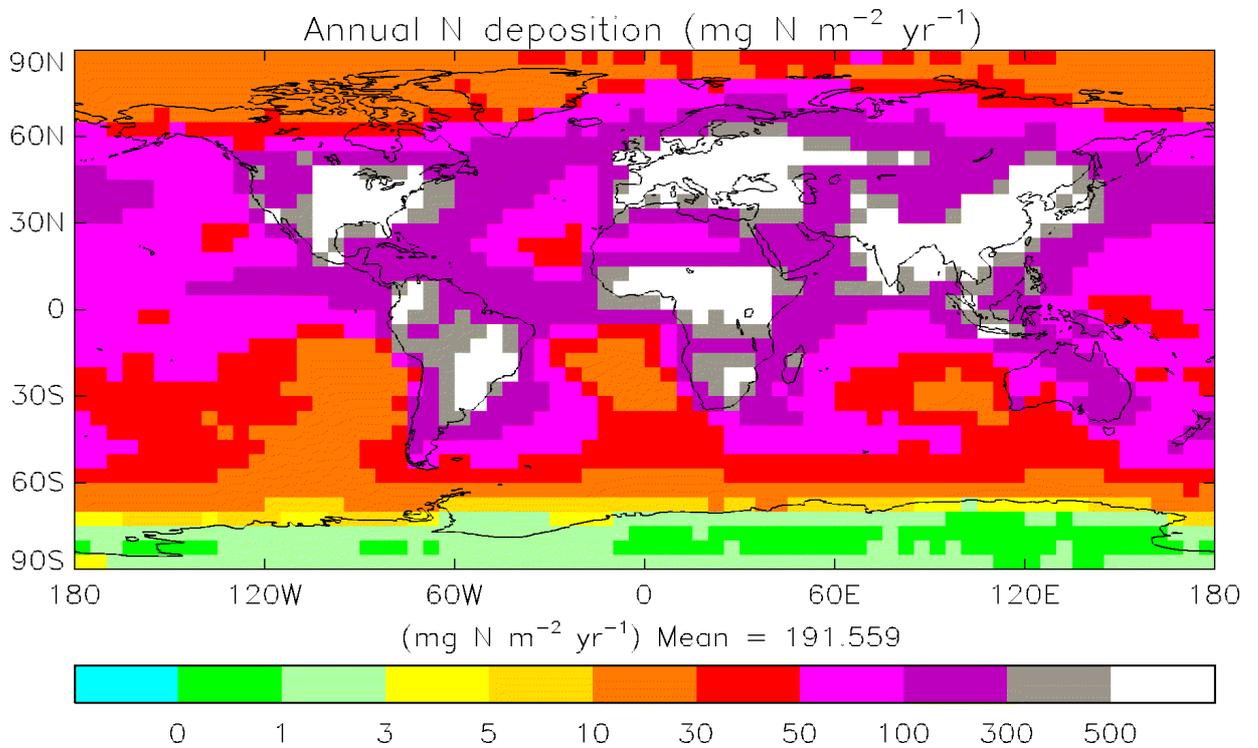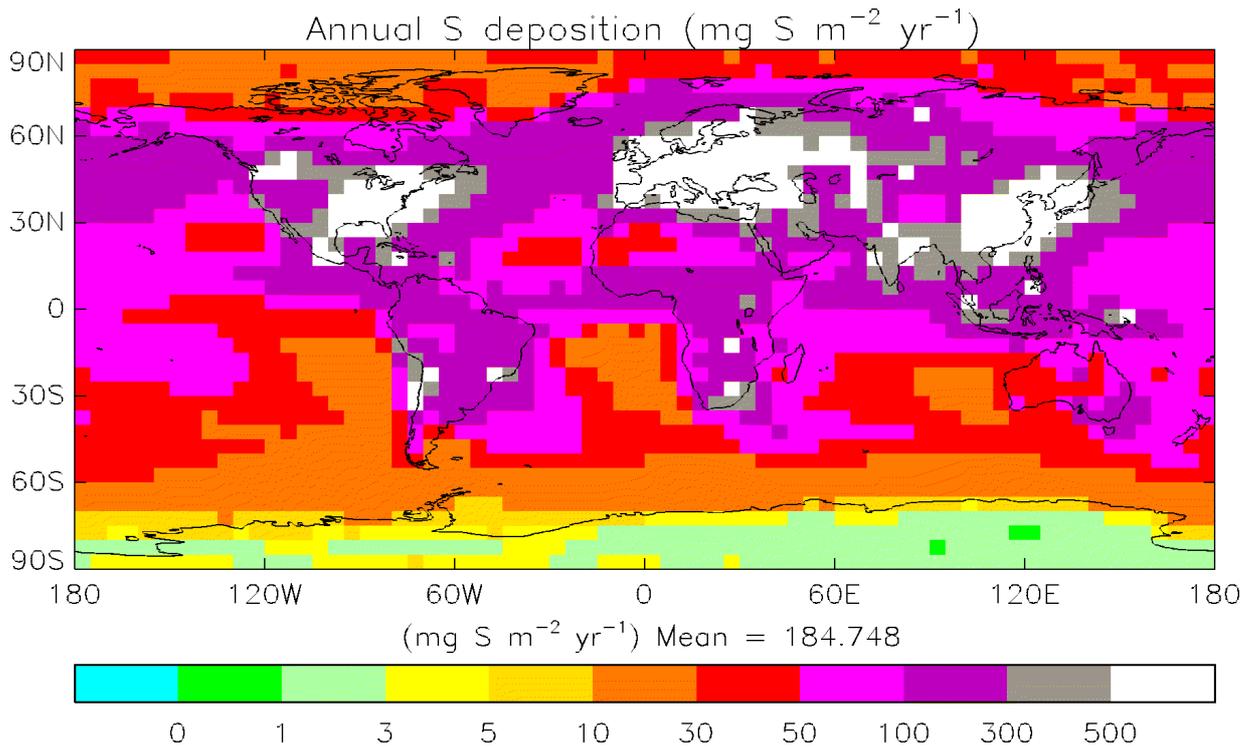
Figure 3.4. Annual deposition fluxes of sulphur and nitrogen compounds from the control run. (a) Annual sulphur deposition fluxes (top panel). (b) Annual nitrogen deposition fluxes (lower panel).

SO2 dry dep flux change when NOx emission halved (mg S m^{-2} yr^{-1})
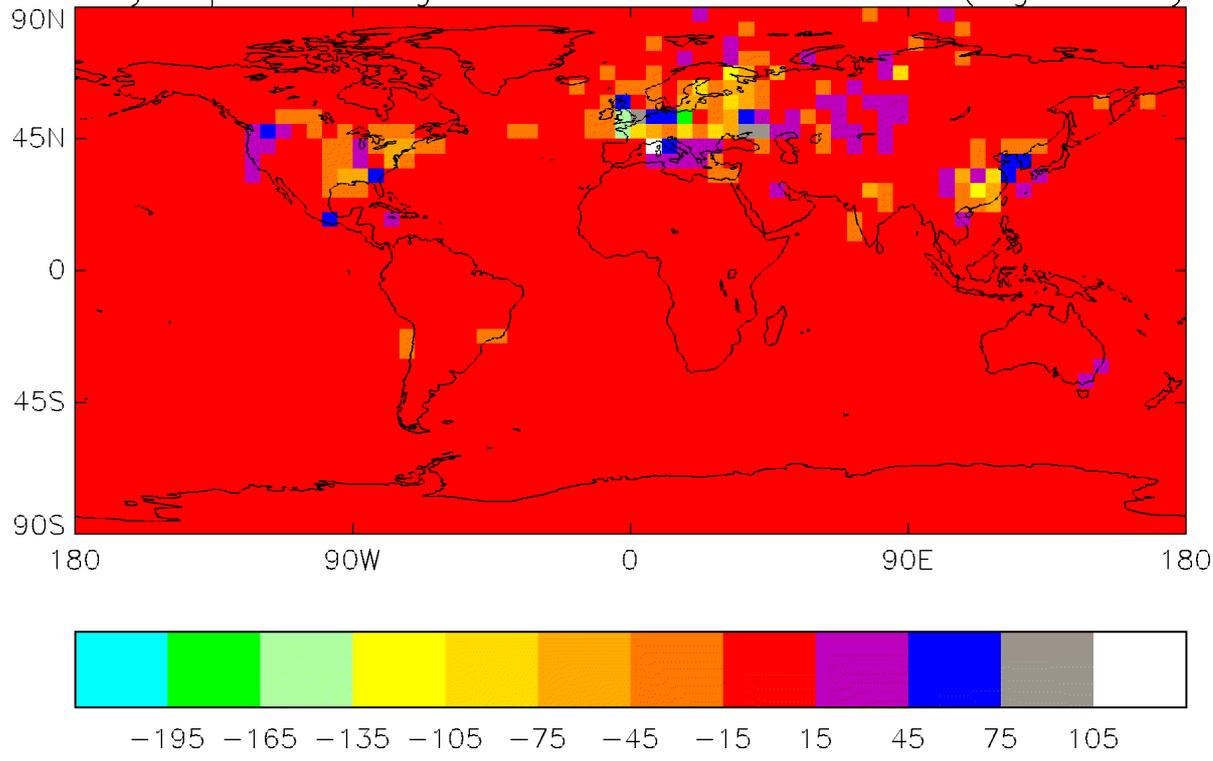

Figure 3.5. Change in annual SO$_2$ dry deposition flux when anthropogenic NO$_x$ emissions are halved.

Total sulphate deposition flux change when NOx emission halved (mg S m^{-2} yr^{-1})
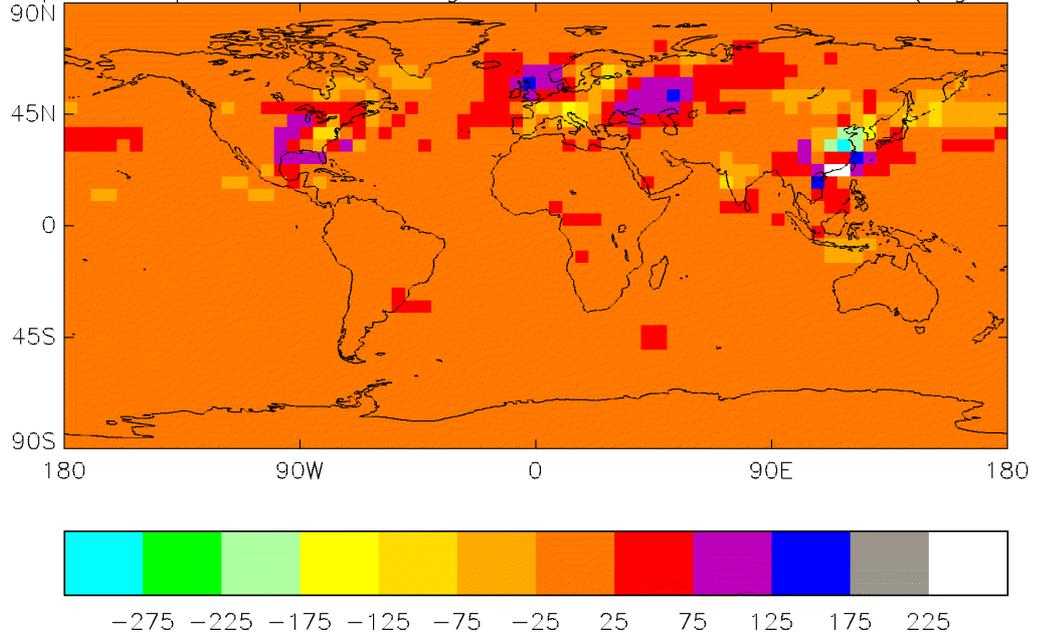
Figure 3.6. Change in annual sulphate total deposition flux when anthropogenic NO$_x$ emissions are halved.
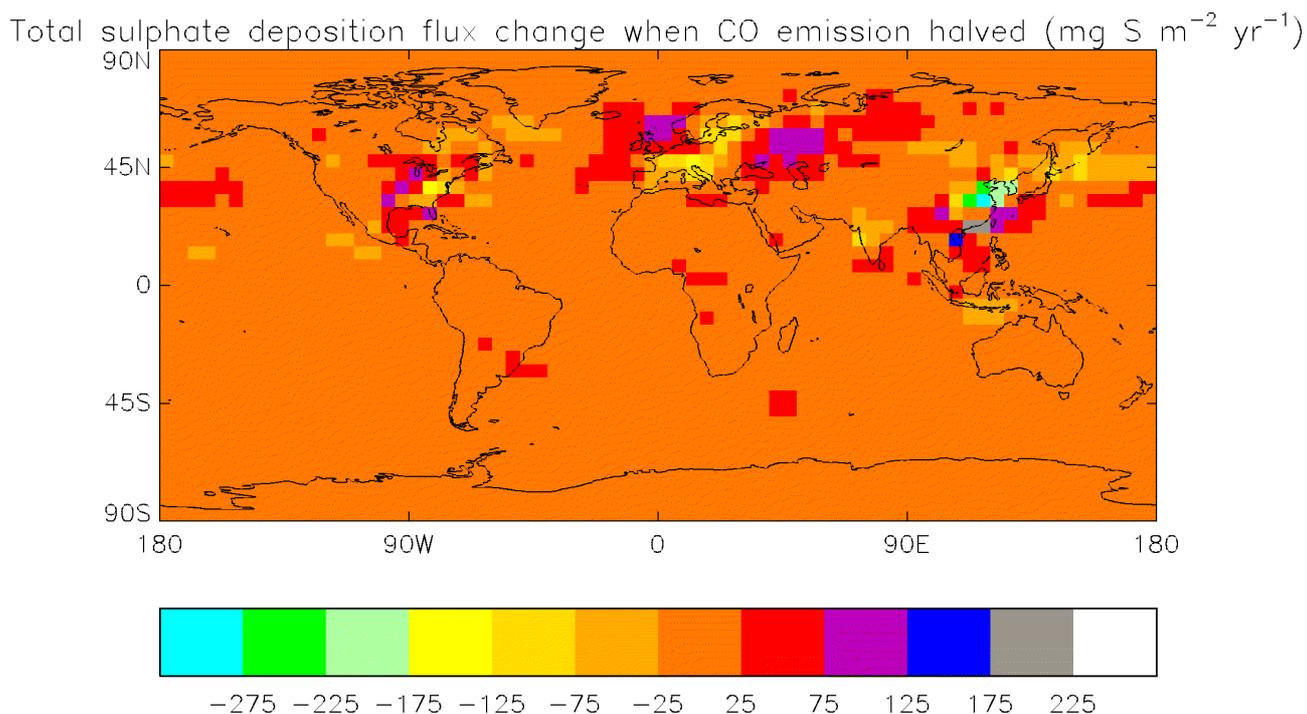
Figure 3.7. Change in annual sulphate total deposition flux when anthropogenic CO emissions are halved.

Figure 3.7 shows the change in total sulphur deposition when the anthropogenic CO emission has been halved. The changes in the pattern of total sulphur deposition are similar to those seen when the anthropogenic NO_x emission has been halved, except the magnitudes are smaller.

3.7 Comparison of Model Depositions with Observations

The model predictions for total sulphate, ammonium and nitrate deposition are compared to measurements made at various European sites in 1992 and 1999 in Figure 3.8. The agreement between the model and observations is generally good with the majority of the model results within a factor of two of the observations. All measurements were made in Europe as part of the EMEP network.

Annual deposition fluxes of reduced nitrogen (NH_x), oxidised nitrogen (NO_y) and sulphate (SO_4^{2-}) over Europe and North America are shown in Figures 3.9-3.14 respectively. The reduced nitrogen compounds are ammonia (NH_3) and ammonium sulphate ((NH_4)$_2SO_4$). The oxidised nitrogen compounds are nitric acid (HNO_3) and
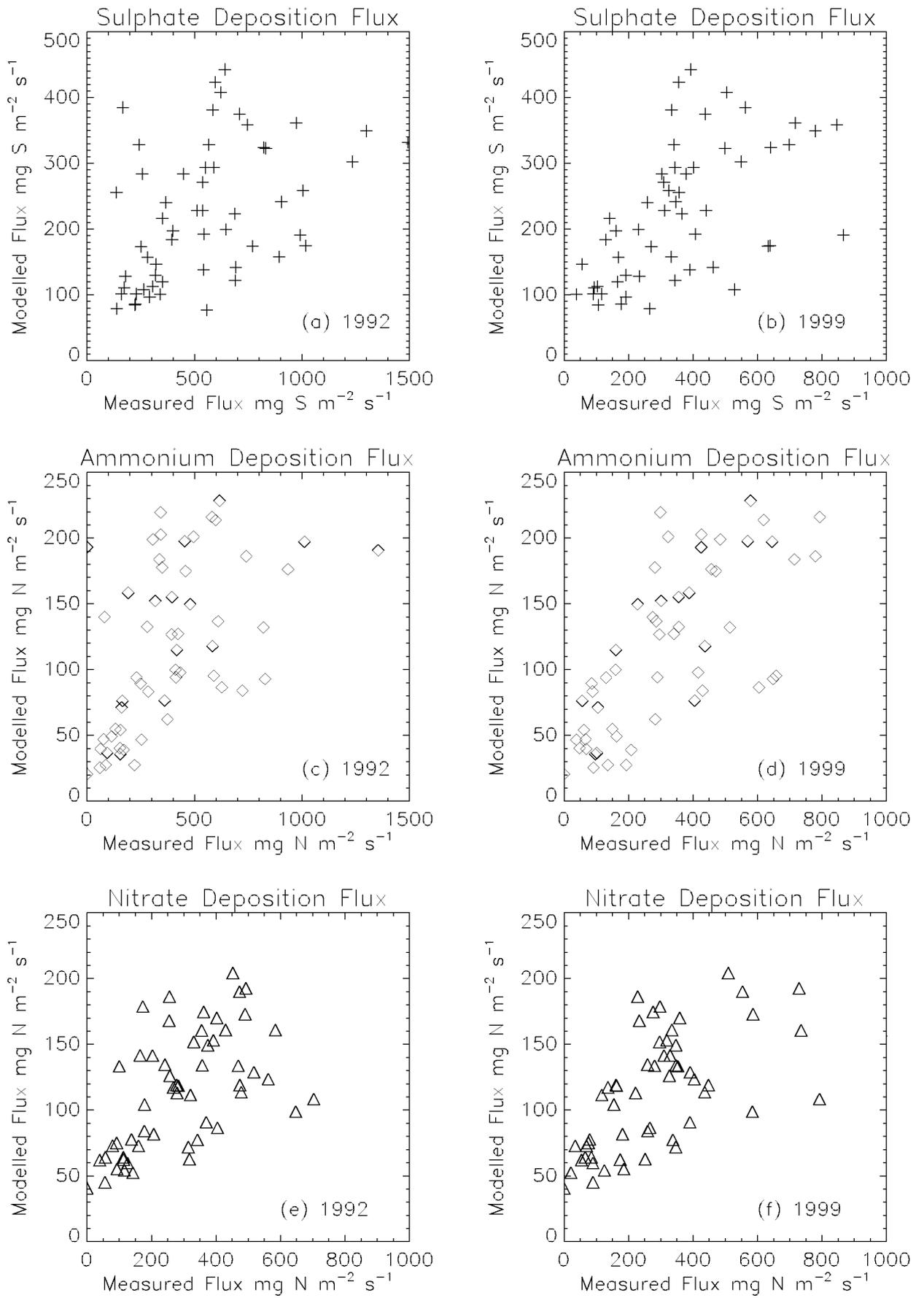
Figure 3.8. Comparison of modelled and measured fluxes of sulphate, ammonium and nitrate.
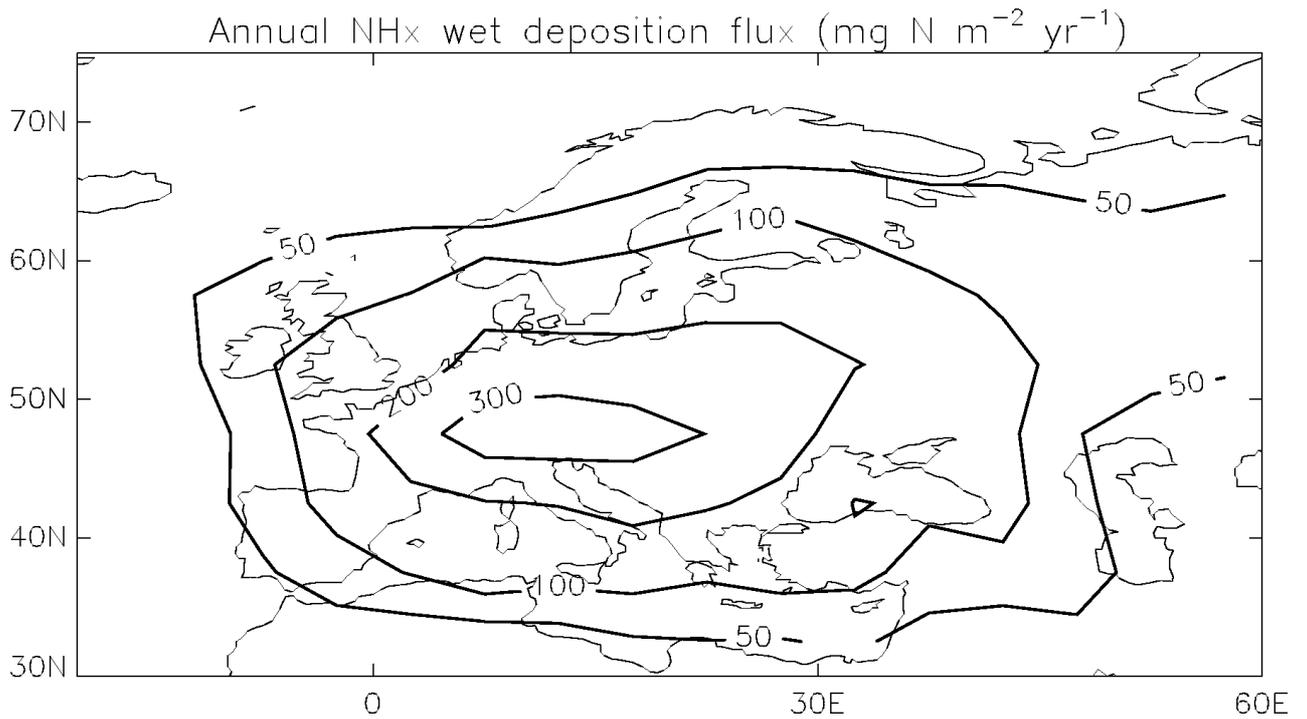
Figure 3.9. Annual wet deposition flux of reduced nitrogen (NH_x) over Europe. The contours are in units of mg N m^{-2} yr^{-1}.
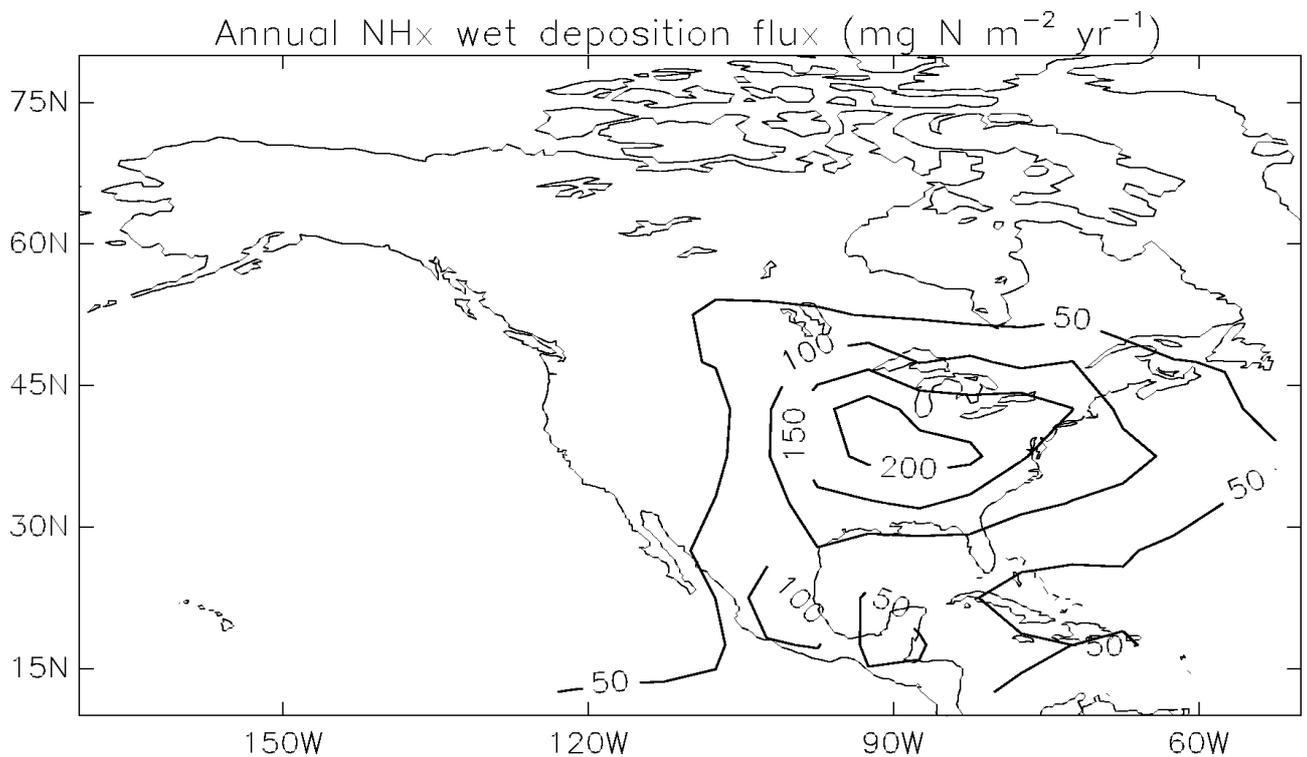
Figure 3.10. Annual wet deposition flux of reduced nitrogen (NH_x) over North America. The contours are in units of mg N m^{-2} yr^{-1}.

53
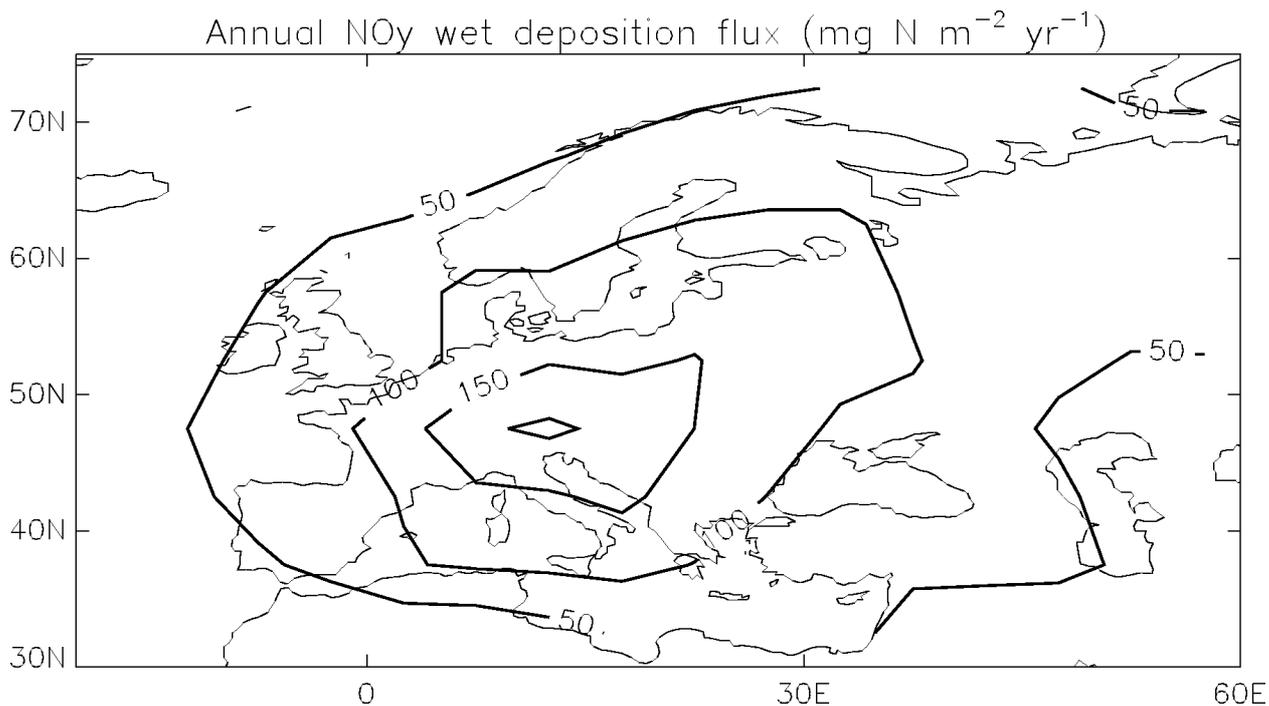
Figure 3.11. Annual wet deposition flux of oxidised nitrogen (NO_y) over Europe. The contours are in units of mg N m^{-2} yr^{-1}.
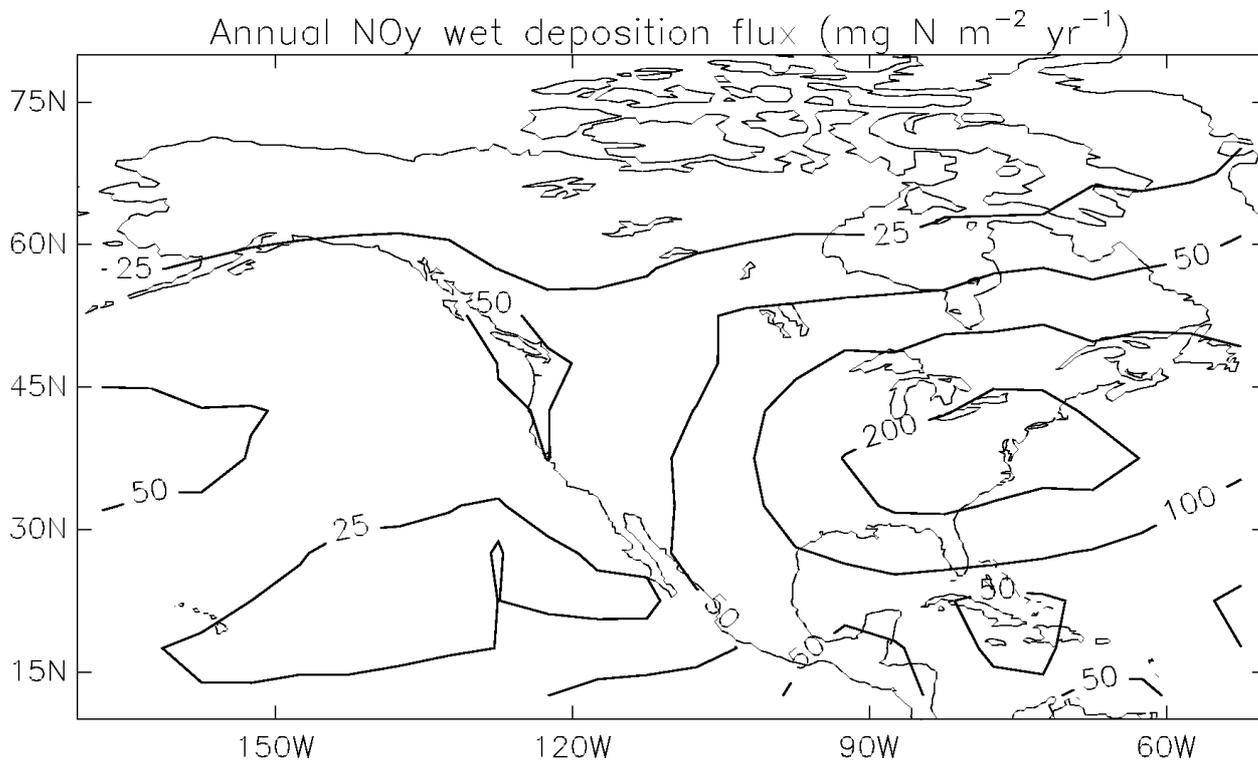
Figure 3.12. Annual wet deposition flux of oxidised nitrogen (NO_y) over North America. The contours are in units of mg N m^{-2} yr^{-1}.
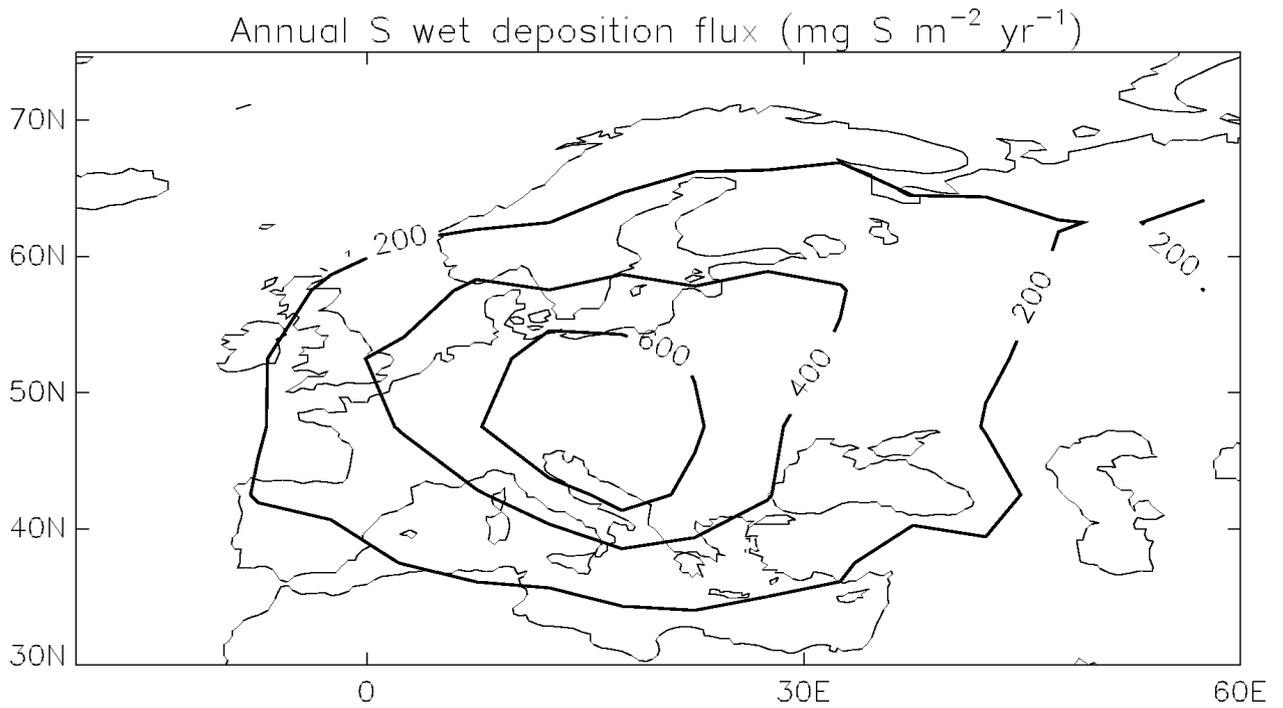
Figure 3.13. Annual wet deposition flux of sulphur over Europe. The contours are in units of mg S m^{-2} yr^{-1}.
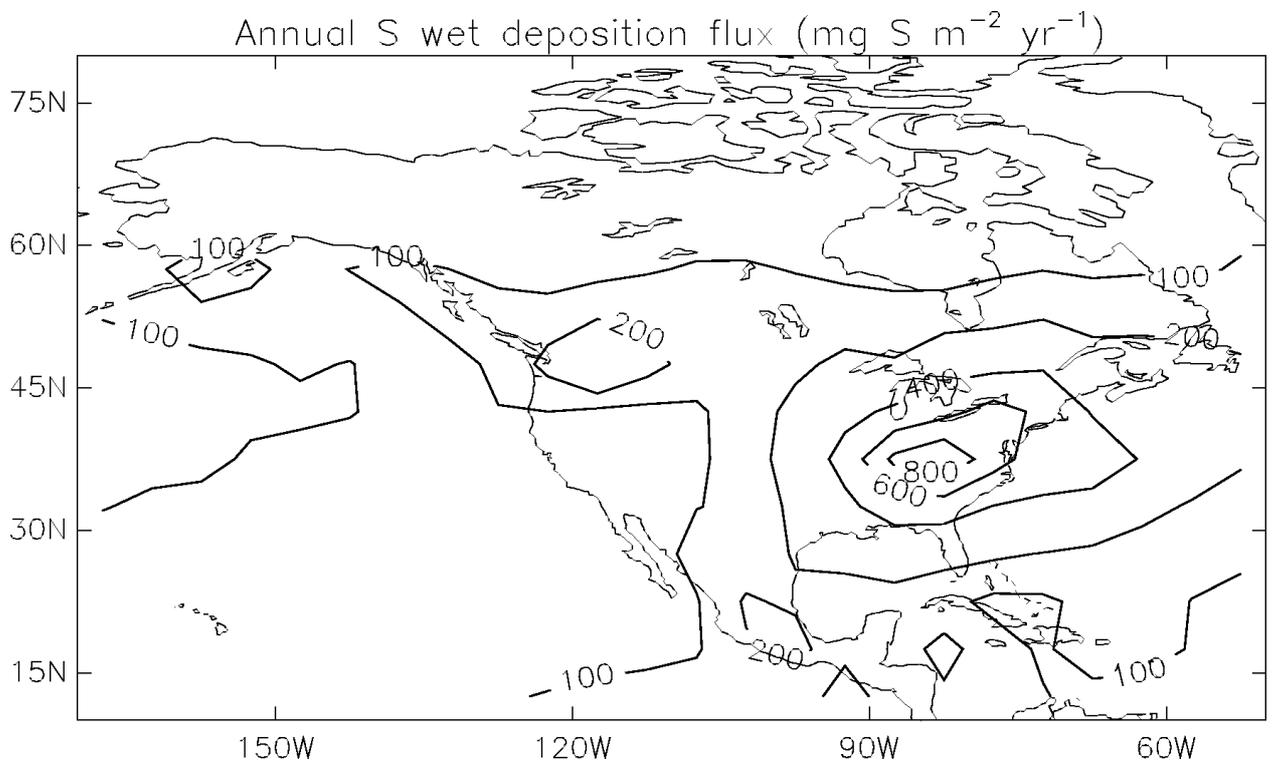

Figure 3.14. Annual wet deposition flux of sulphur over North America. The contours are in units of mg S m^{-2} yr^{-1}.

nitrate aerosol. The sulphate fluxes are the sumof the wet deposition of sulphuric acid aerosols (H_2SO_4) and ammonium sulphate. For each continent, the deposition maxima of the three classes of compounds are located over the source regions, showing that the compounds have a short lifetime.

3.8 Climate Change and Future Sulphur Deposition

As the global climate system warms up during the 21st century and the tropospheric oxidising capacity increases in response to the build-up of greenhouse gases, there is the possibility that changes may occur in the pattern of wet deposition across the British Isles which may act to reinforce or counteract the influence of regional pollution strategies. This possibility has been investigated using the coupled chemistry climate model (STOCHEM) of the Meteorological Office and the emissions scenarios developed by the Intergovernmental Panel on Climate Change.

Figures 3.15 and 3.16 show the wet sulphur deposition for the year 2030 in the IPCC B2 scenario for the year 2030 with (2030 meteorology) and without (1990 meteorology) climate change. Both deposition maps have been calculated with identical 2030 emissions and show similar features. The impact of Asian SO_2 emissions on the wet sulphur deposition fields is clearly apparent across much of the northern hemisphere. Also, the trans-continental transport of acidic sulphur compounds across the North Atlantic Ocean is clearly apparent following the implementation of strict SO_2 emission controls in Europe.

Nevertheless, the differences between Figures 3.15 and 3.16 are small. There is an indication of increased export across the North Atlantic Ocean into the British Isles but it is difficult to say whether this is a robust feature of the future deposition patterns. It may well be that 2030 is too early for dramatic shifts in future deposition patterns.
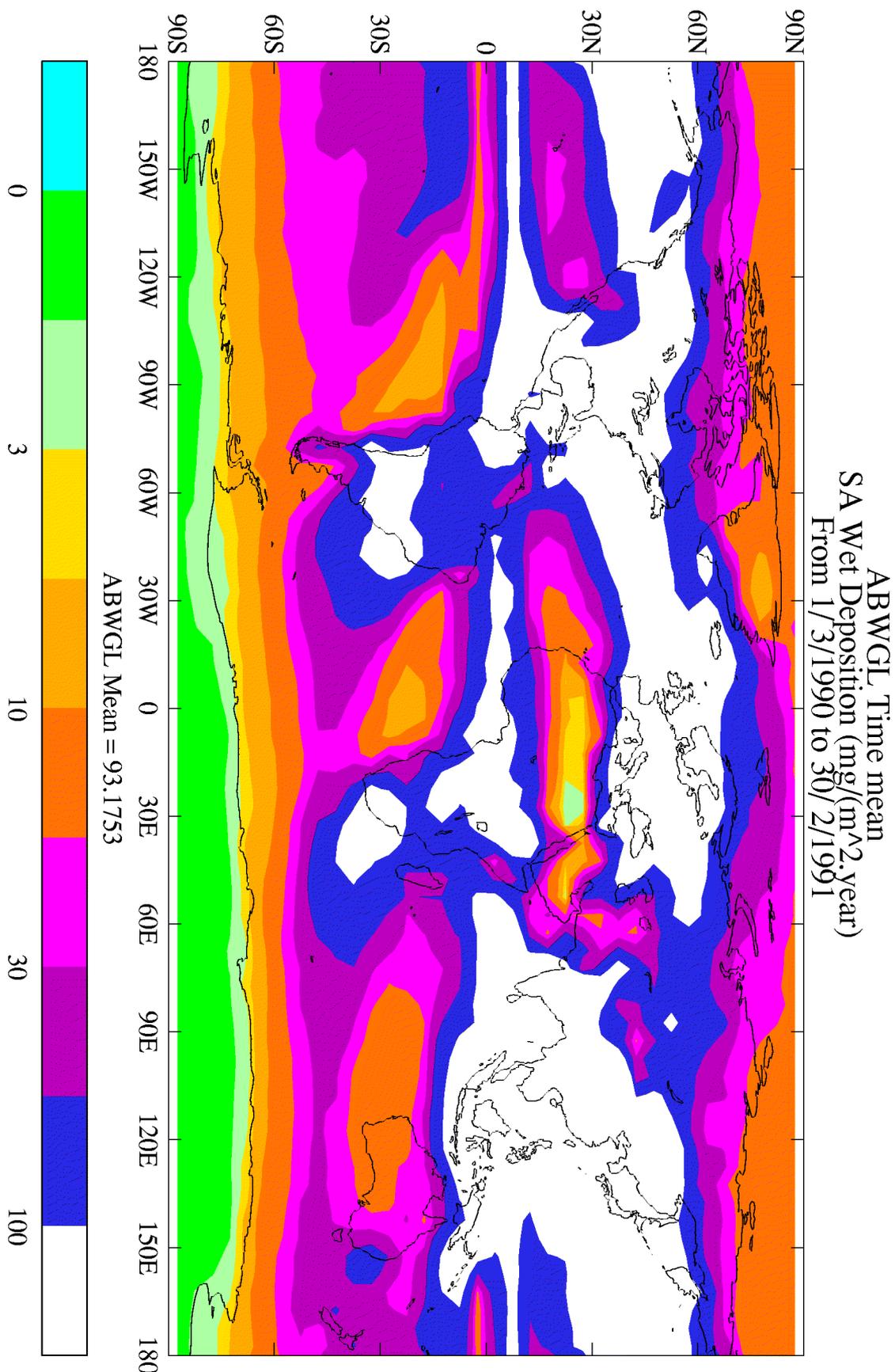
Figure 3.15. The wet deposition flux of SO$_2$ calculated with 2030 emissions and the meteorology of 1990.
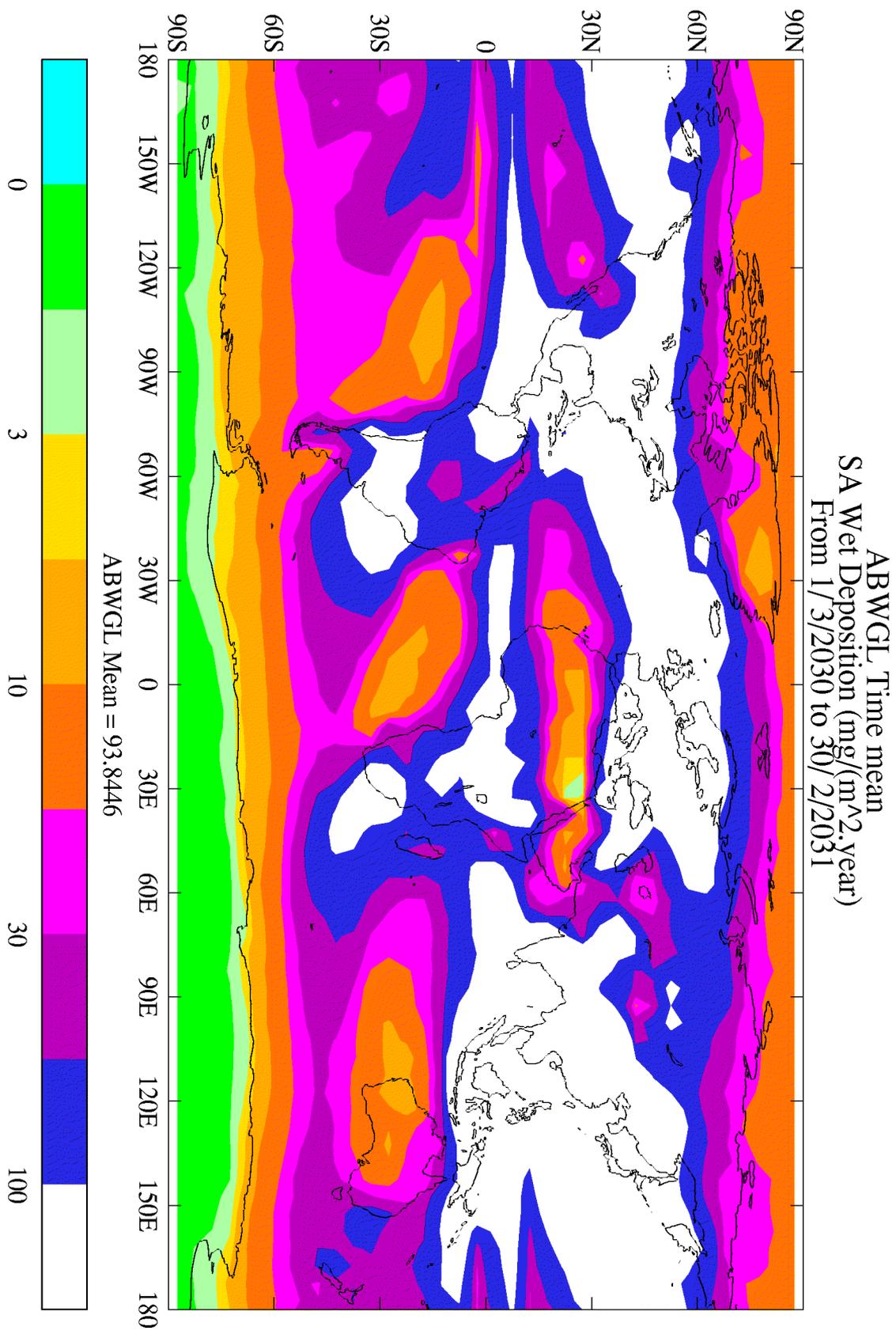
Figure 3.16. The wet deposition flux of SO$_2$ calculated with 2030 emissions and the
meteorology of 2030.

3.9 Global Distributions of Secondary Aerosol Species

Figures 3.17–3.20 present the global distributions of sulphate, nitrate, ammonium and organic aerosols for the emissions and meteorological conditions appropriate to the 1990s. The sulphate aerosol distribution in Figure 3.17 takes into account the oxidation of SO_2 from human activities by both hydroxyl radicals in photochemical oxidation and by reactions in clouds with hydrogen peroxide, ozone and ammonia. The oxidation of dimethyl sulphide from the ocean biosphere is fully treated taking into account reaction with OH during daytime and NO_3 at night. The oxidation of DMS yields methane sulphonic acid, SO_2 and sulphuric acid. The global mean surface concentration of sulphate aerosol was found to be 392 ng S m^{-3}.

The nitrate aerosol distribution in Figure 3.18 takes into account the oxidation of NO_2 by OH during daylight and the nightime and wintertime oxidation of NO_2 by ozone to form N_2O_5. It is assumed that HNO_3 and N_2O_5 react with sea-salt and soil dust aerosol to form coarse particle nitrate. No account has been taken for the formation of fine particle ammonium nitrate so, in principle, the model results are lower limits. However, global ammonia emission inventories are highly unreliable at present and it is difficult to represent adequately the formation of ammonium nitrate. The global mean surface concentration of nitrate aerosol was found to be 128 ng N m^{-3}.

The global distribution of ammonium aerosol is shown in Figure 3.19 and results from the uptake of gaseous ammonia into cloud droplets and there subsequent aqueous phase conversion to ammonium. Ammonium aerosol is formed when these cloud droplets subsequently re-evaporate. The global mean surface concentration of ammonium aerosol was found to be 173 ng N m^{-3}.

The global distribution of secondary organic aerosols in Figure 3.20 takes into account the formation of semi-volatile organic compounds from the oxidation of α-pinene. It is assumed that all biogenic hydrocarbon emissions can be represented by α-pinene and that a range of semi-volatile degradation roducts are formed following its reactions with O_3, OH and NO_3. α-pinene can be taken as a surrogate for the terpene species since it represents more than on half of the speciated emissions from
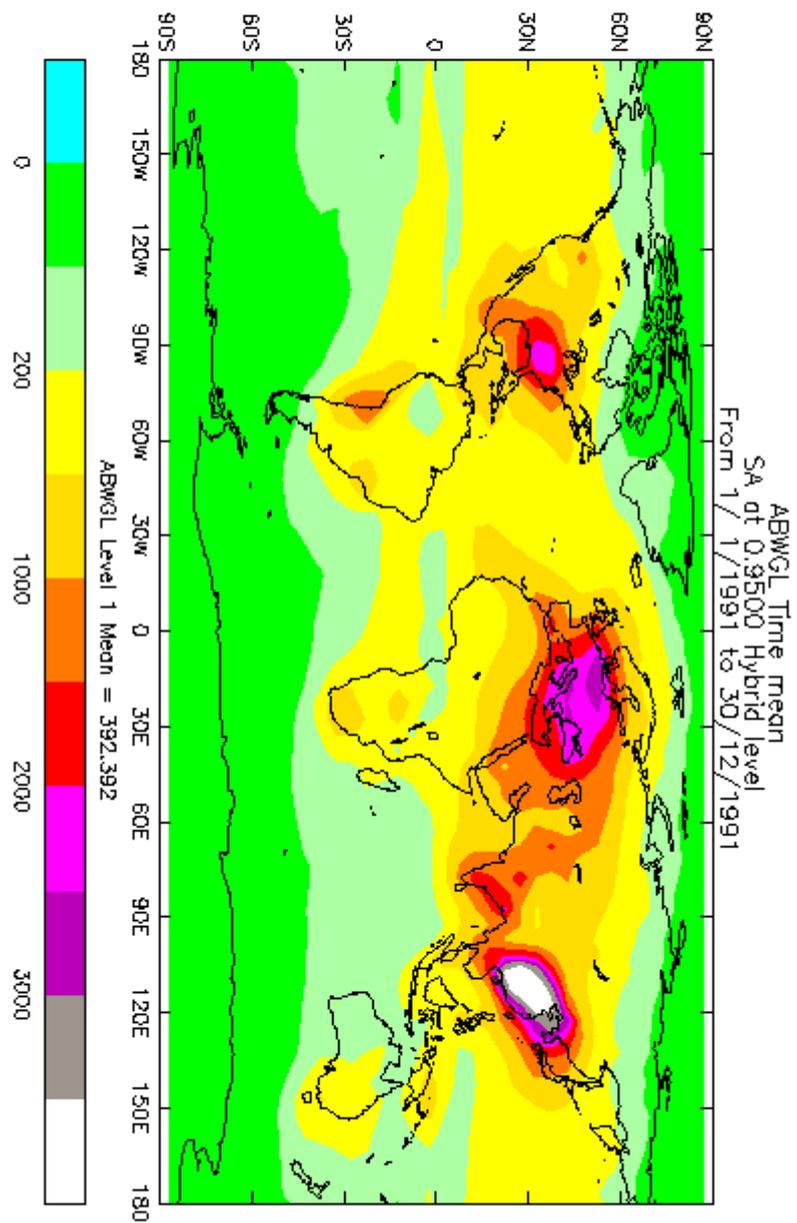
FIGURE 3.17. The global distribution of sulphate aerosol in ng S m^{-3} from STOCHEM for 1990 emissions and meteorology.
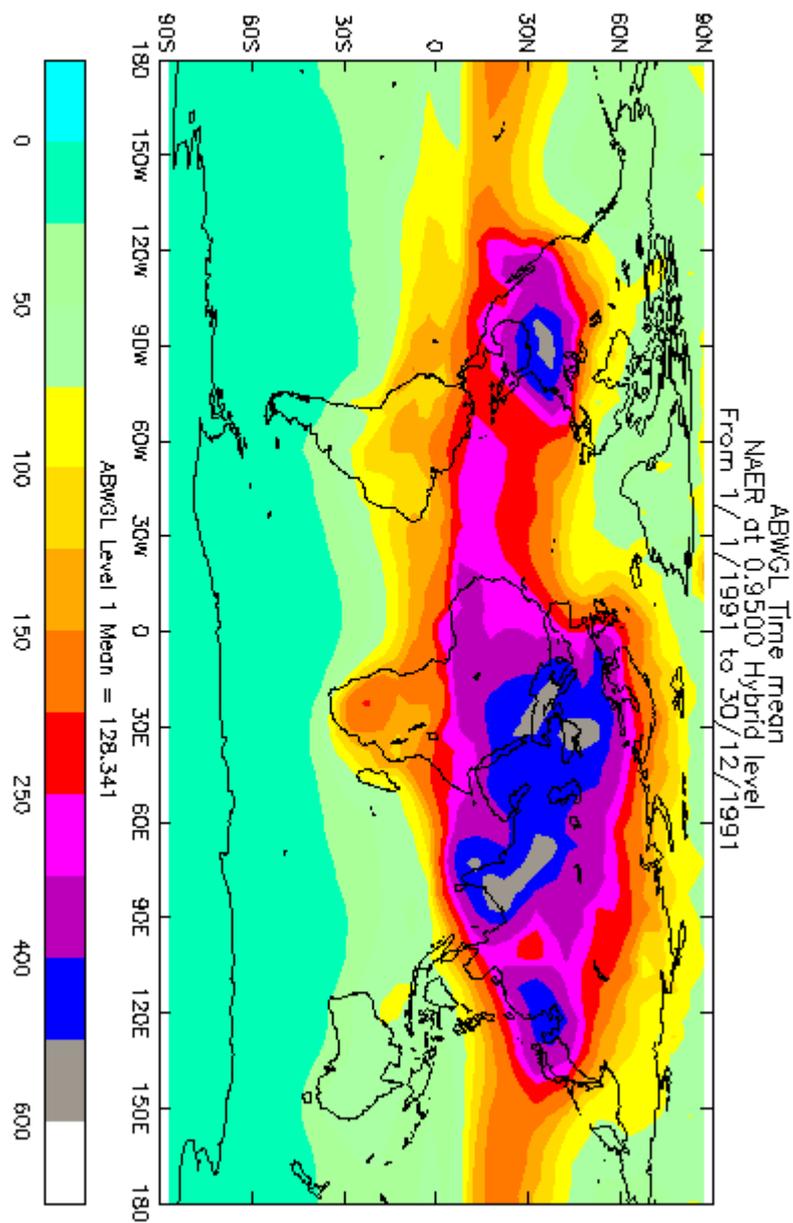
FIGURE 3.18. The global distribution of nitrate aerosol in ng N m^{-3} from STOCHEM for 1990 emissions and meteorology.
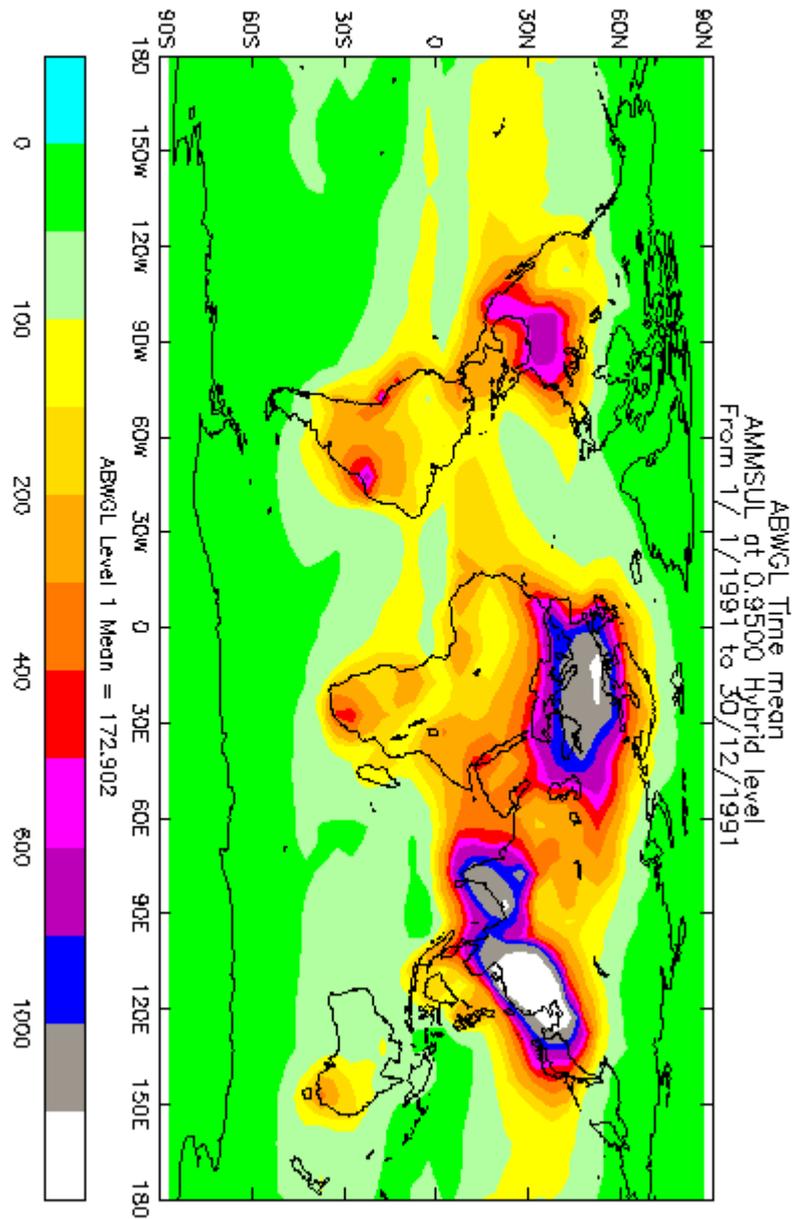
FIGURE 3.19. The global distribution of ammonium aerosol in ng N m^{-3} from STOCHEM for 1990 emissions and meteorology.
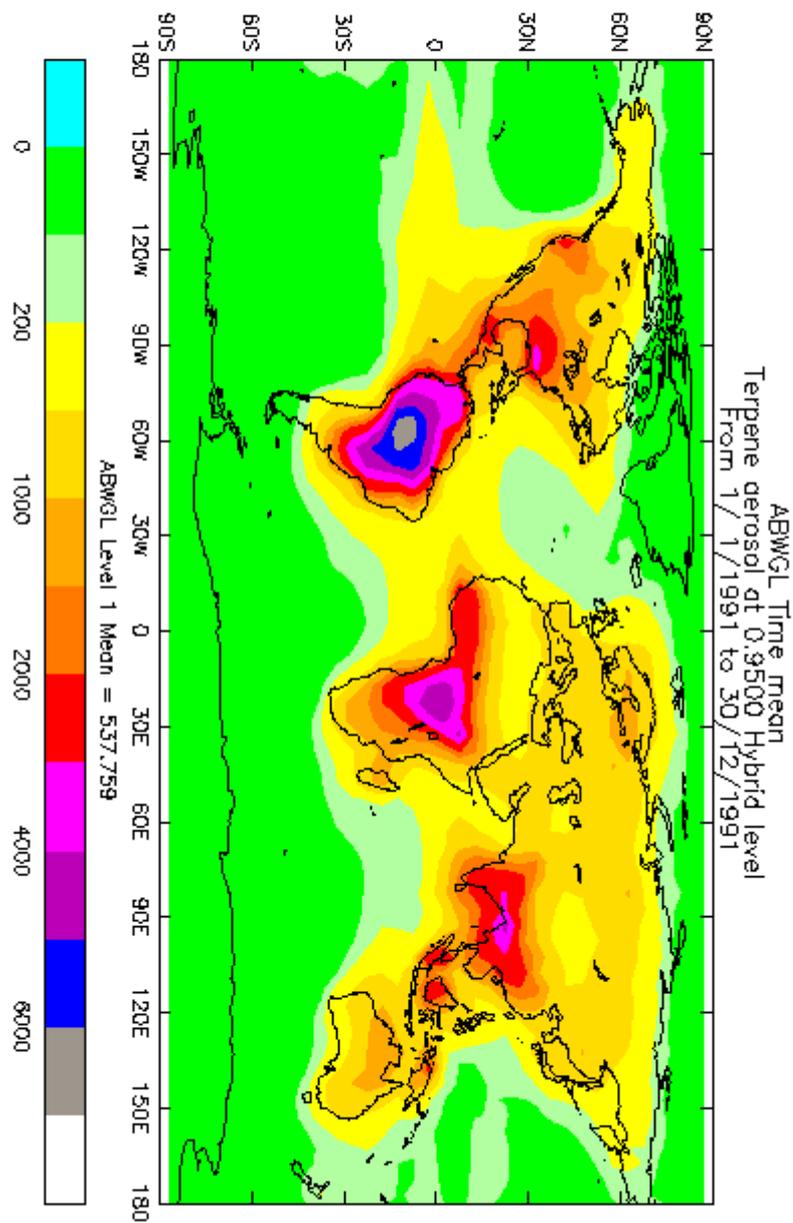
FIGURE 3.20. The global distribution of secondary organic aerosol in ng m^{-3} from STOCHEM for 1990 emissions and meteorology.

natural biogenic sources. These semi-volatile products are scavenged by the pre-existing aerosol in competition with further degradation. The global mean surface concentration of terpene-derived secondary organic aerosols was 538 ng m^{-3}.

These aerosol distributions have been compared carefully with observations for Europe, North America and for a range of remote baseline sites world-wide. For sulphate aerosol, STOCHEM appears to perform as well as the EMEP model whilst removing some of the simplifying assumptions made in the EMEP model concerning oxidation mechanisms and oxidant concentrations. For nitrate and ammonium, there are considerable concerns about the quality of the observations which make detailed comparisons difficult. For organic aerosols, few measurements exist and there are no speciated observations which would make comparisons between models and observations more conclusive.

4. Global and Regional Distributions of Ozone

4.1 Future Surface Ozone Concentrations

Ozone is one of the most reactive pollutants in the lower atmosphere and its global distribution has been heavily influenced by human activities over the period since the industrial revolution. Elevated ozone concentrations cause a wide range of adverse environmental impacts, particularly upon human health and upon crops, plants and natural vegetation. Concerns in North America and Europe about these impacts have driven local- and regional-scale pollution control measures that act to reduce emissions of the ozone precursors, hydrocarbons and nitrogen oxides. Ozone is also an important greenhouse gas and global warming is another adverse consequence of the global-scale build-up of ozone in the lower atmosphere due to human activities.

In the recently published scientific assessment of global warming (IPCC 2001), the radiative impacts of a wide range of radiative forcing agents including greenhouse gases and aerosols and other forcing mechanisms have been quantified. In order of importance, carbon dioxide, methane and ozone are ranked as the three most important drivers of human-induced climate change over the century to 2100.

Ozone is not emitted directly into the atmosphere but is formed there by chemical reactions driven by sunlight involving the oxidation of carbon monoxide, methane and organic compounds in the presence of oxides of nitrogen. Ozone is present throughout the atmosphere but the ozone that contributes most to global warming is that found in the lower atmosphere, mainly in the middle and upper troposphere in the 5-10 km altitude range. Ozone is most strongly radiatively-active in the 5-10 km altitude range because ozone in this region has the maximum temperature contrast relative to the earth's surface. The chemical reactions that generate ozone involve carbon monoxide (CO), methane (CH_4), non-methane hydrocarbons (VOCs) and nitrogen oxides (NO_x), all trace gases with large man-made sources. It is anticipated that as these emissions continue to grow in line with the IPCC emission scenarios (Nakicenovic 2000), that the elevated ozone produced in the cold regions of the middle and upper troposphere will induce additional global warming. Since the Framework Convention on Climate

Change does not include ozone in its basket of greenhouse gases, then no global-scale emission controls are envisaged to contain this ozone build-up.

A surprising conclusion from the analysis performed by the IPCC (2001) was that surface ozone concentrations are also expected to increase through to the year 2100, in addition to upper tropospheric concentrations. So, for example, surface ozone concentrations during the summer months over the continental land masses are currently about 30-40 ppb. In the IPCC SRES A2 and A1FI emission scenarios, the corresponding values become 45-50 ppb in 2030, 60 ppb in 2060 and 70 ppb in 2100. These concentrations are well above the internationally-accepted environmental criteria values (WHO 1987) set to protect human health, sensitive crops and vegetation. This prospect is in store for all of the continental areas of the northern hemisphere, despite the strenuous measures being made to improve urban- and regional-scale ozone air quality in North America and Europe.

The mechanisms and processes leading to the steady increase anticipated in middle and upper tropospheric ozone concentrations have been steadily unravelled. Because of the low water vapour concentrations in the upper troposphere, ultraviolet photolysis is a relatively inefficient ozone destruction process and ozone lifetimes approach and exceed one to two months. Ozone becomes relatively well-mixed around latitude circles at this altitude and so any perturbation due to human activities rapidly spreads and assumes global proportions. Because ozone destruction is relatively inefficient, ozone production can proceed with relatively low NO_x concentrations (Jaegle et al. 2001). In the upper troposphere, NO_x and hence ozone production is controlled by aircraft emissions, convective updrafts bringing surface or biomass burning emissions, lightning and stratospheric injection (Derwent and Friedl 1999). Human influences will act through increased aircraft emissions and the increased supply of surface and biomass burning emissions through convection. In this context, the rapidly increasing Asian NO_x emissions have some particular significance for surface air quality in the western United States (Jacob et al. 1999).

Whilst the mechanisms underpinning the future global-scale increases in the middle and upper tropospheric ozone have been straightforward to unravel, those involved

with the increase in future surface ozone over the northern hemisphere continents have not. That this is not straightforward can be seen from Figures 4.1-4.3. These figures display model surface ozone concentrations from Johnson et al. (2001). The increasing future continental surface concentrations can be contrasted with near constant concentrations over the oceans. In the presence of NO_x, ozone production is stimulated in continental air masses and elevated ozone concentrations are often found in air mass flowing out of the continents and into oceanic regions during summertime. These elevations rapidly decrease as the polluted air masses travel out over the coastline, because of the short lifetime of NO_x. With increasing travel time, ozone production rapidly turns into ozone destruction. If the increased surface ozone concentrations over North America had been driven by the growth in Asian emissions, then this could not have involved increased intercontinental ozone transport at the surface because of ozone destruction over the Pacific Ocean. Similarly, ozone destruction over the North Atlantic Ocean would hinder intercontinental transport at the surface from North America to Europe.

Understanding the mechanisms underpinning the increase in future surface ozone concentrations shown in Figures 4.1-4.3 is intimately connected to our understanding of intercontinental transport. Transport of ozone is efficient and well-understood in the upper troposphere. Transit times around latitude circles at this altitude are of the order of several days. Convective processes in tropical and mid-latitude regions are important in lofting NO_x into the middle and upper troposphere (Pickering et al. 1988). Once there, NO_x can act as an efficient ozone source as one molecule of NO_x can form many ozone molecules during its lifetime. Weather systems in mid-latitudes with their associated fronts can provide another mechanism by which surface-emitted pollutants can be transported to the middle and upper troposphere (Stohl and Trickl 1999).The missing element of the story has been the identification of those meteorological processes that bring upper tropospheric air laden with ozone down to the surface over the continents. These processes may in turn involve convection and the large-scale weather systems that fill mid-latitudes of the troposphere. Man's activities will create a global-scale pool of increased upper tropospheric ozone and this in turn will bring increased surface ozone concentrations to all the Northern Hemisphere continents through the cycle of constantly changing weather patterns.
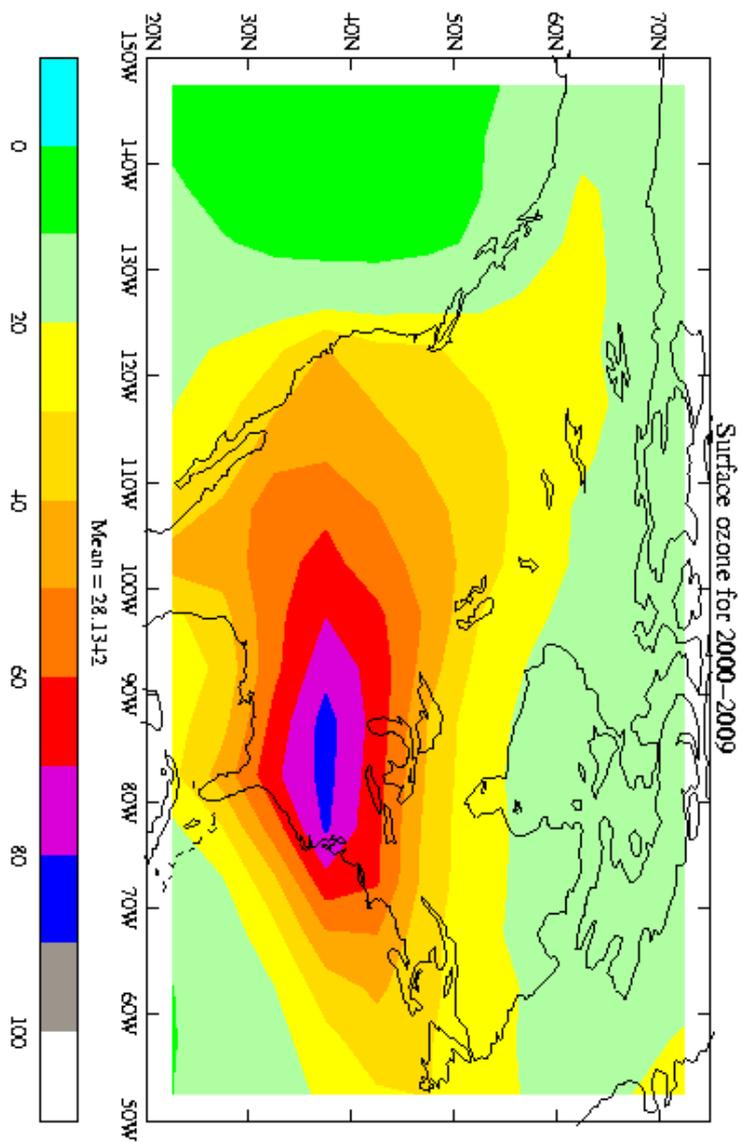
FIGURE 4.1. Surface ozone concentrations over North America during July in ppb for a). the year 2000.
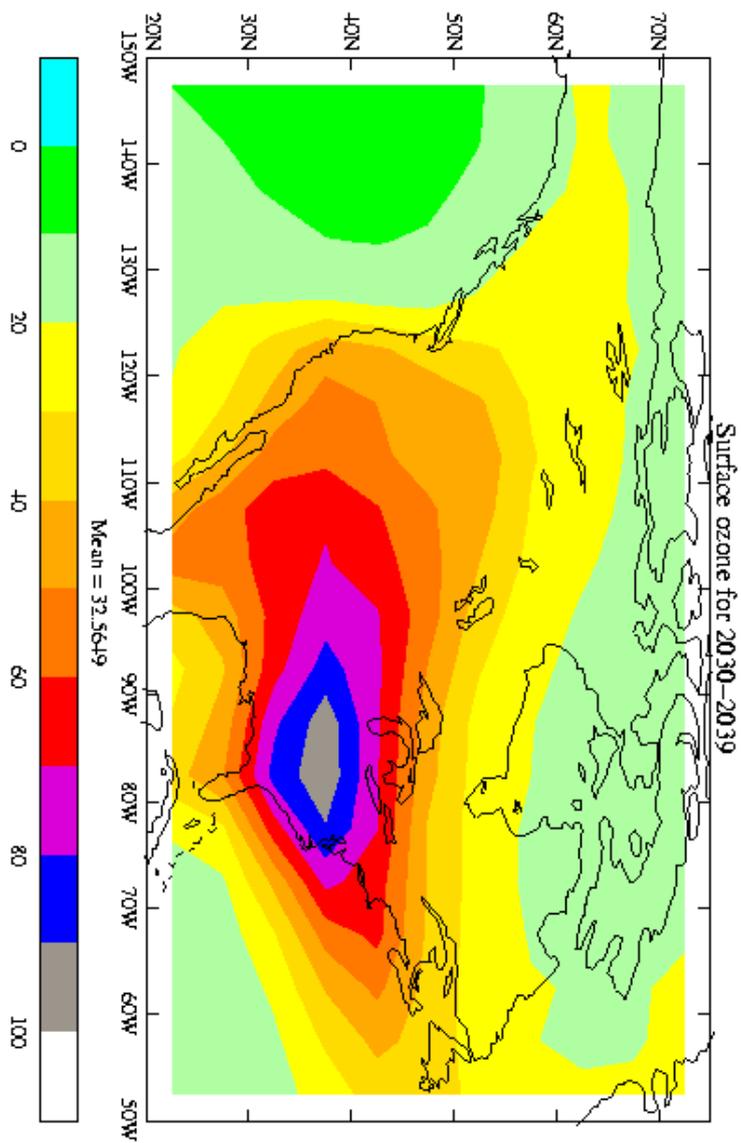
FIGURE 4.1. (Cont.) Surface ozone concentrations over North America during July in ppb for b). the year 2030.
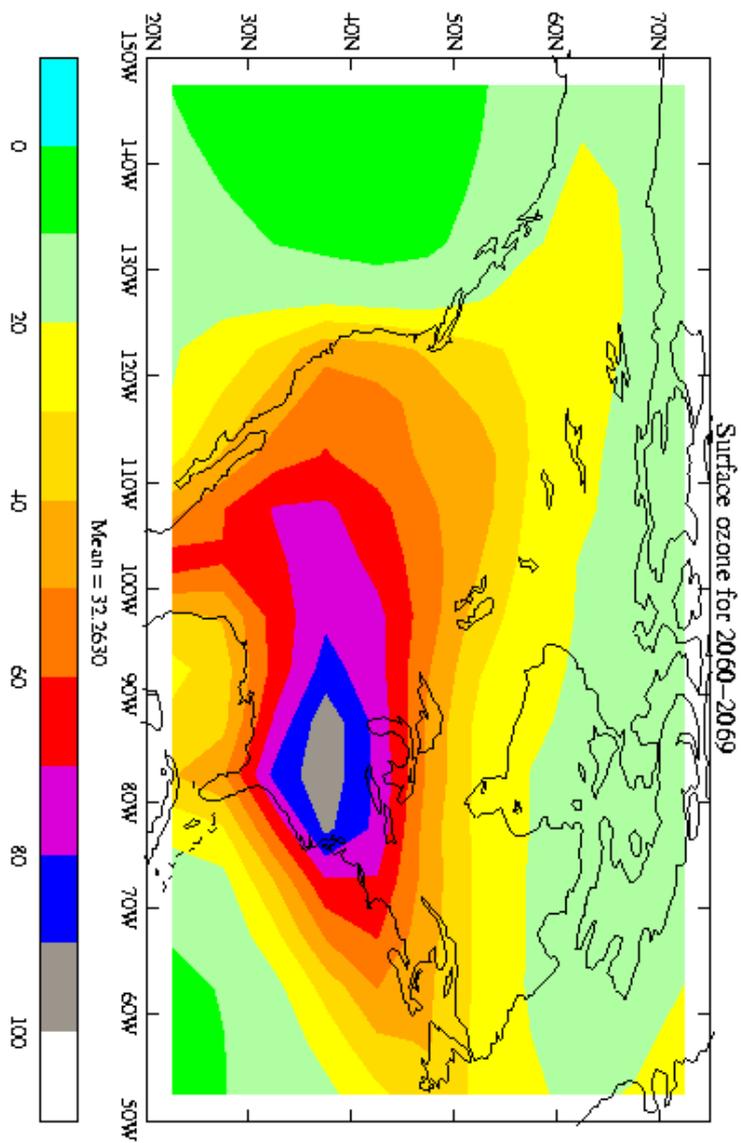
FIGURE 4.1. (Cont.) Surface ozone concentrations over North America during July in ppb for c). the year 2060.
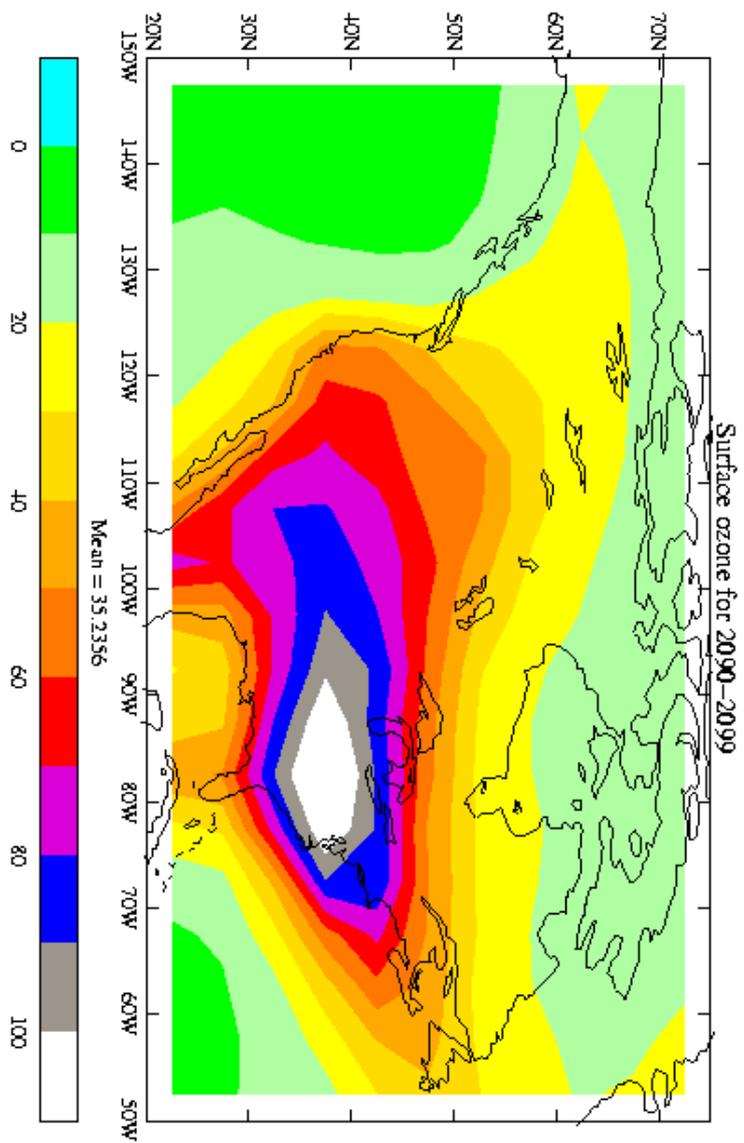
FIGURE 4.1. (Cont.) Surface ozone concentrations over North America during July in ppb for d). the year 2090.
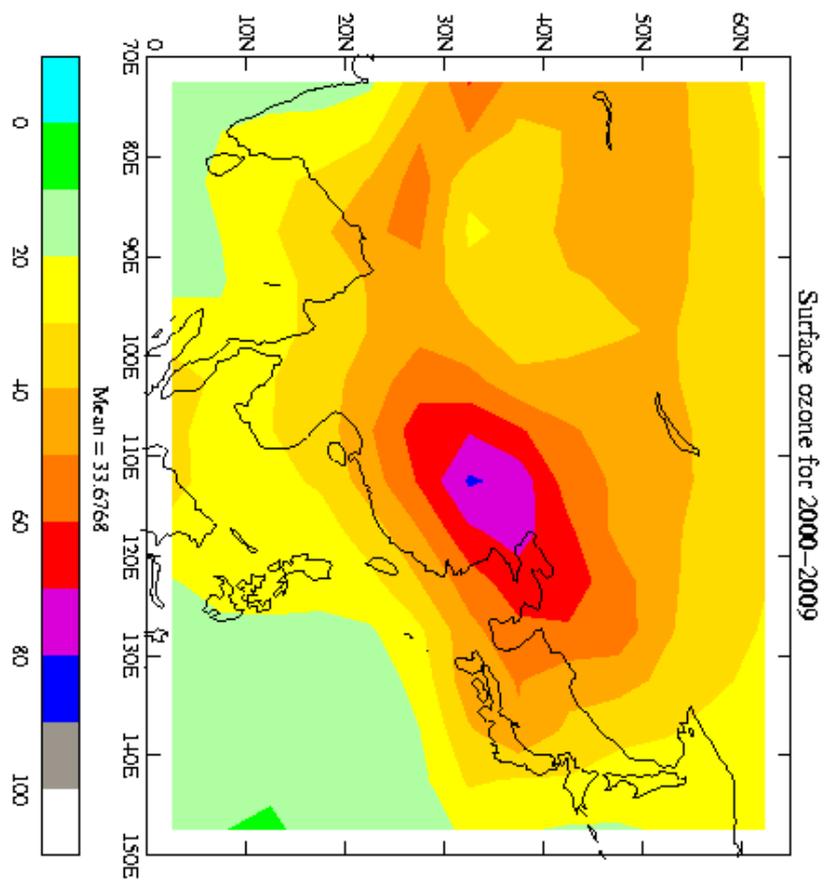
FIGURE 4.2. Surface ozone concentrations over Asia during July in ppb for a). the year 2000.
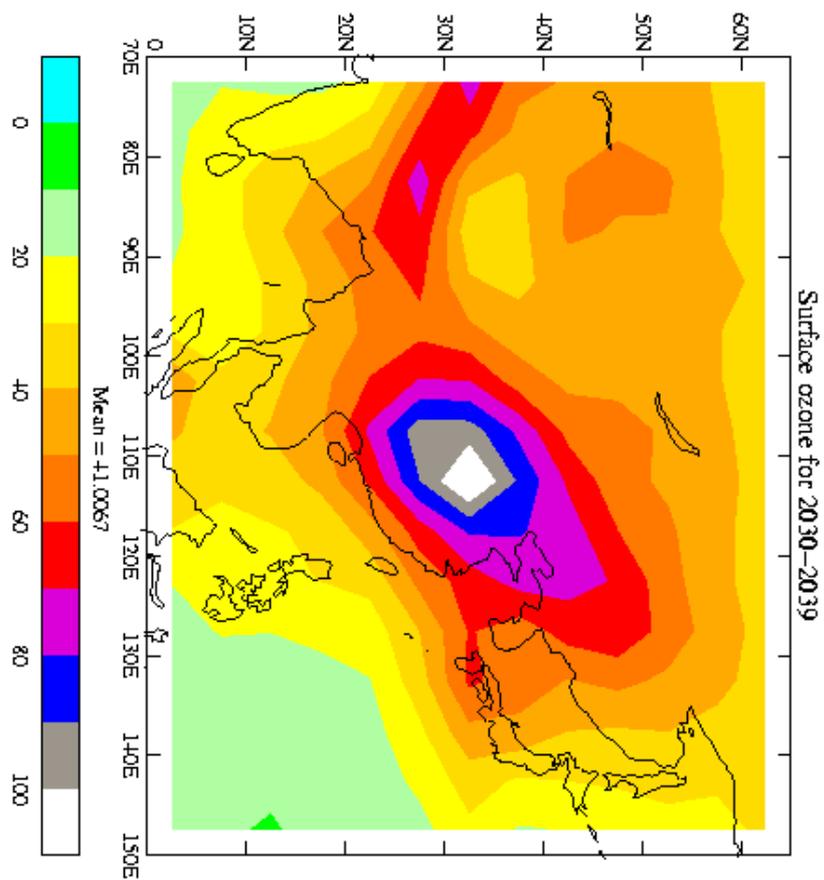
FIGURE 4.2. (Cont.). Surface ozone concentrations over Asia during July in ppb for b). the year 2030.
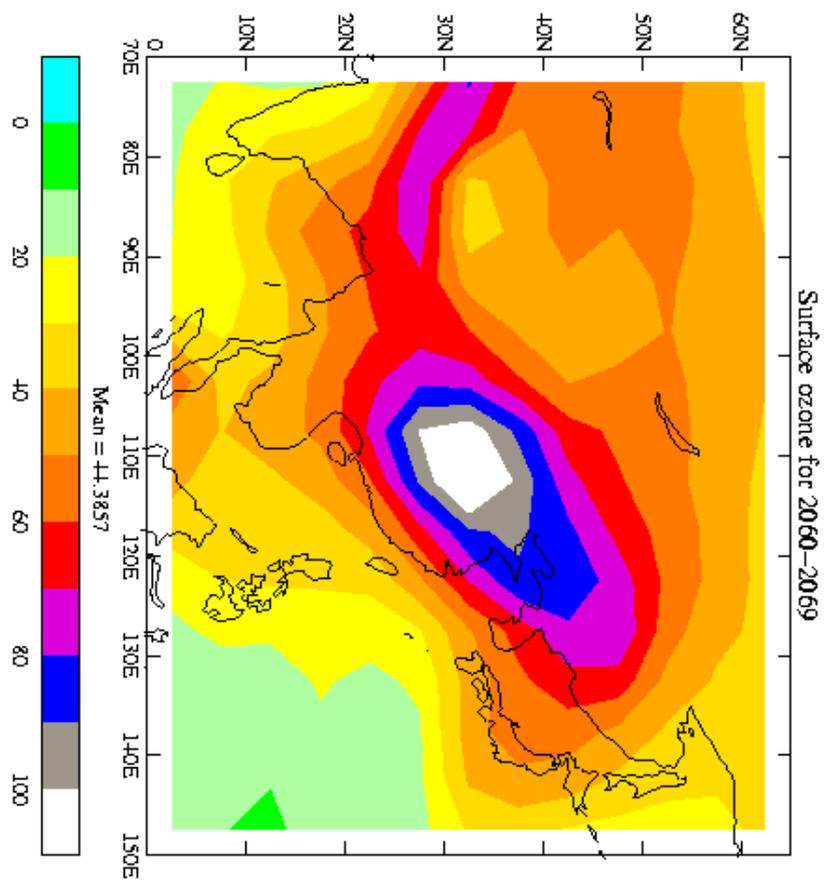
FIGURE 4.2. (Cont.). Surface ozone concentrations over Asia during July in ppb for c). the year 2060.
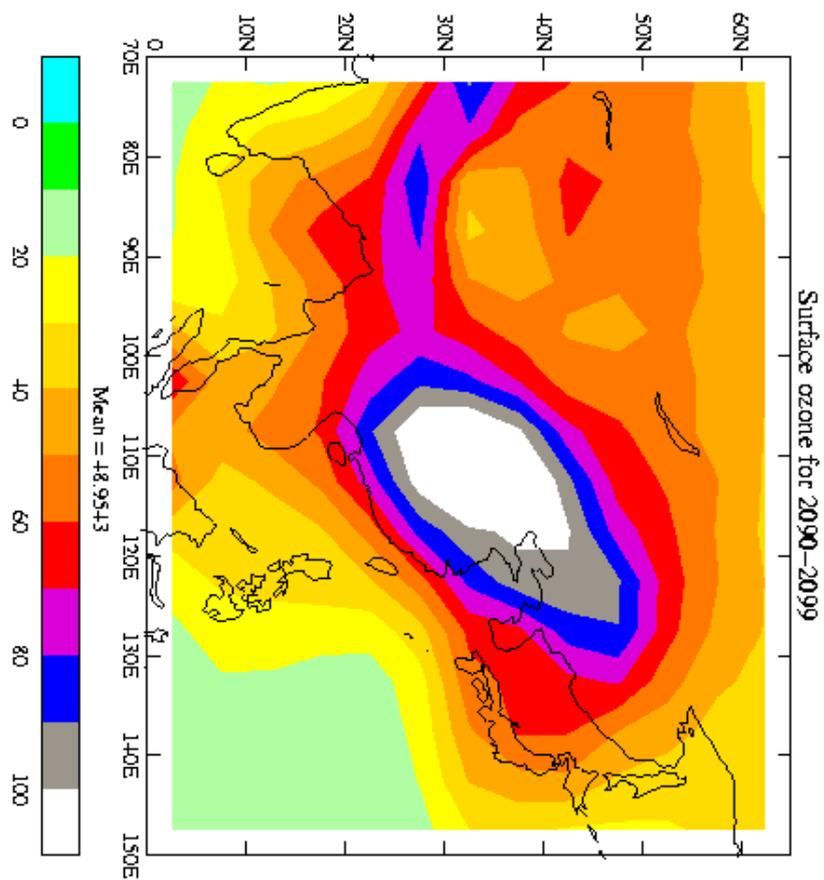
FIGURE 4.2. (Cont.). Surface ozone concentrations over Asia during July in ppb for
d). the year 2090.
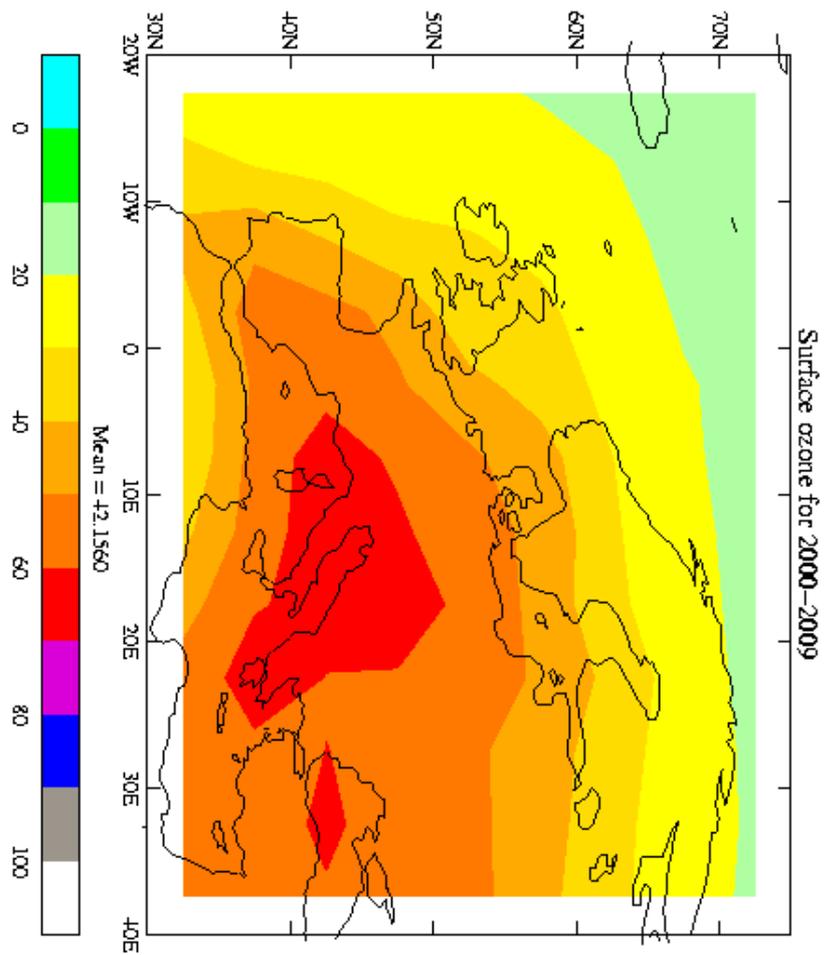
FIGURE 4.3. Surface ozone concentrations over Europe during July in ppb for a). the year 2000.
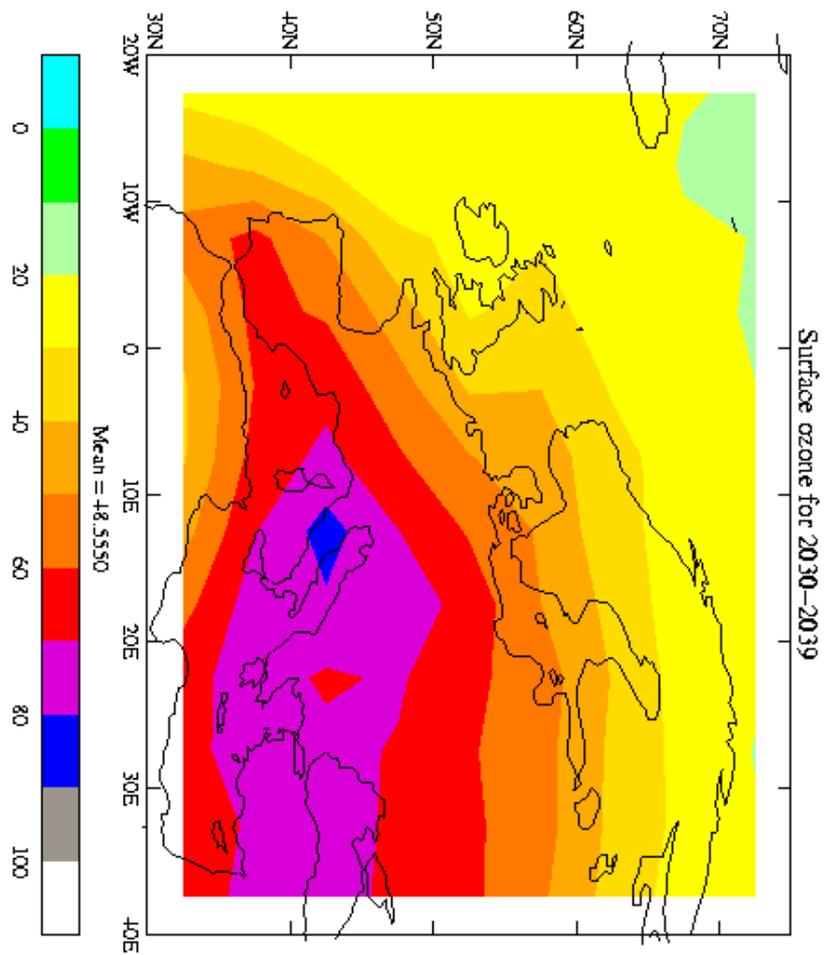
FIGURE 4.3. (Cont.). Surface ozone concentrations over Europe during July in ppb for b). the year 2030.
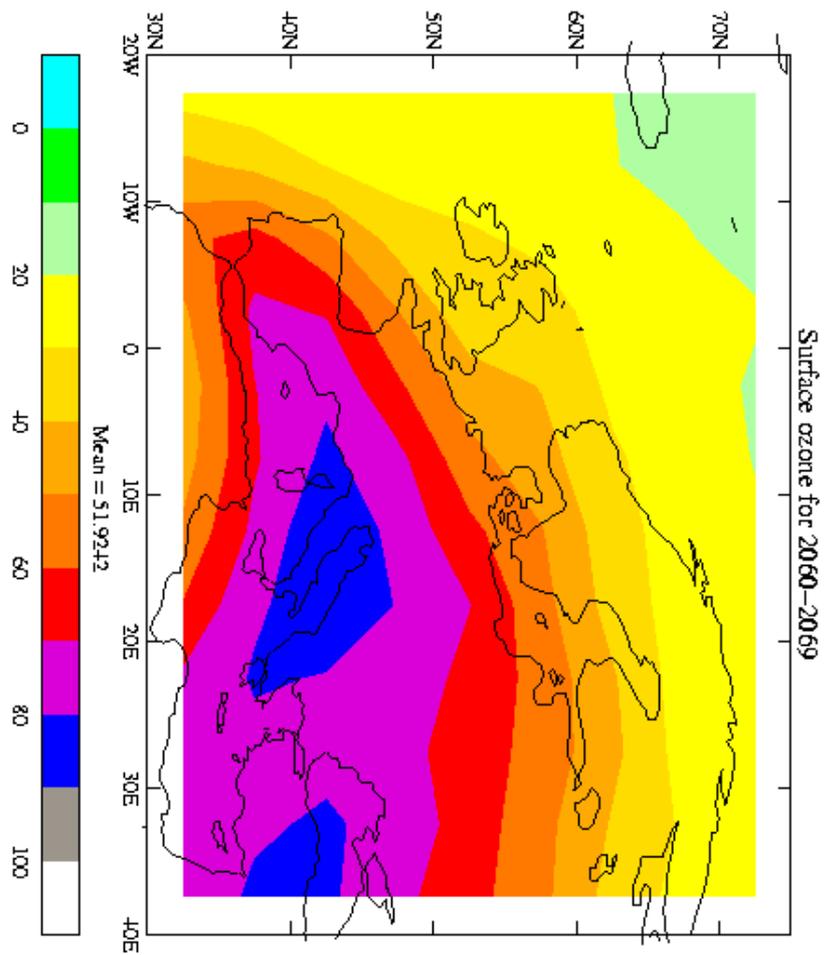
FIGURE 4.3. (Cont.). Surface ozone concentrations over Europe during July in ppb for c). the year 2060.
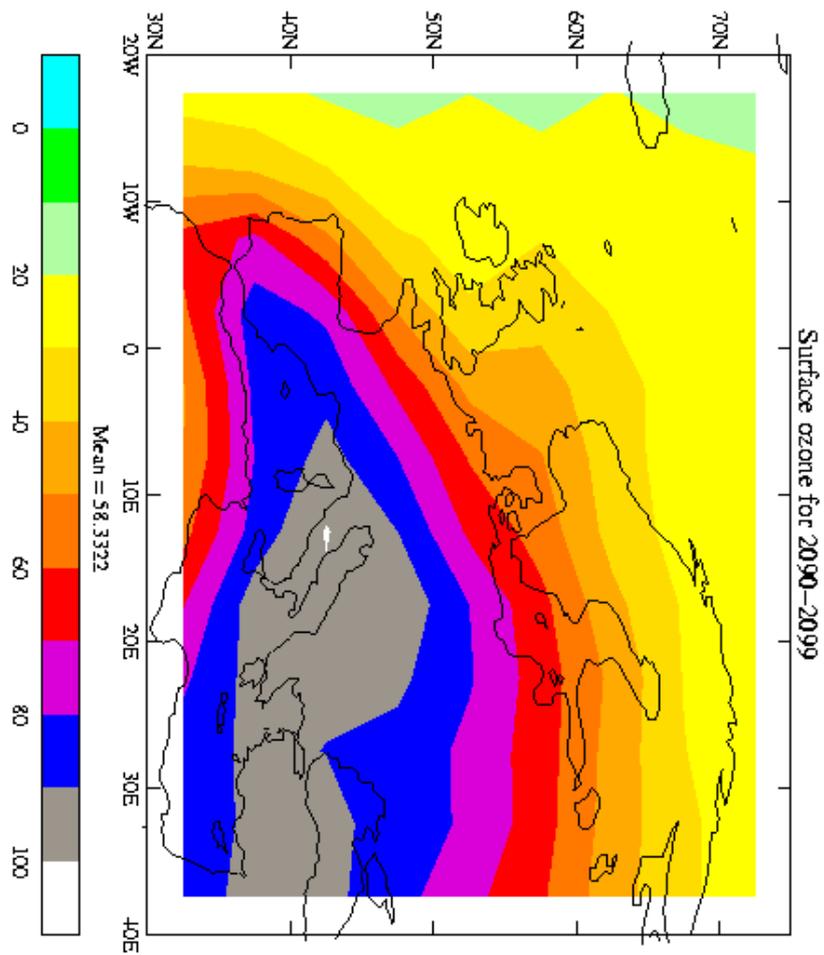
FIGURE 4.3. (Cont.). Surface ozone concentrations over Europe during July in ppb for d). the year 2090.

These ozone increases are more directly relevant to the long term exposure levels of crops and vegetation than to human exposures. However, urban- and regional-scale pollution episodes are built upon these global baseline values. Their future increase may therefore work against regional pollution control strategies, set to reduce exposure levels of both man and vegetation.

4.2 Intercontinental Transport of Ozone and its Global and Regional Distributions

4.2.1 Ozone Tracer Labelling

Each of the 50 000 Lagrangian air parcels carried the mixing ratio of each of 75 model species. The mixing ratio, x_i, of species, i, were calculated with a differential equation of the form:

$$dx_i / dt \ = \ P_i \ - L_i x_i \qquad \qquad \text{(Equation 4.1)}$$

The production rate P_i for each species was calculated at each time step from the local, instantaneous rates of emission and chemical production from the set of 180 reactions. The loss rate $L_i x_i$ for each species was calculated from the local, instantaneous destruction rate due to chemical reaction, dry and wet deposition and aerosol scavenging.

In STOCHEM we have in addition to ozone, additional forms of ozone, such as O_3^A, O_3^B, O_3^C …, in which ozone is labeled by the geographical region in which the ozone was formed, such that:

$$P_{O3} = P_{O3}{}^A \ + \ P_{O3}{}^B \ + \ P_{O3}{}^C \ + \ … \qquad \qquad \text{(Equation 4.2)}$$

Each additional form of ozone has the same loss coefficient, Li, so that:

$$x_{O3} \ = \ x_{O3}{}^A \ + \ x_{O3}{}^B \ + \ x_{O3}{}^C \ + \ … \qquad \qquad \text{(Equation 4.3)}$$

which is to say that the sum of all of the mixing ratios of the different forms of ozone in each air parcel adds up to the overall mixing ratio of ozone. We will call this quantity total ozone to differentiate it from the additional labeled forms of ozone.

The total ozone production rate has the form:

$$P_{O3} = k_1[O][O_2][M] + E_{STE} \qquad \text{(Equation 4.4)}$$

$$O + O_2 + M = O_3 + M \qquad \text{(Reaction 4.1)}$$

where k_1 is the rate coefficient for reaction 1 and E_{STE} is the local, instantaneous ozone production rate from stratosphere-troposphere exchange. If the label A represents ozone of stratospheric origins then:

$$P_{O3}{}^{A} = E_{STE} \qquad \text{(Equation 4.5)}$$

The origins of the other ozone tracer labels involve the rate of production of oxygen atoms through reaction 1 above. Oxygen atoms in the ground electronic state (O^3P) and electronically-excited (O^1D) oxygen atoms are linked to ozone by the following reactions (4.2) to (4.5) in addition to reaction (4.1):

$$O_3 + h\nu = O + O_2 \qquad \text{(Reaction 4.2)}$$
$$O_3 + h\nu = O^1D + O_2 \qquad \text{(Reaction 4.3)}$$
$$O^1D + M = O + M \qquad \text{(Reaction 4.4)}$$
$$O^1D + H_2O = OH + OH \qquad \text{(Reaction 4.5).}$$
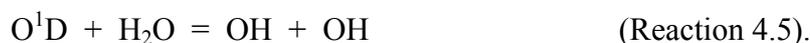
In addition, oxygen atoms and ozone are linked to nitric oxide and nitrogen dioxide by the photostationary state reactions:

$$NO_2 + h\nu = NO + O \qquad \text{(Reaction 4.6)}$$
$$NO + O_3 = NO_2 + O_2 \qquad \text{(Reaction 4.7)}$$
$$NO + HO_2 = OH + NO_2 \qquad \text{(Reaction 4.8)}$$
$$NO + RO_2 = RO + NO_2 \qquad \text{(Reaction 4.9).}$$

The differential equation representing the ozone mixing ratio becomes:

$$dx_{O3}/dt = k_1[O][O_2][M] - k_2[O_3] - k_3[O_3] - \text{other } O_3 \text{ loss terms} \quad \text{(Equation 4.6)}$$

where the other loss terms for ozone involve loss through its reactions with OH, HO_2, NO_2 and its ozonolysis reactions with ethylene, proylene and isoprene. Putting electronically excited oxygen atoms and ground state oxygen atoms in steady state, then:

$$= k_6[NO_2] - k_3[O^1D][H_2O] - \text{other } O_3 \text{ loss terms} \quad \text{(Equation 4.7)}$$

Applying the photostationary state, then:

$$dx_{O3}/dt = k_8[HO_2][NO] + k_9[RO_2][NO] - k_3[O^1D][H_2O]$$
$$- \text{other } O_3 \text{ loss terms} - \text{other } NO_2 \text{ loss terms} \quad \text{(Equation 4.8)}$$

where the other NO_2 loss terms include its reactions with OH, peroxy acyl radicals, NO_3 radicals and ozone. The two terms $k_8[HO_2][NO]$ and $k_9[RO_2][NO]$ were then used to drive the rate of ozone production of the ozone tracer labels. If the air parcel was located in the air column above the geographical region of North America, then:

$$P_{O3}^{B} = k_8[HO_2][NO] + k_9[RO_2][NO], \quad \text{(Equation 4.9)}$$

and if the air parcel was located over Europe, then:

$$P_{O3}^{C} = k_8[HO_2][NO] + k_9[RO_2][NO] \quad \text{(Equation 4.10)}$$

And, if the air parcel was located over Asia, then:

$$P_{O3}^{D} = k_8[HO_2][NO] + k_9[RO_2][NO], \quad \text{(Equation 4.11)}$$

otherwise, $P_{O3}{}^E = k_8[HO_2][NO] + k_9[RO_2][NO]$. Since the selected regions fill the entire model domain, then the tracers satisfy equation (4.2) and the mixing ratios of the ozone tracers could be determined along with the other 73 model species.

4.2.2 Comparison of Model with Observed Seasonal Cycles in Europe

Because this study focusses on the origins of ozone observed at the surface in Europe, attention is first given to how well the STOCHEM model describes the seasonal cycle of ozone across Europe. Here, the model results for ozone of all origins are used, the results for the so-called 'total ozone'. The chosen model quantity is the daily maximum ozone calculated for each particular location. Since STOCHEM is a Lagrangian model with a rather limited number of air parcels, uniform and complete cell occupancy is not guaranteed and there may not be an air parcel close to each particular location at each time-step. A record is kept of the air parcels which are in the vicinity of particular locations and their ozone mixing ratios are noted at each time step when they are close enough. Figure 4.4 plots out the highest of the ozone mixing ratios in ppb (1 part in 10^9 parts by volume) during each day of 1998 at each of 21 selected site locations in the EMEP ozone monitoring network (Hjellbrekke 2000). Over the set of 21 site locations, model points are plotted for 87% of the days in 1998.

Also plotted on Figure 4.4, as stepped lines are the observed monthly mean daily maximum ozone mixing ratios from the EMEP network database for each site location, also for 1998 taken from Hjellbrekke (2000). The model points appear to scatter around the line at most sites during much of the year. Clearly, there are problems with the observations at Laheema in Finland, Monte Vehlo in Portugal and Starina in Slovakia. Otherwise, the model is well able to describe the observed seasonal cycles at each of the 21 selected locations. The 21 locations out of the 97 available were chosen to achieve a broad representation of the reporting countries within the EMEP network and to avoid, if possible, mountain-top and high altitude locations that may have strong, local mesoscale meteorological influences that would not be captured by the coarse-scale chemistry-transport model. Details of the latitudes, longitudes, siting criteria and measurement techniques for the 21 remote rural locations are given in Hjellbrekke (2000).
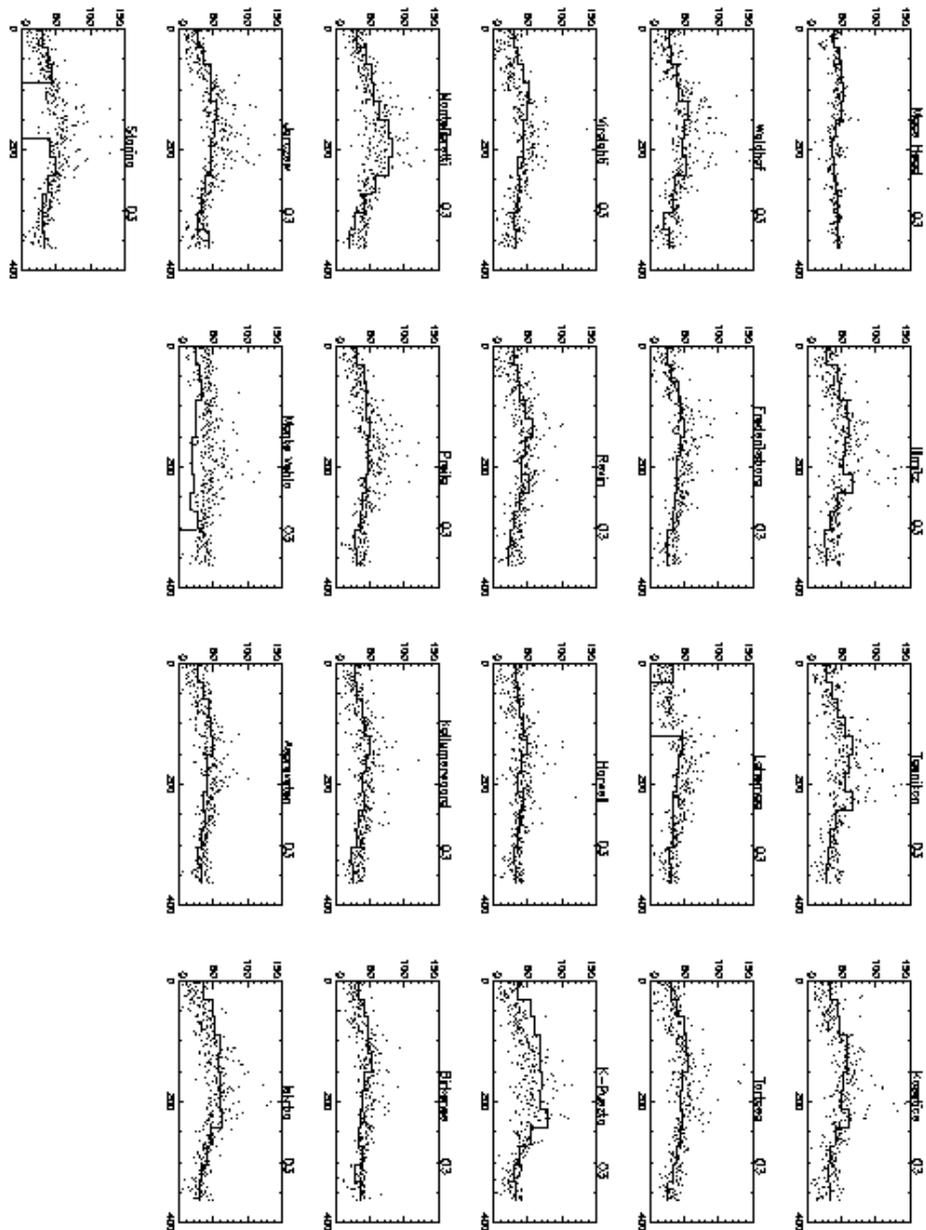
FIGURE 4.4. Observed mean monthly daily maximum ozone concentrations and daily maximum model calculated ozone concentrations for 1998 at 21 selected EMEP ozone monitoring network sites in Europe.

Seasonal cycles are a common feature of most surface ozone time series. Spring-time maxima have been observed at some surface sites and most mountain-top sites in Europe and were originally attributed to stratosphere-troposphere exchange. Summertime maxima are seen at most central European sites and are attributed to European photochemical ozone production. Seasonal cycles are clearly evident in both observations and model results in Figure 4.4. At most sites, summertime ozone peaks dominate the seasonal patterns. However at some of the more sites, secondary maxima are apparent during the springtime. Such maxima are evident in Figure 4.4 at Mace Head in Ireland, Frederiksborg in Denmark, Laheema in Estonia, Tortosa in Spain, Virolahti in Finland, Revin in France, Harwell in the United Kingdom, Preila in Lithuania, Kollumerwaard in Netherlands, Birkenes in Norway, Jarczew in Poland and Aspreveten in Sweden. At each of these locations, the model points also show elevated spring-time levels. At Illmitz in Austria, Taenikon in Switzerland, Kosetice in Czech Republic, K-puszta in Hungary, Waldhof in Germany, Montilibretti in Italy, and Iskrba in Slovenia, the observations reveal a summertime maximum that is also reproduced faithfully by the model.

On this basis, it is concluded that the model exhibits some skill in reproducing qualitatively the observed seasonal cycles at a range of selected site locations in Europe. A clear geographical pattern has emerged from both the observations and the model calculations, with summertime maxima dominating in the Mediterranean region and central Europe and with some evidence of secondary springtime maxima in Scandinavia, and in the Atlantic Ocean fringes of north and west Europe.

In Table 4.1, the seasonal cycles in the observations and in the model calculations are compared in a more rigorous manner. To do this, the average of all the model results for each site during each month are calculated. The averages of the 12 monthly values for the observations and model results are then tabulated. The biases, (model-observation) are calculated for each month and then averaged over the year. This average bias is then expressed as a fraction of the mean of the observations. A normalised mean square error is calculated from the 12 monthly results using:

$$\sum_{n=12} (model - obs)^2 \ / \ (mean_{model} * mean_{obs})$$

TABLE 4.1. Summary of the comparison of observed and model calculated monthly mean daily maximum ozone concentrations at 21 selected locations across Europe in 1998.

Location	Model mean, ppb	Obs mean, ppb	Mean bias, ppb	Mean fractional bias, ppb	Normalised mean square error	Fraction within ± 20%
Mace Head	40.7	42.8	-2.06	-0.049	0.0156	0.92
Illmitz	45.6	44.3	1.31	0.029	0.0490	0.42
Taenikon	41.4	44.6	-3.20	-0.074	0.0436	0.58
Kosetice	43.2	44.1	-0.88	-0.020	0.0357	0.67
Waldhof	39.2	37.0	2.23	0.059	0.0351	0.67
Frederiksborg	37.7	34.6	3.06	0.085	0.0451	0.33
Laheema	33.8	34.2	-0.43	-0.013	0.0886	0.33
Tortosa	44.3	41.0	3.34	0.078	0.0319	0.67
Virolahti	33.3	38.5	-5.24	-0.146	0.1126	0.58
Revin	39.3	37.9	1.43	0.037	0.0417	0.67
Harwell	37.8	37.1	0.77	0.020	0.0133	0.92
K-puszta	44.4	54.9	-10.49	-0.211	0.1063	0.50
Montelibretti	49.0	51.4	-2.39	-0.047	0.0454	0.58
Preila	39.2	38.7	0.46	0.012	0.0538	0.33
Kollumerwaard	36.3	34.4	1.90	0.054	0.0418	0.58
Birkenes	38.6	38.1	0.48	0.012	0.0543	0.58
Jarcsew	42.8	40.9	1.83	0.044	0.1093	0.25
Monte Vehlo	40.7	23.6	17.07	0.531	0.3727	0
Aspreveten	36.7	36.6	0.09	0.003	0.0595	0.42
Iskrba	44.5	48.0	-3.48	-0.075	0.0506	0.67
Starina	43.1	36.3	6.77	0.170	0.0985	0.11

The fraction of the model results for each month that are within the range of the observation – 20% and observation + 20% (about ± 7 ppb) are then tabulated. Clearly the entries in Table 4.1 for K-puszta in Hungary and Monte Vehlo in Portugal have been unduly affected by the incomplete observational record for these sites during 1998.

Taking the sites highlighted above with the clearly observed springtime maxima, mean biases fall in the range –2.06 to 3.34 ppb, -5 % to 8.5 %, with an average of 1.3 ppb. The sites showed a wide range in performance as indicated by the fraction of monthly means within ± 20%, from 0.11 to 0.92 and the normalised mean square errors from 0.02 to 0.11. For the sites highlighted for their summertime maxima, mean biases fell in the range –3.5 to 2.2 ppb, -7.5 % to 5.9%, with an average of –1.1 ppb. They showed a much narrower range in performance compared to the sites with spring-time maxima, as indicated by the fraction of monthly means within ± 20% of 0.42 to 0.67, and normalised mean square errors of 0.035 to 0.051.

Taking the springtime and summertime maxima sites together, it appears that the model is capable of reproducing observed mean daily maximum surface ozone mixing ratios with an accuracy of ± 1.3 ppb, or so, during 1998 and about two-thirds of individual monthly mean values within ± 20% of the observations. This is a workable level of model performance that gives some confidence in the model-derived continental attributions which follow.

4.2.3 Intercontinental Attribution of the Origins of Surface Ozone in Europe

By using the tracer-labelling technique, the model is able to give an indication of the geographical origins of where the ozone was produced in each air parcel which has arrived at each location. By averaging over all the air parcels arriving during 1998, a picture has been built up of the geographical origins of the ozone calculated for each of the 21 selected locations and this is presented in Table 4.2. Broadly speaking, adding up the columns across Table 4.2 gives the annual mean 'total' model ozone mixing ratio and these fall in the range 30-45 ppb. As the previous section shows, these 'total' values are directly comparable with the surface observations. The

columns in Table 4.2, present our best estimate from the model of the ozone mixing ratios that can be attributed to the particular source regions.

TABLE 4.2. Contributions to the annual mean daily maximum ozone concentrations in ppb from the different source areas calculated for 21 selected locations across Europe.

Location	Stratosphere-troposphere	Europe	North America	Asia

Contributions in ppb

Location	Stratosphere-troposphere	Europe	North America	Asia
Mace Head	10.6	9.5	12.2	6.6
Illmitz	6.9	27.4	7.7	3.9
Taenikon	7.0	22.2	8.4	4.4
Kosetice	7.5	24.5	8.3	4.4
Waldhof	7.7	21.5	8.5	4.7
Frederiksborg	7.8	16.8	8.1	5.0
Laheema	6.0	16.9	5.9	4.2
Tortosa	6.9	21.8	9.2	4.0
Virolahti	5.8	15.9	5.8	4.2
Revin	8.0	18.3	9.5	4.9
Harwell	8.8	15.1	10.8	5.3
K-puszta	6.1	27.8	7.0	3.7
Montelibretti	6.2	31.5	6.9	3.5
Preila	7.3	19.7	7.1	4.7
Kollumerwaard	8.7	15.9	9.5	5.5
Birkenes	8.2	15.2	8.8	5.6
Jarcsew	6.3	26.6	6.9	3.8
Monte Vehlo	7.5	16.6	9.7	4.2
Aspreveten	7.5	16.5	7.4	4.9
Iskrba	5.7	28.6	6.7	3.6
Starina	6.2	25.2	7.2	3.8
Average	7.3	20.7	8.2	4.5

The annual mean ozone mixing ratios at the 21 selected locations across Europe due to stratosphere-troposphere exchange fell in the range from 5.7-10.6 ppb, with Iskrba at the lowest end and Mace Head at the highest end of the range. Mace Head being the westerly most location, is the location that is most exposed to the weather systems travelling up the North Atlantic Ocean. These weather systems are thought to account for much of the stratosphere-troposphere exchange found in northerly midlatitudes. Iskrba, on the other hand, is one of the easterly most locations in Table 4.2 and is thus farthest removed from the influence of the weather systems travelling up the North Atlantic Ocean Averaged over the 21 locations and over 1998, stratosphere-troposphere exchange contributed about 7.3 ppb to surface ozone mixing ratios over Europe.

Table 4.2 indicates that the bulk of the ozone calculated in air parcels arriving at the 21 selected locations carried the 'European' label. The European contribution in the third column of Table 4.2, covered the range 9.5-31.5 ppb, with Mace Head at the lowest and Montelibretti at the highest end of the range. Mace Head is the location in Table 4.2 with the least exposure to European regionally-polluted air masses, receiving European air on 32% of occasions during the 1990-1994 period (Simmonds et al. 1997). Montelibretti, on the other hand, is surrounded by centres of European population and industry in all directions and so is greatly influenced by European ozone production. Averaged over the 21 locations and 1998, European ozone production contributed about 20.7 ppb to surface ozone mixing ratios over Europe and provided the largest single source area contribution.

The North American continental region contributed surface ozone mixing ratios over Europe in the range 5.8-12.2 ppb, as shown by the fourth column of Table 4.2. Virolahti and Laheema, both Baltic Sea locations, received the least North American contribution and Mace Head the highest. As we have remarked above, Mace Head is the location most exposed to the weather systems moving up the North Atlantic Ocean and these systems appear to provide a mechanism for the intercontinental transport of ozone as well as stratosphere-troposphere exchange. The behaviour seen for stratosphere-troposphere exchange and North American intercontinental transport appear somewhat different pointing perhaps to different geographical patterns in

influence from these two mechanisms across Europe. Averaged over the 21 locations and 1998, North American continental ozone production contributed about 8.2 ppb to surface ozone mixing ratios over Europe.

The Asian continental region contributed surface ozone mixing ratios in the range 3.5-6.6 ppb, as shown in the fifth column of Table 4.2. Montelibretti and Iskrba received the least Asian contribution and Mace Head the highest. The spatial pattern of the contributions from Asian sources and stratosphere-troposphere exchange show similarities, confirming the possible importance of North Atlantic weather systems. Averaged over the 21 locations and 1998, Asian continental ozone formation contributed about 4.5 ppb to surface ozone mixing ratios over Europe.

4.2.4 Sensitivity of the Intercontinental Attribution of Ozone in Europe to Global Emission Source Strengths

In this section, the sensitivities of the model surface ozone mixing ratios in Europe to the global emission source strengths of carbon monoxide and NO_x are examined. They were studied by reducing by one half the global man-made source strengths in two separate model experiments. The 50% reductions were applied across-the-board, with no geographical or seasonal dependence.

Table 4.3 presents the impact of an across-the-board 50% reduction in global man-made NO_x emissions at each of the 21 selected locations on the ozone mixing ratios attributed to each continental source region. The absolute reductions in NO_x emissions in each continental region were roughly similar at about 10 million tonnes as NO_x per year. No entries are provided for stratosphere-troposphere exchange because the ozone mixing ratios from this source were unaffected by the reductions in carbon monoxide or NO_x emissions. The reductions in ozone mixing ratios due to the 50% reduction in global NO_x emissions were largest for the European source region, 0.9-4.3 ppb, least for the Asian source region, 0.5-0.7 ppb, with North America 0.8-1.9 ppb. On a percentage change basis, the reductions in surface ozone attributed to the European source region were between 6-18%, to North America, 14-16% and to Asia, 12-14%. The percentage changes were broadly similar in the ozone attributed to the different continental source regions but with that for Europe somewhat the smallest.

TABLE 4.3. The impact on the contribution to the annual mean daily maximum ozone concentrations from each source area following a 50% reduction in global man-made NO$_x$ emissions.

Location	Europe	North America	Asia

Changes in contributions in ppb

Location	Europe	North America	Asia
Mace Head	1.2	1.9	0.9
Illmitz	4.2	1.2	0.5
Taenikon	3.1	1.3	0.6
Kosetice	3.3	1.3	0.6
Waldhof	1.7	1.3	0.6
Frederiksborg	2.1	1.2	0.7
Laheema	2.6	0.8	0.5
Tortosa	4.0	1.5	0.6
Virolahti	2.4	0.9	0.5
Revin	2.0	1.4	0.7
Harwell	1.0	1.7	0.7
K-puszta	4.3	1.1	0.5
Montelibretti	5.4	1.1	0.5
Preila	2.6	1.1	0.6
Kollumerwaard	0.9	1.5	0.7
Birkenes	2.3	1.3	0.7
Jarcsew	3.6	1.0	0.5
Monte Vehlo	3.0	1.5	0.6
Aspreveten	2.3	1.1	0.7
Iskrba	4.0	1.0	0.5
Starina	3.8	1.1	0.5
Average	2.8	1.3	0.6

TABLE 4.4. The impact on the contribution to the annual mean daily maximum ozone concentrations from each source area following a 50 % reduction in global man-made CO emissions.

Location	Europe	North America	Asia

Changes in contributions in ppb

Location	Europe	North America	Asia
Mace Head	0.3	0.3	0.2
Illmitz	0.7	0.2	0.1
Taenikon	0.6	0.2	0.1
Kosetice	0.7	0.2	0.1
Waldhof	0.6	0.2	0.1
Frederiksborg	0.5	0.2	0.1
Laheema	0.4	0.1	0.1
Tortosa	0.5	0.2	0.1
Virolahti	0.4	0.1	0.1
Revin	0.5	0.2	0.1
Harwell	0.4	0.3	0.1
K-puszta	0.7	0.2	0.1
Montelibretti	0.8	0.2	0.1
Preila	0.5	0.2	0.1
Kollumerwaard	0.4	0.2	0.1
Birkenes	0.4	0.2	0.1
Jarcsew	0.7	0.2	0.1
Monte Vehlo	0.4	0.2	0.1
Aspreveten	0.4	0.2	0.1
Iskrba	0.7	0.2	0.1
Starina	0.6	0.2	0.1
Average	2.8	1.3	0.6

The impact of an across-the-board 50% reduction in global man-made carbon monoxide emissions on the surface ozone attributed to each continental source region are presented in Table 4.4, for each of the 21 selected locations. The reductions in ozone mixing ratios were again largest for the ozone attributed to the European source region, 0.4-0.8 ppb, least for the Asian source region, 0.1-0.2 ppb, with North American ozone reduced by 0.1-0.3 ppb. On a precentage basis, a 50% reduction in carbon monoxide emissions reduced surface ozone from Europe by 2.3-3.2%, from North America by 1.7-3.0% and from Asia by 1.8-3.0%. These responses to a 50% reduction in CO emissions appear to be largely independent of ozone production region, on a percentage basis.

4.3 Influence of Regional Emission Controls on the Global-scale Build-up of the Greenhouse Gases.

The STOCHEM model has been used to look at the global scale impact of NO_x and CO emissions on the build-up of the greenhouse gases: methane and ozone. The build-up of methane is controlled by competition between its emissions and its destruction by tropospheric OH radicals:

$OH + CH_4 = $ removal
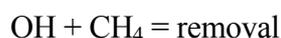
Any process which acts to increase the tropospheric OH abundance will act to increase methane removal and decrease it build-up. Equally well, any process which acts to decrease the tropospheric OH abundance will increase its build-up. Increasing carbon monoxide emissions act to decrease the tropospheric OH abundance through:

$OH + CO = HO_2 + CO_2$
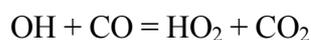
and so increase methane build-up. Increasing NO_x emissions, increase the tropospheric OH aboundance through:

$HO_2 + NO = OH + NO_2$
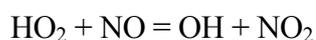
and so decrease the methane build-up. Increasing both CO and NO_x emissions, however, lead to increased ozone production and hence increases in the build-up of ozone.

By changing the location and season of an emitted pulse of NO_x or CO, differing impacts on methane and ozone build-up have been found for pulses emitted in Europe, North America and Asia.

TABLE 4.5. Global methane and ozone responses to 40 Tg yr^{-1} emission pulses of carbon monoxide emitted in each continent and month.

Pollutant	Continent	Season	Integrated excess CH_4 burden, Tg years	Integrated excess O_3 burden, Tg years

Pollutant	Continent	Season	Integrated excess CH_4 burden, Tg years	Integrated excess O_3 burden, Tg years
CO	N America	January	23.87	0.4905
		July	23.48	0.4800
	Asia	January	24.09	0.5178
		July	22.64	0.7790
	Europe	January	23.82	0.4658
		July	22.83	0.4034

For CO pulses of 40 Tg yr^{-1} each, slightly differing model global methane and ozone responses have resulted, see Table 4.5 below. The differences in the integrated excess methane burdens are probably within the model error bounds for the different seasons and continents. However, the differences in integrated excess ozone burdens show differences that are beyond the model error bounds for the different seasons and continents.

For NO_x emission pulses of 2 Tg N yr^{-1} each, the globally-integrated methane responses are the most negative for pulses emitted in Asia, followed by North America and least for European pulses. Globally-integrated ozone responses are largest for Asia and least for Europe, see Table 4.6, below. The different model responses to NO_x emission pulses

in the different continents and seasons span a factor of four or more and are much greater than the differences found for CO emission pulses.

TABLE 4.6. Global methane and ozone responses to 2 Tg N yr^{-1} emission pulses of NO$_x$ emitted in each continent and month.

Pollutant	Continent	Season	Integrated excess CH$_4$ burden, Tg years	Integrated excess O$_3$ burden, Tg years

Pollutant	Continent	Season	Integrated excess CH$_4$ burden, Tg years	Integrated excess O$_3$ burden, Tg years
NO$_x$	N America	January	-15.23	0.6685
		July	-19.09	0.4446
	Asia	January	-23.08	0.5510
		July	-49.83	1.2960
	Europe	January	-11.34	0.2502
		July	-12.80	0.2269

Having looked at the global scale impacts of the CO and NO$_x$ emission pulses, the next issue is their impact within Europe on surface ozone. Here, the question might be the policy advantage to be gained within Europe in terms of reducing monthly mean ozone concentrations through emission reductions in the rest of the world. Accordingly, Figures 4.5 (a) and (b) present the model monthly mean surface ozone concentration responses within Europe for the North American and Asian CO emission pulse experiments, respectively.

Figures 4.5 (a) and (b) show the surface ozone responses to CO emission pulses for 5 model grid squares which cover the area defined by: 50-55°N, 5°W-20°E. The ozone responses are slightly higher for the North American CO emission pulses compared with those from Asia. The responses to the July emission pulse are somewhat higher than those for the January pulse for North America but the converse is the case for Asia.

FIGURE 2. Ozone responses in ppb across Europe to North American CO emission pulses.
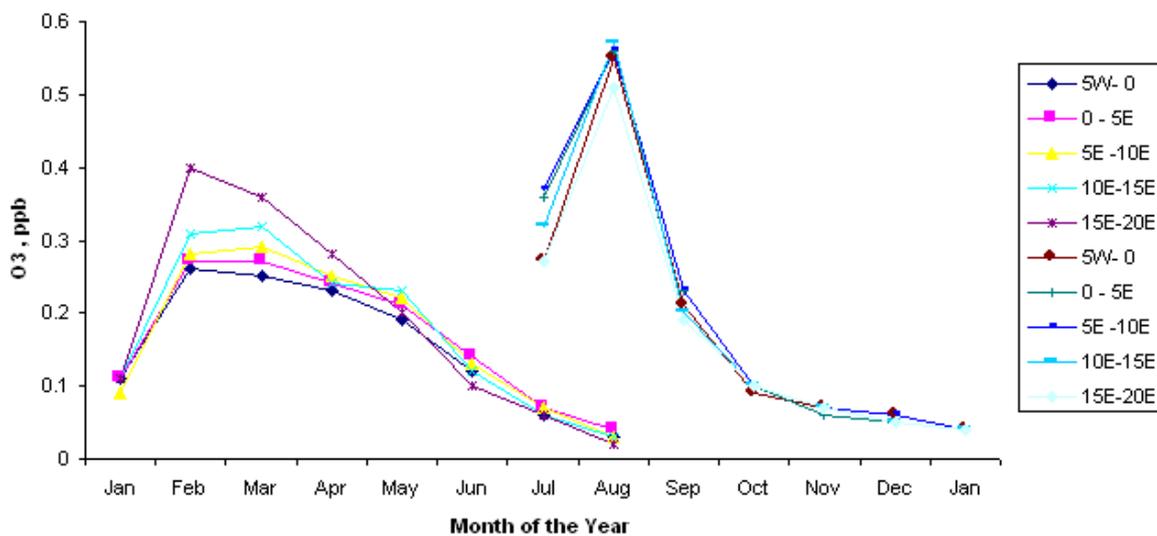
FIGURE 3. Ozone responses in ppb to Asian CO emission pulses.
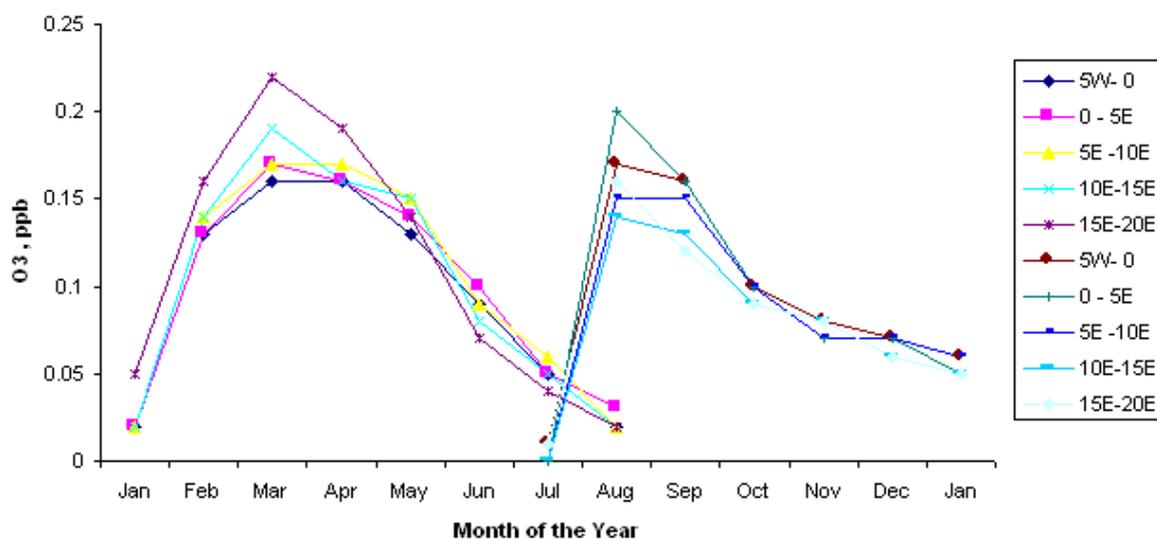
FIGURE 4.5. The model monthly mean surface ozone concentration responses within various latitude bands in Europe for (a). the North American and (b). Asian CO emission pulse experiments.

FIGURE 4. Ozone responses in ppb to North American NOx emission pulses.
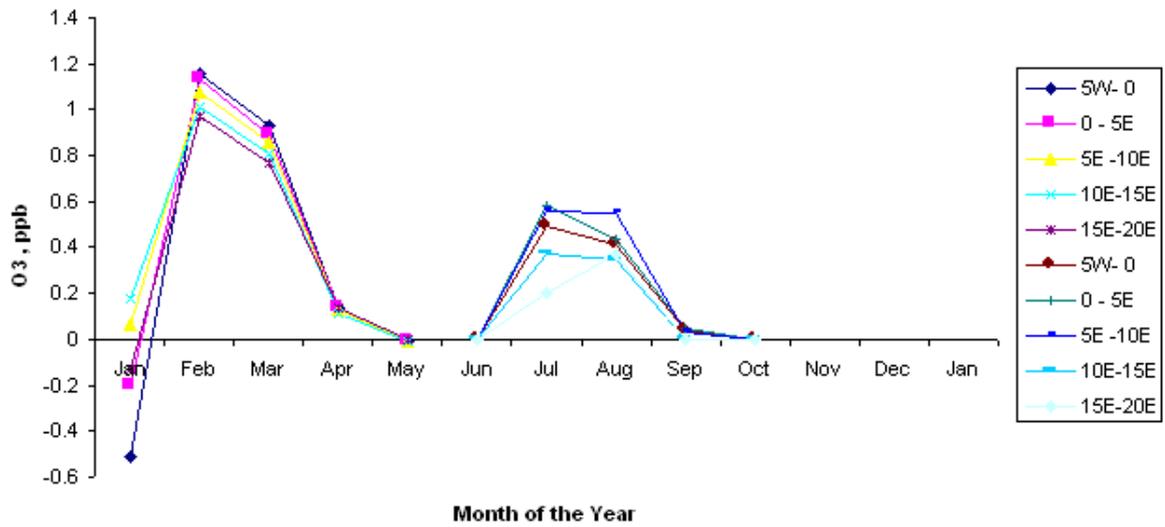
FIGURE 5. Ozone responses to Asian NOx emission pulses.
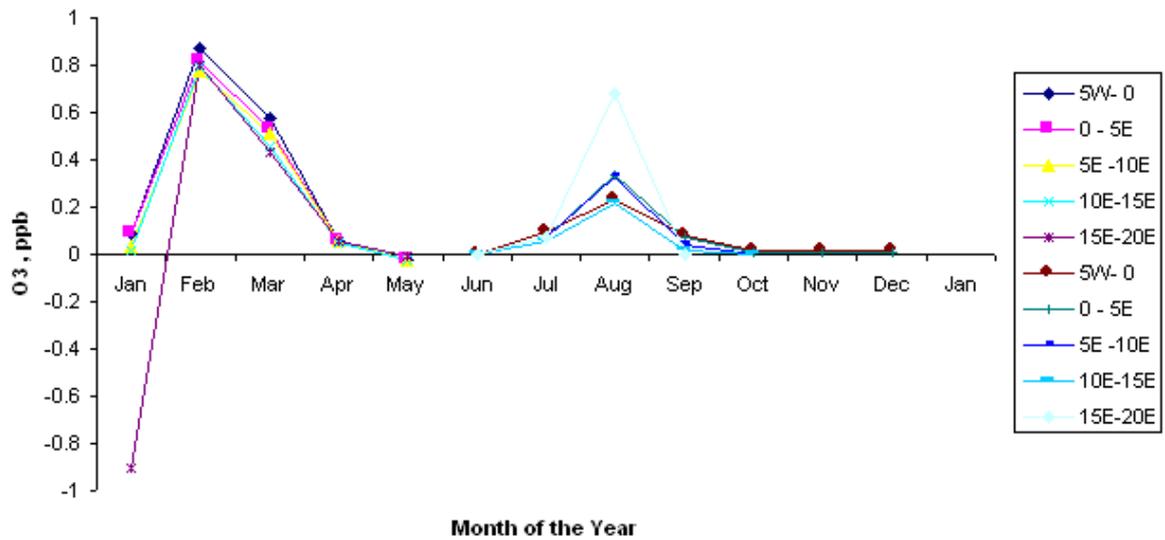
FIGURE 4.6. The model monthly mean surface ozone concentration responses within various latitude bands in Europe for (a). the North American and (b). Asian NO_x emission pulse experiments.

Figures 4.6 (a) and (b) show the surface ozone responses to NO_x emission pulses for the same 5 grid squares across Europe. Again, the ozone responsses are slightly greater for the North American NO_x emission pulses compared with those from Asia and the January responses are greater than those for July.

These results begin to sketch out the basis for a global integrated assessment model. They imply that there are consequences within Europe for emission reduction measures carried out in Asia and North America. This study provides the first quantification of the monthly mean ozone concentration responses within Europe due to CO and NO_x emission changes in the rest of the world. The aim of future work will be to quantify further the European benefits from control measures implemented in the rest of the world.

4.5 Future Ozone Increases and the Growth in Aircraft Emissions

The following scenario cases were examined using the STOCHEM 3-D global Lagrangian chemistry model:

- 1990 Base Case
- 2030 Scenario Case with 1990 Aircraft NOx emissions
- 2030 Scenario Case for all emissions

Emissions for 1990 were based on the EDGAR database and those for 2030 represented those reported for the IPCC SRES B2 scenario. The experiments were integrated using the Hadley Centre fully coupled atmosphere-ocean-chemistry climate model (HadCM3/STOCHEM) initialised with the appropriate climatologies for the 1990s and the 2030s.

Global mean ozone concentrations are summarised in Table 4.7 below. On this basis, it appears that increases in surface emissions between 1990 and 2030 have had a greater influence on the increase in surface ozone concentrations compared with aircraft emissions.

TABLE 4.7. Global mean surface ozone concentrations for four different months in the three scenarios in ppb.

Month	1990 surface and aircraft emissions	2030 surface + 1990 aircraft emissions	2030 surface and aircraft emissions
April	26.45	29.21	29.77
July	24.63	27.08	27.46
October	23.46	25.59	26.03
December	23.96	26.86	27.44

Table 4.8 below summarises the global mean ozone concentrations for each altitude level. On this basis it appears that the increase in aircraft emissions from 1990 to 2030 has a much greater influence on upper tropospheric ozone compared with surface ozone.

TABLE 4.8. Global mean ozone concentrations at four altitude levels during December in the three scenarios in ppb.

Altitude level	1990 surface and aircraft emissions	2030 surface + 1990 aircraft emissions	2030 surface and aircraft emissions
950 mb	23.96	26.86	27.44
750 mb	28.90	32.22	33.00
550 mb	31.80	35.19	36.18
250 mb	62.55	62.50	64.89

5. Global Deposition of Mercury Compounds

5.1 Introduction to the Atmospheric Life Cycle of Mercury and its Compounds

Mercury and its compounds are emitted into the atmosphere from a number of natural processes as well as by human activities. Long range and intercontinental transport of atmospheric mercury and its deposition, followed by the biomethylation and the bioaccumulation of the highly toxic methylmercury compounds in the aquatic food chain, pose serious environmental problems. These concerns have been reflected in the incorporation of mercury within the Geneva Convention of the United Nations Economic Commission for Europe on Long-range Transboundary Air Pollution. A protocol to this Convention was signed at Arrhus in Denmark in June 1998 and addresses the emissions of mercury in addition to those of cadmium and lead.

Man-made emissions of mercury arise from fossil fuel combustion (Carpi 1997), smelting, chlor-alkali plants, incineration and gold mining and have been compiled into a global inventory by Steenhuisen and Wilson (2001). This inventory is available on a 1° x 1° grid globally for the year 1995 for elemental gaseous mercury (Hg^0), for reactive gaseous divalent mercury (Hg^2) and for particulate mercury (Hg^p). Total global man-made emissions are reported as 1447, 775 and 205 tonnes per year, respectively, for Hg^0, Hg^2 and Hg^p. Man-made mercury emissions therefore amount to 2427 tonnes per year. This inventory has been incorporated into the global 3-D Lagrangian chemistry-transport model STOCHEM.

Mercury and its compounds are released or re-emitted into the atmosphere by a number of natural sources and processes. These include volcanoes and other outgassing processes from the earth's crust or mantle, emissions from soils, freshwater (Schroeder et al. 1992) and marine (Wangberg et al. 2001) systems, vegetation and biomass burning (Friedli 2001). Early estimates of the total global mercury emissions from natural sources have been reviewed by Schroeder and Munthe (1998) and values have been reported in the range from 2500 to 30 000 tonnes per year. In view of the inadequacies of the quantification of natural sources, they have not yet been included in STOCHEM.

In the description of the fate and behaviour of atmospheric mercury and its compounds, care must be taken to distinguish between the different chemical forms of the mercury compounds. Elemental gaseous mercury (Hg^0) constitutes the major part, 60%, of the man-made emissions to atmosphere (Steenhuisen and Wilson 2001). Elemental gaseous mercury is relatively unreactive, is removed only slowly by dry deposition and being insoluble in water is not efficiently scavenged by rain. Elemental gaseous mercury therefore has a long atmospheric lifetime, of the order of 1 year (Slemr et al. 1985). It therefore undergoes long range and intercontinental transport and has a well-defined global baseline distribution.

Gaseous divalent mercury (Hg^2) can be present in the atmosphere either as organic compounds such as CH_3HgCl and $Hg(CH_3)_2$ or as inorganic compounds such as $HgCl_2$. Gaseous divalent mercury is sometimes called reactive gaseous mercury RGM because it is readily dry deposited, soluble in water and is efficiently scavenged by rain and so has a relatively short atmospheric lifetime.

Taken together, elemental gaseous mercury and reactive gaseous mercury comprise total gaseous mercury TGM. Continuous monitoring instruments are available for TGM. Generally speaking, elemental gaseous mercury is the major component of TGM since its concentrations are about an order of magnitude higher than those of reactive gaseous mercury (Stratton and Landberg 1995). We will therefore compare STOCHEM fields of elemental gaseous mercury concentrations directly with measurements of TGM.

Divalent mercury may also be scavenged by and attached to suspended particulate matter in the atmosphere and is here termed Hg^p. Particulate mercury originates also from direct emissions and is formed in the atmosphere by the slow oxidation of elemental gaseous mercury. It exists as sub-micron particles and therefore has a low dry deposition velocity, readily undergoing long range transboundary transport. It is, however, readily removed by wet scavenging in rain and so has a relatively short atmospheric lifetime.

It is widely thought that the slow conversion of elemental gaseous mercury to reactive gaseous mercury is controlled by tropospheric ozone (Ryaboshapko et al. 2002). The

kinetics of this oxidation process have been presented by Hall (1995). Recent studies by Somnar et al. (2001) indicate that hydroxyl radicals might also be such an oxidant. Shia et al. (1999) also present a detailed aqueous phase reaction scheme to oxidise elemental to reactive gaseous mercury in cloud droplets. However, this approach based on efficient cloud droplet chemistry appears not to produce an entirely consistent picture of the life cycle of atmospheric mercury and its compounds (Bergan and Rodhe 2001). Conversion of elemental mercury to reactive gaseous mercury has accordingly been described in STOCHEM using the ozone and hydroxyl radical reactions in the gas phase.

The aim of this chapter is to investigate the feasibility of including mercury into the global three-dimensional chemistry transport model STOCHEM. By this means, we can test whether further pollutants, sources, transformations and environmental impacts can be usefully linked together within the framework of an integrated assessment approach.

5.2 Feasibility Study

As a feasibility study, a simplified version of the atmospheric life cycle of mercury and its compounds has been set up within the framework of STOCHEM. The global total emissions from human activities of Hg^0, Hg^2 and Hg^p of 1447, 775 and 205 tonnes yr^{-1}, respectively, were employed based on the work of Steenhuisen and Wilson (2001). No natural emissions were assumed for any of the mercury compounds modelled. Two fates were described for Hg^0 involving the reactions 5.1 and 5.2:

$$Hg^0 + OH = Hg^p \qquad \text{(Reaction 5.1)}$$
$$Hg^0 + O_3 = Hg^p \qquad \text{(Reaction 5.2)}$$

using rate coefficients, 8.7×10^{-14} and 3.0×10^{-20} cm^3 $molecule^{-1}$ s^{-1}, based on the studies of Sommar et al. (2001) and Hall (1995), respectively. Both Hg^2 and Hg^p were removed by wet and dry deposition using the standard scavenging parameters within STOCHEM for a reactive gaseous species and submicron particles.
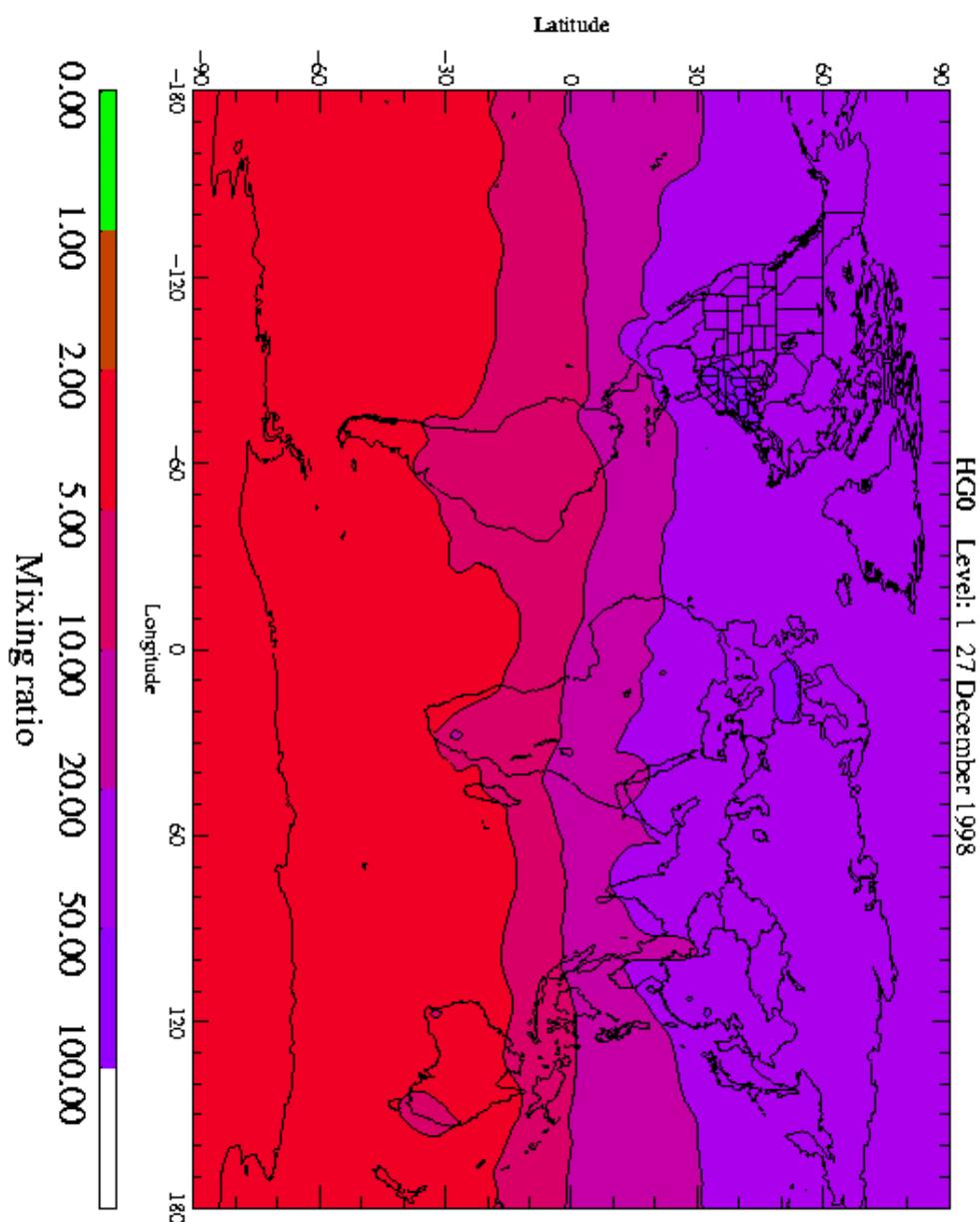
Figure 5.1. Surface distributions of mercury and its compounds from man-made sources in 10^{-15} volume mixing ratios (100×10^{-15} vmr equals 0.84 ng m^{-3}). (a) distribution of Hg^0.
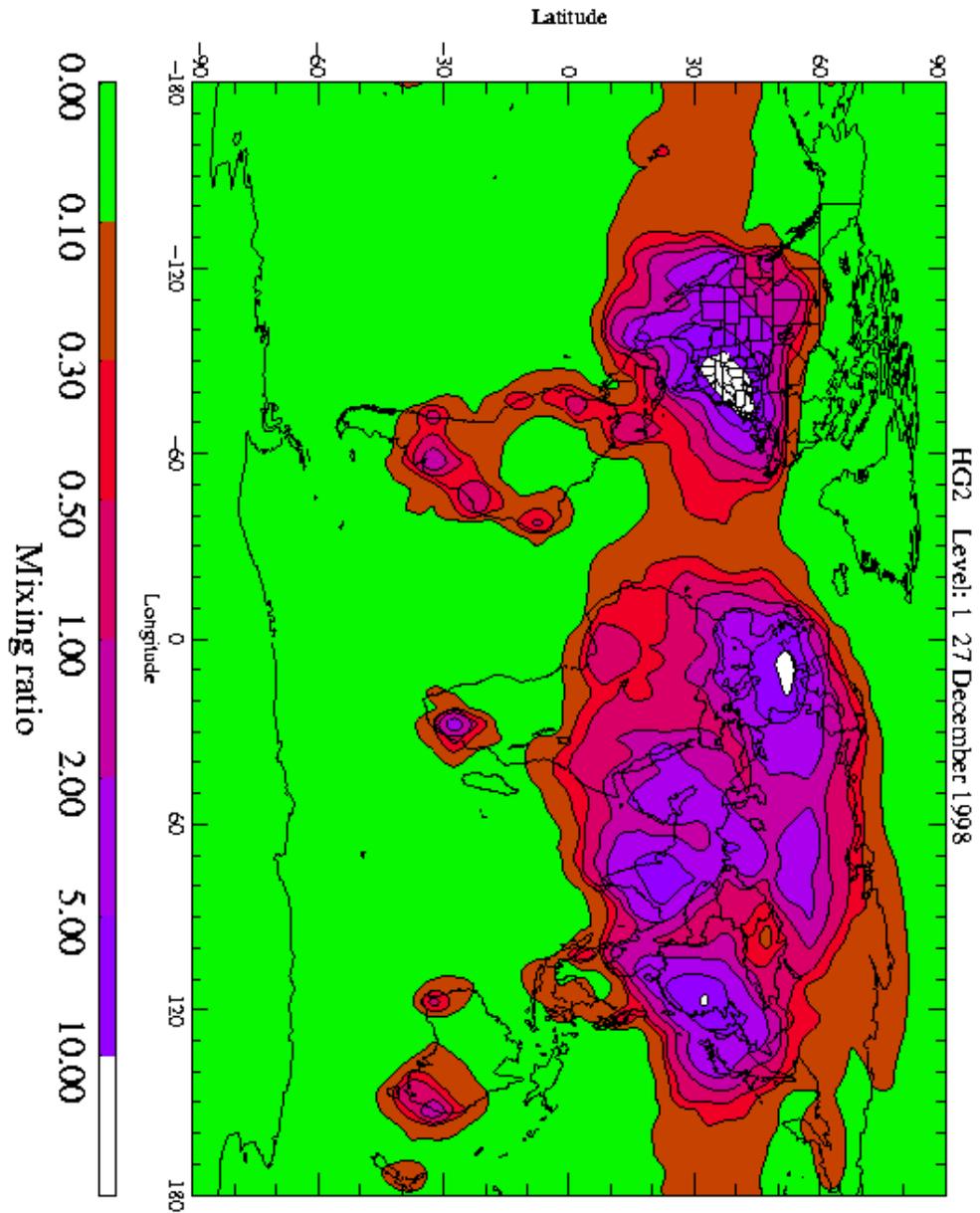
Figure 5.1. (Cont). Surface distributions of mercury and its compounds from man-made sources in 10^{-15} volume mixing ratios (10×10^{-15} vmr equals 0.084 ng m^{-3}). (b) distribution of Hg^2.
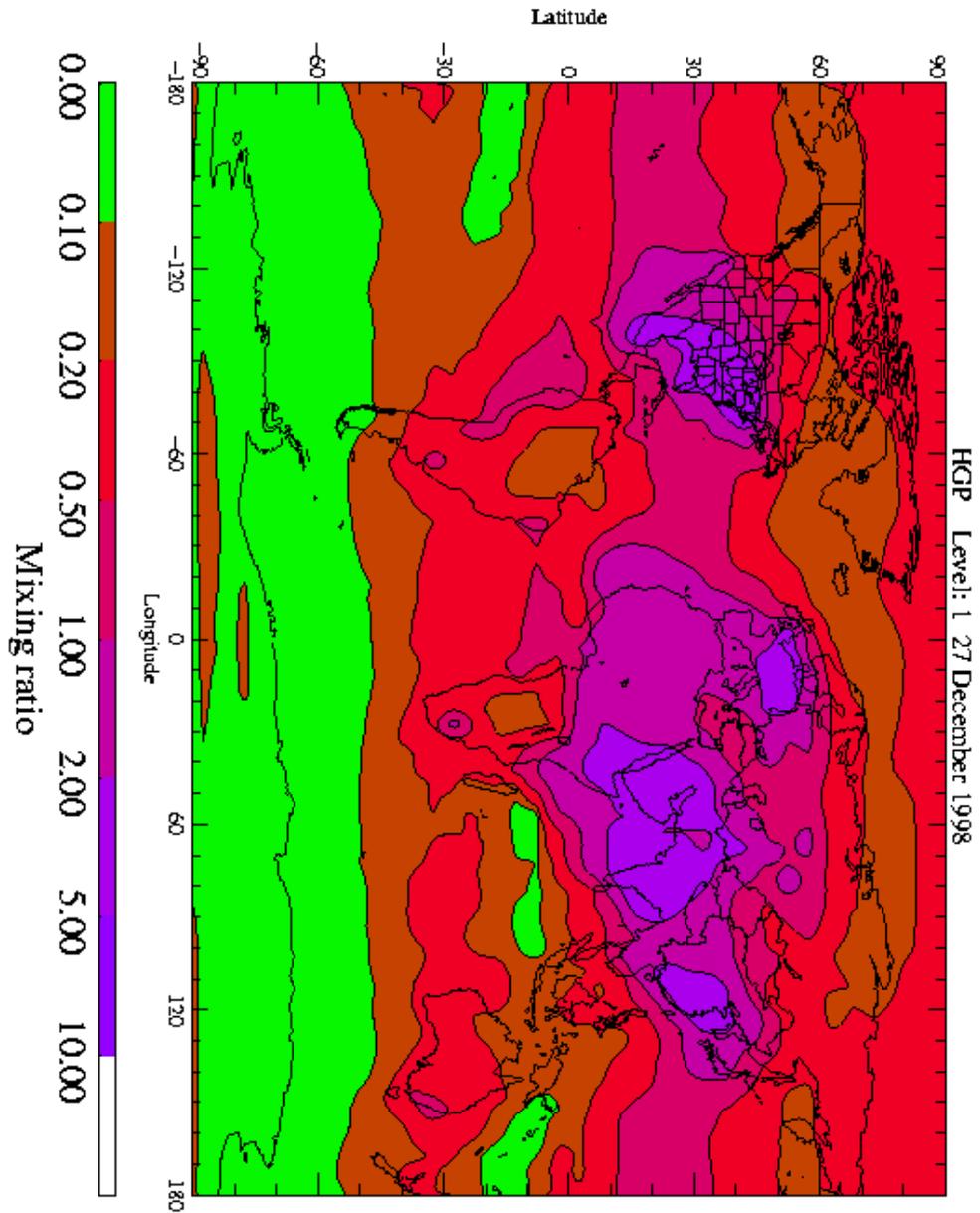
Figure 5.1. (Cont). Surface distributions of mercury and its compounds from man-made sources in 10^{-15} volume mixing ratios (10×10^{-15} vmr equals 0.084 ng m^{-3}). (c) distribution of Hg^{p}.

Figures 5.1 a-c present the global distributions of Hg^0, Hg^2 and Hg^p for mid-December 1998 at the surface, calculated at the end of a 15-month model experiment. The global mean mixing ratios of Hg^0, Hg^2 and Hg^p were found to be 13.9, 0.46 and 0.60 x 10^{-15}, respectively, global mean concentrations of 0.12, 0.004 and 0.005 ng m^{-3}. These global mean concentrations are consistent with current understanding of the observed relative concentrations of the mercury compounds with Hg^0 being the most abundant. The spatial distributions of the different mercury compounds follow similar patterns with highest concentrations over the polluted continents of the northern hemisphere.

The annual mean global inventories of Hg^0, Hg^2 and Hg^p were found to be 373, 7.3 and 21 tonnes, respectively. The mean atmospheric lifetime found for Hg^0 was therefore 95 days which is much lower than the estimate of 460-2430 days given by Bergan and Rodhe (2001). The reason for this apparent discrepancy is because we have included both oxidation routes, 5.1 and 5.2, for the conversion of Hg^0. In this experiment, the annual mean conversion routes through the OH and ozone routes were 1050 and 221 tonnes yr^{-1}, showing that the OH route is by far the most efficient. The turnover time for the ozone route alone was accordingly 620 days which is well within the range of the estimates givrn above based on the ozone oxidation route given by Bergan and Rodhe (2001).

The removal processes for the mercury compounds involve both wet and dry deposition of both Hg^2 and Hg^p. Dry deposition accounts for the removal of 164 and 148 tonnes yr^{-1} of Hg^2 and Hg^p, whereas wet deposition accounts for the removal of 600 and 1323 tonnes yr^{-1}, respectively. The resulting atmospheric lifetimes for Hg^2 and Hg^p are 3.5 and 4.0 days.

A comparison of model calculated man-made concentrations of Hg^0 with the observations made at Mace Head, Ireland by Ebinghaus et al. (2002) is presented in Figure 5.2. The monthly mean observations for baseline air masses arriving off the north Atlantic Ocean show a clearly evident seasonal cycle with a wintertime maximum and a summertime minimum. The annual mean Hg^0 concentration in baseline air masses was 1.58 ng m^{-3}. In comparison, the model results are significantly
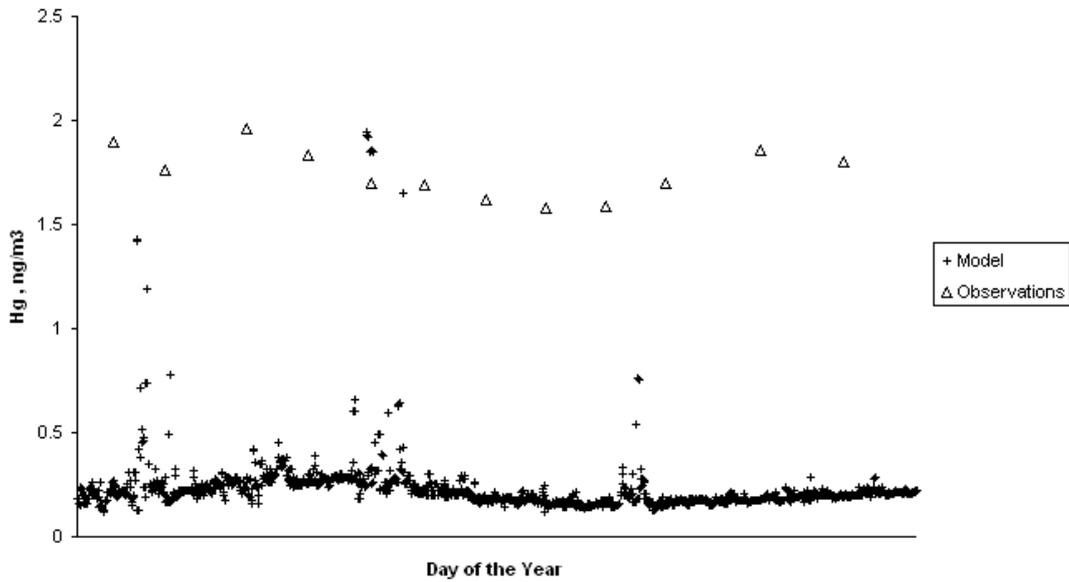
Figure 5.2. Observed mean monthly Hg^0 concentrations in ng m^{-3} in baseline air masses compared with the model calculated concentrations at Mace Head, Ireland.

lower by a factor of between 6 to 10 and span the range 0.15 to 0.25 ng m^{-3}. The neglect of natural mercury sources in the model has clearly influenced the evaluation of model performance against observations.

The model calculations in Figure 5.2 show the presence of sporadic peaks which go up to peak concentrations of about 2 ng m^{-3}, an elevation of about 1.8 ng m^{-3} above the baseline. These peaks coincide with the arrival of regionally-polluted air masses at the Mace Head location and are also a feature of the observations. Ebinghaus et al. (2002) report observed peak concentrations of up to 4.3 ng m^{-3}, an elevation of 2.7 ng m^{-3} above baseline. STOCHEM is clearly giving a more accurate representation of the Hg^0 concentrations in regionally polluted air masses compared with baseline air masses.

In summary, we have shown that it is feasible to fit a simplified treatment of the atmospheric life cycle of mercury and its compounds into the STOCHEM model. The

fields of OH radicals and of ozone calculated within STOCHEM have the required accuracy with which to calculate a quantitative description of the fate and behaviour of the mercury compounds emitted from man-made sources. The proposal is now to extend the STOCHEM mercury model:

- To include natural sources of mercury and its compounds using the MOSES 2.2 surface-exchange scheme.
- To complete a full evaluation of model performance against available observations.
- To use the labelling techniques developed for ozone to provide an indication of the continental origins of the mercury compounds found in the model wet and dry deposition loads.
- To understand the future fate and beahviour of mercury compounds under the influence of climate change.

6. Discussion and Conclusions

The adverse environmental impacts of the long range transport and deposition of acidic sulphur and nitrogen species to the remote and sensitive regions of north west Europe have been recognised for over two decades now. Policy measures to control and abate the emissions of SO_2 and NO_x have been formulated within the aegis of the United Nations Economic Commission for Europe (UN ECE) in Geneva, Switzerland and its international convention on long range transboundary air pollution (CLRTAP). A series of legally-binding protocols have been negotiated to this convention dealing originally with the exchange of research and monitoring data and then the control and abatement of SO_2, NO_x, VOCs, NH_3, trace metals, and persistent organic pollutants.

The latest protocol, signed in Gothenburg in 1999, is the 'Protocol to Abate Acidification, Eutrophication and Ground Level Ozone'. The ultimate goal of this protocol is to achieve levels of the deposition of acidic and eutrophying species which no longer exceed critical loads and to achieve levels of exposure to ozone which no longer exceed critical levels. The formulation of the underpinning science required to support this protocol was laid out by Grennfelt, Hov and Derwent (1994). Grennfelt et al. (1994) envisaged a set of pollutant generating human activities, a set of atmospheric trace gases derived from these activities, and the physico-chemical interations between these trace gases, generating a set of damaging pollutants which cause damage to target ecosystems and human health. Their framework linked SO_2, NO_x, NH_3, VOCs, CO and methane emissions to acidification, euthrophication, regional and free tropospheric ozone formation. This framework formed the basis for the regional-scale integrated assessment modelling adopted within the Gothenburg Protocol. This modelling generated a table of country-specific emission levels for SO_2, NO_x, VOCs and NH_3 which it was envisaged would partially close the gap between the modelled exposure levels and deposition loads in the year 2010 and critical levels and loads for acidification, eutrophication and ground level ozone.

Subsequently, additional air quality policy concerns have been raised. These have addressed fine particles, with human health and climate change as 'receptors'. Furthermore, the growth in tropospheric ozone levels has emerged much more strongly as an air quality issue since the work of Grennfelt et al. (1994). This growth

has impacts on agricultural crops and forests and ultimately on human health since ozone episodes sit on top of a global ozone baseline. When these new links are added into the framework assembled by Grennfelt et al. (1994), the diagram shown in Figure 6.1 results.
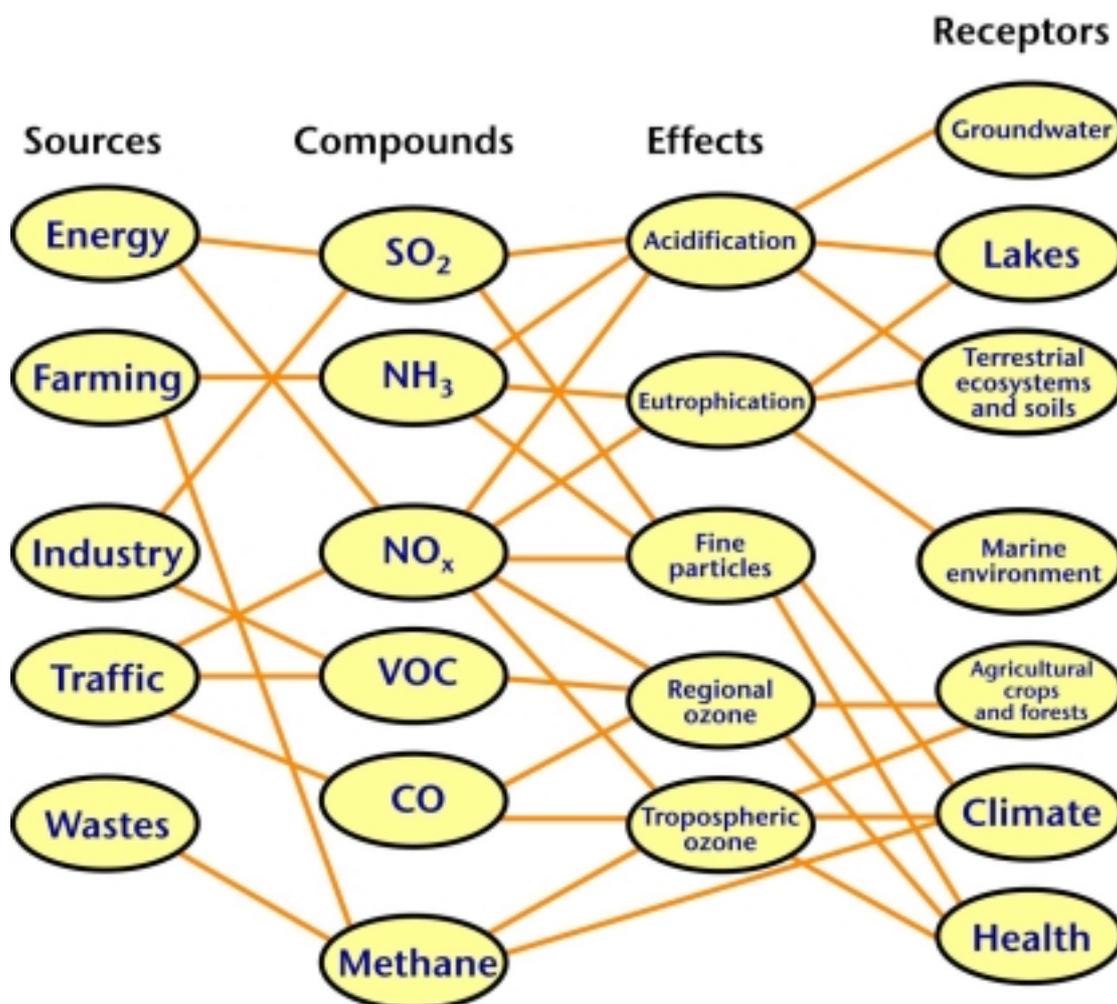
Figure 6.1. Regional air pollution problems in Europe. Relations between dominant sources, emitted compounds and their effects on different receptors.

Having constructed the new and more complete framework in Figure 6.1, the challenge is now to represent it in integrated assessment models. This report has examined a number of the potential linkages in Figure 6.1 and addressed the growing understanding of the importance of the linkages between global and regional-scale air quality problems. These linkages may require new protocols and strategies and may lead potentially to revisions in the existing protocols.

The requirements for future revisions are built in to the individual protocols. Future revisions depend on the successes of the measures taken to reduce emissions and changing perceptions of the environmental impacts addressed. They also reflect improvements in scientific understanding of the processes involved. The models used to describe the emission, transformation, long-range transport and deposition of air pollutants are becoming more sophisticated with time. They are becoming better able to support the pressure for further emission reductions and to provide the more accurate assessments of source-receptor relationships required to identify the crucial remaining sources to be tackled.

The first issue that has been addressed in this study has been the linkage between CO emissions and acidification and eutrophication. Figure 6.1 shows how CO emissions from human activities on the regional scale arise predominantly from traffic and how they influence the formation of ozone on both the regional and global scale. The potential issue is that this involvement of CO in global and regional ozone formation also influences the production of hydrogen peroxide and of hydroxyl radicals. Hydrogen peroxide and hydroxyl radicals are the main oxidants for the SO_2 emitted from human activities. There is the potential therefore for man-made emissions of CO on the regional scale to influence acidification. By the same argument, the involvement of CO in the production of OH radicals could influence the oxidation of NO_x to nitric acid and PAN and to change the deposition of oxidised and reduced nitrogen species, and hence eutrophication.

When man-made CO emissions are reduced by 50 % across-the-board, the total global dry deposition of sulphur compounds is reduced and the dry and wet deposition fluxes of ammonium sulphate are increased slightly. However, the magnitude of these changes is approximately 0.15 Tg yr^{-1} in each case, being just greater than the noise level in STOCHEM of 0.1 Tg yr^{-1}. The spatial patterns of the changes in deposition resulting from the halving of man-made CO emissions involve reduced dry sulphur deposition fluxes over Europe and parts of North America and China. However, there are some regions where this flux has increased - central Europe, and small parts of central Asia, south-east Asia and western North America. However, overall, the dry deposition flux of SO_2 has fallen. These responses to changes in man-made CO

emissions are small and are unlikely to be of any significance in air quality policy terms.

When man-made NO_x emissions are reduced by 50 % across-the-board, total global dry SO_2 deposition is reduced by 0.37 Tg yr^{-1} and dry and wet deposition of ammonium sulphate increase by 0.25 and 0.41 Tg yr^{-1}, respectively. These changes suggest that the transformation of SO_2 to ammonium sulphate is more efficient when man-made NO_x emissions are controlled. The changes in the dry and wet deposition fluxes of H_2SO_4 are within the noise. The dry deposition flux of ammonia has also decreased slightly, which is consistent with an increased production of ammonium sulphate aerosol. The dry and wet deposition rates of the NO_y species have, not surprisingly, decreased. Changes in the spatial pattern of total sulphur deposition generally involve increases in those regions where the SO_2 dry deposition flux has decreased. There are also regions where the total sulphur deposition flux has decreased, over parts of Europe and North America, and particularly northern China. Again, overall these responses are small and are unlikely to have any significance in air quality policy terms.

It is widely recognised that the growth of greenhouse gases will induce through climate change, widespread and significant changes in atmospheric composition and weather patterns. The impact of the growth in greenhouse gas emissions through to 2030 in the IPCC SRES B2 scenario on the deposition of acidifying and eutrophying compounds has been investigated by calculating the deposition patterns for 2030 with identical emissions but with 1990 and 2030 meteorology. Both deposition maps for 2030 have been calculated with identical 2030 emissions and show similar features. The impact of Asian SO_2 emissions on the wet sulphur deposition fields is clearly apparent across much of the northern hemisphere. Also, the trans-continental transport of acidic sulphur compounds across the North Atlantic Ocean is clearly apparent following the implementation of strict SO_2 emission controls in Europe.

Nevertheless, the differences between the deposition maps resulting from changes in meteorology due to climate change are small. There is an indication of increased export across the North Atlantic Ocean into the British Isles but it is difficult to say whether this is a robust feature of the future deposition patterns. It may well be that

2030 is too early for dramatic shifts in the regional deposition patterns of acidifying and eutrophying agents. Nevertheless, such shifts should be taken into account in any wider study of the interaction between climate change and critical loads and levels exceedance over the medium to long term future.

The formation of secondary particles on the global and regional scales has been investigated. The conversion of SO_2 and DMS to particulate sulphur, of NO_x to particulate nitrate, NH_3 to particulate ammonium and terpenes to secondary organic aerosols has been incorporated into STOCHEM. A reasonable description has been obtained of the observed distributions of secondary particles on the regional and global scales. On the global scale, the fraction of secondary particle mass predicted to be present as sulphate was found to be 0.52, with the fractions of nitrate, ammonium and organics found to be 0.22, 0.09 and 0.17, respectively. This implies that the links between the climate impacts of particles and regional emissions of SO_2, NO_x and NH_3 in Figure 6.1 are likely to be of strong policy concern. However, the UN Framework Convention on Climate Change as currently formulated does not address the aerosol precursor gases in the basket of gases under control. The links between SO_2, NO_x and NH_3 emissions and secondary particles and human health on the regional scale came too late for the Gothenburg Protocol as originally formulated though may well feature strongly in its revision. Man-made VOCs have been found to about an order of magnitude less important for secondary organic aerosol formation compared with natural biogenic VOCs (Derwent and Malcolm 2000) so it will not be pressing to include such a linkage in Figure 6.1. Overall, there are cogent reasons for extending the Gothenburg Protocol and the UN Framework Convention on Climate Change to include secondary aerosol species and their precursors: SO_2, NO_x and NH_3.

Evidence has begun to accumulate concerning the intercontinental and interhemispheric scales of long range transport for some of the trace gases and air pollutants of concern in Figure 6.1. It has, for example, been long recognised that particulate sulphate can travel from North America and Eurasia to the Arctic contributing to the Arctic haze problem. It has only recently been recognised that North American ozone precursor emissions may exert an influence on ozone levels in Europe. Similarly, intercontinental transport processes can lead to the export of ozone from Europe to Asia, Asia to the North America and North America to Europe.

Labelling techniques have been employed within STOCHEM to ascertain the continental origins of the ozone observed at the surface at each of 21 selected ozone monitoring sites across Europe. The bulk of the ozone calculated in air parcels arriving at the 21 selected locations during 1998 carried the 'European' label. The European contribution to mean ozone levels covered the range 9.5-31.5 ppb, with Mace Head, Ireland at the lowest and Montelibretti, Italy at the highest end of the range. Averaged over the 21 locations and 1998, European ozone production contributed about 20.7 ppb to surface ozone mixing ratios over Europe and provided the largest single source area contribution.

The North American continental region contributed surface ozone mixing ratios over Europe in the range 5.8-12.2 ppb, with Virolahti, Finland and Laheema, Estonia on the both Baltic Sea receiving the least North American contribution and Mace Head, Ireland the highest. As we have remarked above, Mace Head is the location most exposed to the weather systems moving up the North Atlantic Ocean and these systems appear to provide a mechanism for the intercontinental transport of ozone as well as stratosphere-troposphere exchange. The behaviour seen for stratosphere-troposphere exchange and North American intercontinental transport appear somewhat different pointing perhaps to different geographical patterns in influence from these two mechanisms across Europe. Averaged over the 21 locations and 1998, North American continental ozone production contributed about 8.2 ppb to surface ozone mixing ratios over Europe.

The Asian continental region contributed surface ozone mixing ratios in the range 3.5-6.6 ppb, with Montelibretti, Italy and Iskrba, Slovenia receiving the least Asian contribution and Mace Head, Ireland the highest. The spatial pattern of the contributions from Asian sources and stratosphere-troposphere exchange show similarities, confirming the possible importance of North Atlantic weather systems. Averaged over the 21 locations and 1998, Asian continental ozone formation contributed about 4.5 ppb to surface ozone mixing ratios over Europe.

In view of the importance of intercontinental transport from North America and Asia in determining mean ozone concentrations over Europe, the question remains as to the magnitude of ozone changes resulting in Europe from ozone precursor emission

reductions in North America and Asia. It may be that such changes due to policy actions in North America and Asia are not negligible and may need to be taken into account in the revision of the Gothenburg Protocol.

The impact of an across-the-board 50% reduction in global man-made NO_x emissions on the ozone mixing ratios attributed to each continental source region was studied 21 selected locations across Europe. The reductions in annual mean ozone mixing ratios due to the 50% reduction in global NO_x emissions were largest for the ozone formed within the European source region, amounting to 0.9-4.3 ppb, least for the Asian source region, 0.5-0.7 ppb, with North America 0.8-1.9 ppb. On a percentage basis, the reductions in surface ozone resulting from a 50% reduction in man-made NO_x emissions were between 6-18% when the reduction was made in Europe, between 14-16% from North America and 12-14% from Asia. It is likely, therefore, that changes in man-made NO_x emissions made in North America and Asia will have an impact on annual mean ozone levels across Europe, particularly on the Atlantic Ocean seaboard of north west Europe and in Scandinavia.

The impact of an across-the-board 50% reduction in global man-made carbon monoxide emissions was studied in a similar manner as that for NO_x emission reductions. The reductions in ozone mixing ratios were again largest for the ozone attributed to the European source region, 0.4-0.8 ppb, least for the Asian source region, 0.1-0.2 ppb, with North American ozone reduced by 0.1-0.3 ppb. On a precentage basis, a 50% reduction in carbon monoxide emissions reduced surface ozone from Europe by 2.3-3.2%, from North America by 1.7-3.0% and from Asia by 1.8-3.0%. These responses to CO emissions appear to be close to the level of noise within the STOCHEM model and may be of borderline air quality policy significance.

The STOCHEM model has been used to look at the global scale impact of the regional emissions of NO_x and CO and their control on the build-up of the greenhouse gases: methane and ozone. By changing the location and season of an emitted pulse of NO_x or CO, but not its magnitude, differing impacts on methane and ozone have been found for NO_x and CO emitted in Europe, North America and Asia.

For CO emissions in North America, Europe and Asia, slightly differing global methane and ozone responses have resulted. The differences in the integrated excess methane burdens and hence global mean radiative forcing, are probably within the model error bounds for the different seasons and continents. However, the differences in integrated excess ozone burdens show differences that are beyond the model error bounds for the different seasons and continents. For NO_x emissions, the globally-integrated methane responses and hence radiative forcing are the most negative for pulses emitted in Asia, followed by North America and least negative for European pulses. Globally-integrated ozone responses are largest for Asia and least for Europe. The different model responses to NO_x emissions arising from the different continents in different seasons, span a factor of four or more and are much greater than the differences found for CO emissions.

The influence of the regional emissions of CO and NO_x and their control on the global mean radiative forcing due to methane and ozone and hence on climate change, are large and are likely to be of air quality policy significance. The UN Framework Convention on Climate Change does not currently have tropospheric ozone precursors within its basket of greenhouse gases. It is therefore not possible currently for Europe to claim credit or disbenefit in climate change terms for actions taken on the regional scale to control NO_x and CO emissions.

STOCHEM has been used to follow the build-up of methane and ozone in the troposphere during the 21st century and to understand the mechanisms involved in the feedback between the chemical development and the changing weather patterns which result from climate change. A surprising conclusion from the analysis was that surface ozone concentrations are also expected to increase through to the year 2100, in addition to upper tropospheric concentrations. So, for example, surface ozone concentrations during the summer months over the continental land masses are currently about 30-40 ppb. In the IPCC SRES A2 and A1FI emission scenarios, the corresponding values become 45-50 ppb in 2030, 60 ppb in 2060 and 70 ppb in 2100. These concentrations are well above the internationally-accepted environmental criteria values (WHO 1987) set to protect human health, sensitive crops and vegetation. This prospect is in store for all of the continental areas of the northern hemisphere, despite the strenuous measures being made to improve urban- and regional-scale ozone air quality in North America and Europe. These ozone increases

are more directly relevant to the long term exposure levels of crops and vegetation than to human exposures. However, urban- and regional-scale pollution episodes are built upon these global baseline values and so the future medium to long term increases in the latter may therefore work against regional pollution control strategies, set to reduce exposure levels of both man and vegetation.

Finally, the STOCHEM model has been used to study the feasibility of adding the life cycle of mercury to Figure 6.1. Mercury and its compounds are emitted into the atmosphere from a number of natural processes as well as from human activities. Long range and intercontinental transport of atmospheric mercury and its deposition, followed by the biomethylation and the bioaccumulation of the highly toxic methylmercury compounds in the aquatic food chain, pose serious environmental problems. These concerns have been reflected in the incorporation of mercury within the Geneva Convention of the United Nations Economic Commission for Europe on Long-range Transboundary Air Pollution. A protocol to this Convention was signed at Arrhus in Denmark in June 1998 and addresses the emissions of mercury in addition to those of cadmium and lead. In the context of Figure 6.1, mercury could be added as a substance emitted by coal combustion and from industrial processes. Its oxidation in the atmosphere is driven by ozone and hydroxyl radicals which are controlled by VOCs, CO, methane and NOx. The receptors for mercury would be the aquatic food chain and human health in the Arctic environment.

We have shown that it is feasible to fit a simplified treatment of the atmospheric life cycle of mercury and its compounds into the STOCHEM model. The fields of OH radicals and of ozone calculated within STOCHEM have the required accuracy with which to calculate a quantitative description of the fate and behaviour of the mercury compounds emitted from man-made sources.

In summary, therefore we have identified a number of reasons why present agreements, protocols and strategies need extending and supplementing with new protocols and strategies. These are in no particular order:

- As concentration levels and deposition loads are progressively reduced by regional pollution controls, originally small and uncontrolled sources within

the UN ECE framework assume more significant proportions. Examples include marine sulphur sources from shipping in the North Atlantic Ocean, North Sea, Baltic Sea and Mediterranean Sea. Such sources may have a significant influence on critical load exceedance in sensitive ecosystems on the Atlantic Ocean seaboard of north west Europe and Scandinavia.

- Global baseline levels of ozone in Europe have been rising due to increased man-made emissions elsewhere in the northern hemisphere and threaten to erode the improvements made through European regional pollution controls on NO_x and VOCs. There is currently no framework within European regional air quality policy formulation to address the consequences of changes in global baseline ozone concentrations due to precursor emission changes in North America and Asia.

- Reductions in European regional emissions of CO and NO_x may have a significant influence on the global scale build-up of methane and ozone, the second and third most important greenhouse gases. The UN Framework Convention on Climate Change does not include tropospheric ozone precursor gases within its basket of greenhouse gases. There is therefore no mechanism for Europe to claim any credit or disbenefit in terms of climate change mitigation for it actions to reduce ozone precursor emissions on the regional scale.

- European emissions of SO_2, NO_x and NH_3 play a significant role in the global scale formation of secondary aerosol particles which may have a significant influence on climate change. The UN Framework Convention on Climate Change does not include aerosol precursor gases within its basket of greenhouse gases. Again, there is no mechanism for Europe to claim credit or disbenefit in terms of climate change mitigation for its actions to reduce aerosol precursor emissions on the regional scale.

- Mercury deposition over Europe is driven partly by local European emissions of mercury compounds and by the deposition of mercury compounds derived from the global mercury circulation. This material of global origins is not addressed currently by the Arrhus Protocol on heavy metals.

7. Recommendations for Further Work

In completing this work, it has become clear that we have not been able to take all the issues through to completion. We have identified areas where further work needs to be done to reinforce and extend the policy conclusions developed in section 6 above.

On the issue of background ozone, further work is recommended to provide a detailed focus for the emission projections on the year 2020. This will allow a move to be made away from the straight-jacket of the IPCC SRES emission scenarios. The model output needs to be extended to address AOT_{40} exposure levels in addition to monthly mean ozone concentrations. An assessment is required of the origins and spatial variations in the ozone trends across Europe during the 1990s and the role played by intercontinental transport from North America and Asia. Further studies are required of the extent to which the growing ozone background will influence ozone levels within Europe in the period after the implementation of the UN ECE Gothenburg Protocol and the EU National Emissions Ceilings Directive for discussion within the CAFÉ policy formulation process.

We recommend further modelling work on the environmental impact of marine SO_2 and NO_x emissions. This could include a further analysis of the long range transport of acidic sulphur species into the western fringes of Europe and their impact on the trends in acidic deposition there. We need to understand the role played by marine NO_x emissions in the intercontinental transport of ozone into Europe from North America. There is a potential issue of the importance of marine NO_x emissions in the ozone problems of the Mediterranean region.

Further model development is required in the representation of meteorological and chemical processes in STOCHEM. Further studies are required of the import of ozone into Europe from North America and Asia and of the export of ozone into Asia from Europe. There is a need to validate the model representation of intercontinental transport against field studies of mechanism and processes.

We recommend further work on global mercury modelling through the application of tracer labelling techniques to show how much mercury deposition in Europe comes from mercury emissions in other continents and from the southern hemisphere.

Finally, we recommend further work on the links between climate change and regional air quality. Policies have been set in hand to reduce deposition loads with the aim of reaching critical loads in the long term. At some stage in the future, global climate change will start to influence the critical loads for soils and freshwaters and the critical levels for natural vegetation and crops through changes in the physical and ecological environment. So, climate change will ultimately influence regional air quality policy targets. Over the same timescale, actions on the regional scale to reduce emissions of ozone precursors will influence the tropospheric OH abundance and hence the build-up of the greenhouse gases, methane and ozone. There will be a feedback between regional air quality and global climate change through the ozone precursor gases. Regional pollution controls will reduce regional aerosol loadings and induce another feedback between regional air quality and global climate change. Climate change will bring about changes in the emissions from natural biogenic sources with possible impacts on trace gas concentrations and regional air quality. We

are just at the beginning of the process of understanding how to construct the model experiments required to quantify the links between regional air quality and global climate change.

8. References

Barrie L.A., Bottenheim J.W., Schnell R.C., Crutzen P.J., and Rasmussen R.A. (1988). Ozone destruction and photochemical reactions at polar sunrise in the lower arctic atmosphere. Nature **334**, 138-141.

Bergan T. and Rodhe, H. 2001. Oxidation of elemental mercury in the atmosphere; Constraints imposed by global scale modelling. Journal of Atmospheric Chemistry **40**, 191-212.

Borrmann S., Solomon S., Dye J.E. and Luo B. (1996). The potential of cirrus clouds for heterogeneous chlorine activation. Geophysical Research Letters **23**, 2133-2136.

Carpi A. 1997. Mercury from combustion sources: A review of the chemical species emitted and their transport in the atmosphere. Water Air and Soil Pollution **98**, 241-254.

Chatfield R.B. and Delany A.C. (1990). Convection links biomass burning to increased tropical ozone: However, models will tend to overpredict O3. Journal of Geophysical Research **95**, 18473-18488.

Collins, W.J., Stevenson, D.S., Johnson, C.E. and Derwent, R.G., 1997, Tropospheric ozone in a global-scale three-dimensional Lagrangian model and its response to NO_x emissions controls. Journal of Atmospheric Chemistry **26**, 223-274.

Collins, W.J., Stevenson, D.S., Johnson, C.E. and Derwent, R.G., 1999, The role of convection in determining the budget of odd hydrogen in the upper troposphere. Journal of Geophysical Research **104**, 26927-26941.

Derwent, R.G. and Friedl, R. 1999. Impacts of Aircraft Emissions on Atmospheric Ozone, In: Aviation and the Global Atmosphere. Eds: J.E. Penner et al.; Cambridge University Press, UK.

Derwent, R.G. and Malcolm, A.L. 2000. Photochemical generation of secondary particles in the United Kingdom. Phil. Trans. Roy. Soc. London **A358**, 2643-2657.

Friedli, H.R., Radke, L.F. and Lu, J.Y. 2001. Mercury in smoke from biomass fires. Geophyscial Research Letters **28**, 3223-3226.

Gauss, M., Myhre, G., Pitari, G., Prather, M.J., Isaksen, I.S.A., Berntsen, T.K., Brasseur, G.P., Dentener, F.J., Derwent, R.G., Hauglustaine, D.A., Horowitz, L.W., Jacob, D.J., Johnson, M., Law, K.S., Mickley, L.J., Muller, J.-F., Plantevin, P.-H., Pyle, J.A., Rogers, H.L., Stevenson, D.S., Sundet, J.K., van Weele, M., and Wild, O. 2002. Radiative forcing in the 21st century due to ozone changes in the troposphere and lower stratosphere. Journal of Geophysical Research **108**, 4292, doi:10.1029/2002JD002624.

Grennfelt, P., Hov, O. and Derwent, R.G. 1994. Second generation abatement strategies for NO_x, NH_3, SO_2 and VOCs. Ambio **23**, 425-433.

Hjellbrekke, A.-G. 2000. Ozone measurements 1998. EMEP/CCC-Report 5/2000. Norwegian Institute for Air Research, Kjeller, Norway.

Hall, B. 1995. The gas-phase oxidation of elemental mercury by ozone. Water Air and Soil Pollution **80**, 301-315.

IPCC, 1999, Special Report on Aviation and the Global Atmosphere. Intergovernmental Panel on Climate Change. Cambridge University Press, Cambridge.

IPCC, 2001, Climate change 2001: The scientific basis. Intergovernmental Panel on Climate Change, Cambridge University Press, Cambridge, UK.

Jacob, D.J. et al. 1999. Effect of rising Asian emissions on surface ozone in the United States. Geophysical Research Letters **26**, 2175-2178.

Jaegle, L.; et al. Chemistry of HO_x radicals in the upper troposphere. Atmospheric Environment **35**, 469-489, 2001.

Johns T.C., Carnell R.E., Crossley J.F., Gregory J.M., Mitchell J.F.B., Senior C.A., Tett S.F.B. and Wood R.A. (1997). The second Hadley Centre coupled ocean-atmosphere GCM: model description, spinup and validation. Climate Dynamics **13**, 103-134.

Johnson, C.E. et al.; Role of Climate Feedback on methane and ozone studied with a coupled ocean-atmosphere-chemistry model. Geophysical Research Letters **28**, 1723-1726, 2001.

Kanikadou M., et al. (1999). 3-D global simulations of tropospheric CO distributions – Results of the GIM/IGAC intercomparison 1997 exercise. Chemosphere: Global Change Science **1**, 263-282.

Komhyr, W.D., Oltmans, S.J., Franchois, P.R., Evans, W.F.J. and Matthews, W.A. 1989. The latitudinal distribution of ozone to 35 km altitude from ECC ozonesonde observations. pp 147-150. Ozone in the Atmosphere. A. Deepak, Hampton, Virginia, USA.

Li, D., and Shine, K., 1995, A 4-dimensional ozone climatology for UGAMP models. UGAMP Internal Report, University of Reading, UK.

Murphy, D.M. and Fahey, D.W., 1994, An estimate of the flux of stratospheric reactive nitrogen and ozone into the troposphere. Journal of Geophysical Research **99**, 5325-5332.

Nakicenovic, N. et al. 2000. Special Report on Scenarios: A Special Report of Working Group III of the Intergovernmental Panel on Climate Change. Cambridge University Press, Cambridge, UK.

Olivier, J.G.J., Bouwman, A.F., van der Maas, C.W.M., Berdowski, J.J.M., Veldt, C., Bloos, J.P.J., Visschedijk, A.J.H., Zandveld, P.Y.J., and Haverlag, J.L. 1996. 'Description of EDGAR version 2.0', RIVM Report nr. 771060 002, Bilthoven, Netherlands.

Olson J., Prather M., Berntsen T., Carmichael G., Chatfield R., Connell P., Derwent R., Horowitz L., Jin S., Kanakidou M., Kasibhatla P., Kotamarthi R., Kuhn M., Law K., Penner J., Perliski L., Sillman S., Stordal F., Thompson A. and Wild O. (1997). Results from the Intergovernmental Panel on Climate Change photochemical model intercomparison (Photocomp). Journal of Geophysical Research **102**, 5979-5991.

Oltmans, S.J. and Levy, H. II 1994. Surface ozone measurements from a global network. Atmospheric Environment **28**, 9-24.

Pickering, K.E. et al.; Trace gas transport in the vicinity of frontal convective clouds. Journal of Geophysical Research **93**, 759-773, 1988.

Ryaboshapko, A., Bullock, R., Ebinghaus, R., Ilyin, I., Lohman, K., Munthe, J., Petersen, G., Seigneur, C., and Wangberg, I. 2002. Comparison of mercury chemistry models. Atmospheric Environment **36**, 3881-3898.

Schroeder, W.H. and Munthe, J. 1998. Atmospheric mercury – an overview. Atmospheric Environment **32**, 809-822.

Schroeder, Lindqvist, O., Munthe, J. and Xiao, Z. 1992. Volatilization of mercury from lake surfaces. Science of the Total Environment **125**, 47-66.

Shia, R.L., Seigneur, C. Pai, P., Ko, M., and Sze, N.D. 1999. Global simulation of atmospheric mercury concentrations and deposition fluxes. Journal of Geophysical Research **104**, 23747-23760.

Slemr, F., Schuster, G. and Seiler, W. 1985. Distribution, speciation and budget of atmospheric mercury. Journal of Atmospheric Chemistry **3**, 407-434.

Stohl, A.. and Trickl, T. 1999. A textbook example of long-range transport: Simultaneous observation of ozone maxima of stratospheric and North American origin in the free troposphere over Europe. Journal of Geophysical Research **104**, 30445-30462.

Somnar, J., Gardfelt, K., Stromberg, D., and Feng, X. 2001. A kinetic study of the gas-phase reaction between the hydroxyl radical and atomic mercury. Atmospheric Environment **35**, 3049-3054.

Steenhuissen, F. and Wilson, S. 2001. 1995 global anthropogenic mercury emissions; Spatial data distribution and mapping project. Arctic Monitoring and Assessment Programme (AMAP). PO Box 8100 Dep. N-0032 Oslo, Norway.

Stevenson, D.S., Collins, W.J., Johnson, C.E., and Derwent, R.G., 1998, Intercomparison and evaluation of atmospheric transport in a Lagrangian model (STOCHEM), and an Eulerian model (UM), using ^{222}Rn as a short-lived tracer. Quarterly Journal of the Royal Meteorological Society **124**, 2477-2491.

Stratton, W.J. and Lindberg, S.E. 1995. Use of a refluxing mist chamber for measurement of gas-phase mercury (II) species in the atmosphere. Water Air and Soil Pollution **80**, 1269-1278.

Walton, J., MacCracken, M., and Ghan, S. (1988). A global-scale Lagrangian trace species model of transport, transformation, and removal processes. Journal of Geophysical Research **93**, 8339-8354.

Wangberg, I., Schmolke, S., Schager, P., Munthe, J., Ebinghaus, R., and Iverfelt, A. 2001. Estimates of air-sea exchange of mercury in the Baltic Sea. Atmospheric Environment **35**, 5477-5484.

WHO 1987. Air Quality Guidelines for Europe; World Health Organisation Regional Publications, European Series No. 23, World Health Organisation, Copenhagen, Denmark, 1987.

Winkler P. 1988. Surface ozone over the Atlantic Ocean. Journal of Atmospheric Chemistry **7**, 73-91.

Annex A. Published Papers and Reports from this Project

1. W.J. Collins, R.G. Derwent, C.E. Johnson, D.S.Stevenson. The impact of human activities on the photochemical production and destruction of tropospheric ozone. Quarterly Journal of the Royal Meteorological Society, **126**, 1925-1951, (2000).

2. D.S. Stevenson, C.E. Johnson, W.J. Collins, R.G. Derwent. The impact of climate change upon the future radiative forcing from tropospheric ozone and methane. Proc. Quadrennial Ozone Symposium Sapporo 2000, pp185-186, NASDA, Japan, (2000).

3. W.J. Collins, R.G. Derwent, C.E Johnson. Input of stratospheric ozone into the troposphere studied with a Lagrangian model. Proc. Quadrennial Ozone Symposium Sapporo 2000, pp. 227-228, NASDA, Japan, (2000).

4. C.E. Johnson, D.S. Stevenson, W.J. Collins and R.G. Derwent. Role of climate feedback on methane and ozone studied with a coupled ocean-atmosphere-chemistry model. Geophysics Research Letters, **28**, 1723-1726, (2001).

5. R.G. Derwent, W.J.Collins, C.E Johnson, D.S Stevenson. Transient behaviour of tropospheric ozone precursors in a global 3-D CTM and their indirect greenhouse effects. Climatic Change, **49**, 463-487, (2001).

6. W.J. Collins, R.G. Derwent, C.E. Johnson, D.S. Stevenson. The origins of an early spring maximum in the global tropospheric ozone burden in a 3-D chemistry-transport model. TOR-2 Annual Report, pp.147-150. EUROTRAC-2 ISS, GSF National Research Center for Environment and Health, Munich, Germany, (2001).

7. D.S. Stevenson, R.G. DErwent, W.J. Collins, C.E. Johnson. Comparison of the observed and 3-D CTM model calculated seasonal cycles in surface ozone concentrations. TOR-2 Annual Report, pp.151-154. EUROTRAC-2 ISS, GSF National Research Center for Environment and Health, Munich, Germany, (2001).

8. W.J. Collins, R.G. Derwent, C.E. Johnson and D.S. Stevenson (2002). The oxidation of organic compounds and their global warming potentials. Climatic Change **52**, 453-479.

9. W.J. Collins, R.G. Derwent, C.E. Johnson and D.S. Stevenson (2002). A comparison of two schemes for the convective transport of chemical species in a Lagrangian global chemistry model. Quarterly Journal of the Royal Meteorological Society **128**, 991-1009.

10. C.E. Johnson, D.S. Stevenson, W.J. Collins and R.G. Derwent (2002). Interannual variability in methane growth rate simulated with a coupled ocean-atmosphere-chemistry model. Geophysical Research Letters, **29**, 10.1029/2002GL015269.

11. R.G.Derwent, W.J.Collins, C.E. Johnson and D.S. Stevenson (2002). Global ozone concentrations and regional air quality. Environmental Science and Technology, **36**, 379A-382A.

12. R.G.Derwent, W.J.Collins, C.E. Johnson and D.S. Stevenson (2002). Projections for future ozone change driven by changes in climate and precursor emissions. In: Air Pollution as a Climate Forcing: A Workshop. pp59-60. Goddard Institute for Space Studies, New York.

13. A.F.Bouwman, D.P. Van Vuuren, R. G. Derwent and M.Posch (2002). A global analysis of acidification and eutrophication of terrestrial ecosystems. Water Air and Soil Pollution, **141**, 349-382, (2002).

14. R.G Derwent. Key pollutants – ground level ozone. Part 2 2002-2052. In: The Clean Air Revolution: 1952-2052. pp 42-48. National Society for Clean Air, Brighton, (2002).

15. W.J. Collins, R.G. Derwent, M.E. Jenkin, C.E. Johnson and D.S. Stevenson. The global distribution of secondary particulate matter in a 3-D Lagrangian chemistry transport model. Journal of Atmospheric Chemistry, **44**, 57-95, (2003).

16. A.Volz-Thomas et al. Tropospheric ozone and its control. Chapter 3. pp73-122. Towards Cleaner Air for Europe. Science, Tools and Applications. Part 1. Margraf Publishers, Leiden, The Netherlands, (2003).

17. D.S. Stevenson, C.E. Johnson, E.J. Highwood, V. Gauci, W.J. Collins and R.G. Derwent (2002). Atmospheric impact of the 1783-1784 Laki eruption: Part I. Chemistry modelling. Atmospheric Chemistry Physics Discussions, **3**, 551-596, (2003).

18. W.J. Collins, R.G. Derwent, B.Garnier, C.E. Johnson, M.G. Sanderson, D.S Stevenson (2002). The effect of stratosphere-troposphere exchange on the future tropospheric ozone trend. Journal of Geophysical Research, **108**, 4292, 10.1029/2002JD002617, (2003).

19. Gauss. M., Myhre, G., Pitari, G., Prather, M.J., Isaksen, I.S.A., Bernsten, T.K., Brasseur, G.P., Dentener, F.J., Derwent, R.G., Hauglustaine, D.A., Horowitz, L.W., Jacob, D.J., Johnson, M., Law, K.S., Mickley, L.J., Muller, J.-F., Plantevin, P.-h., Pyle, J.A., Rogers, H.L., Stevenson, D.S., Sundet, J.K., van Weele, M., and Wild, O. Radiative forcing in the 21st century due to ozone changes in the troposphere and the lower stratosphere. Journal of Geophysical Research, **108**, 4292, doi:10.1029/2002JD002624.

20. M. G. Sanderson, W.J. Collins, R.G. Derwent, C.E. Johnson (2002). Simulation of global hydrogen levels using a Lagrangian three-dimensional model. Journal of Atmospheric Chemistry, in press.

21. Sanderson, M.G., Jones, C.D., Collins, W.J., Johnson, C.E. and Derwent, R.G. (2003). Effect of climate change on isoprene emissions and surface ozone levels. Geophysical Research Letters, submitted.

Annex B. Meetings Attended.

Results from this project were presented at the following meetings.

1. European Geophysical Assembly, Nice, France, March 2001.

2. EMEP Task Force on Measurement and Modelling, Portoroz, Slovenia, May 2001.

3. Gordon Research Conference, Newport, Rhode Island, June 2001.

4. US EPA/EMEP Joint workshop on intercontinental transport, Palisades, New Jersey, June 2001.

5. GEIA/GIM workshop, Paris, France, July 2001.

6. IAMAP meeting, Innsbruck, Austria, August 2001.

7. EMEP Task Force on Measurement and Modelling, Geneva, Switzerland, April 2002.

8. NASA/GISS workshop on air pollution as a climate forcing, Hawaii, May 2002.

9. Gordon Research Conference, Oxford, August 2002.

10. IGAC meeting, Crete, August 2002.

11. Joint US EPA/UBA workshop on interhemispheric pollution, Bad Breisig, Germany, October 2002.

12. Great Smog Conference, London, December 2002.

13. Atmospheric Chemistry Specialist Group, Royal Meteorological Society, Oxford, March 2003.

14. Task Force on Integrated Assessment Modelling, Vienna, March 2003.

15. Joint European Geophysical Assembly/AGU Meeting, Nice, France, April 2003.

16. Joint SPARC/IGAC workshop, Giens, France, April 2003.

17. Haagen-Smit Symposium, Lake Arrowhead, California, May 2003.